An Experimental Investigation of Spanwise Vortices Interacting with Solid and Free Surfaces

by

Martin J. Donnelly

Dissertation submitted to the faculty of the Virginia Polytechnic Institute and State University in partial fulfillment of the requirements for the degree of

Doctor of Philosophy
In
Engineering Mechanics

D.P. Telionis, Chairman
S.L. Hendricks
J. Lesko
S.A. Ragab
J. Schetz

June 12, 2006
Blacksburg, Virginia

Keywords: vortex interaction, turbulent boundary layer, free surface

An Experimental Investigation of Spanwise Vortices Interacting with Solid and Free Surfaces

Martin J. Donnelly

(ABSTRACT)

Coherent vortices are generated in flow fields due to flow interaction with sharp solid surfaces. Such vortices generate significant disturbances in the flow and affect its further development. In this dissertation attention is focused on the interaction of vortices with solid or free liquid/air surfaces. We examine vortices with their axis parallel or normal to the surface. Three main cases were examined: the interaction of a vortex pair propagating towards a solid boundary, the interaction of spanwise vortices in a turbulent boundary layer, and finally the interaction of spanwise vortices with a flat-plate wake and a free liquid surface. These problems hold significance in several engineering applications, including investigations into trailing wing tip vortices and their interaction with the ground, vortical effects on the development of turbulent boundary layers and free surface signatures and their detection in ship/submarine wakes. Data are acquired with a laser Doppler velocimetry system (LDV) and with Particle-Image Velocimetry (PIV), using a high-speed digital video camera. The LDV system measures two components of velocity along appropriately chosen planes. Grids of data were acquired for different pitch rates of a disturbing flap that generates vortices. Phase-averaged vorticity and turbulence level contours are estimated and presented. It is found that vortices with diameter the order of the boundary layer quickly diffuse and disappear while their turbulent kinetic energy spreads uniformly across the entire boundary layer.

Larger vortices have a considerably longer life span and in turn feed more vorticity into the boundary layer. Trailing edge vortices are generated in a water tunnel by sharp hinged motions of a flap. These vortices are allowed to reconnect with the free surface and mix with a turbulent free shear layer. The flow is conditionally sampled via frame grabbing of free surface shadowgraphs. It is found that the vortex core bends away from the plane of the shear layer. Moreover, contrary to earlier findings, organized velocity fluctuations decrease as the free surface is approached.

Acknowledgements

Foremost appreciation goes to my wife and partner of 13 years, Kerri. It was your belief, support, love, and encouragement that allowed me to complete this dissertation after so many years.

To my parents, John and Norah, you always told me I could do anything I set my mind too. Your unconditional love and respect have allowed me to accomplish everything I have set out to do.

To my advisor and mentor, Dr. Demetri Telionis, your ideas, support, encouragement, and guidance brought me to this point. Even after many years away you never gave up on me completing these requirements, for that I an extremely grateful.

I wish to thank my colleagues in the Engineering Science and Fluid Mechanics Laboratory, Dr. Michael Wilder, Dr. Othon Rediniotis, Dr. Sandie Klute, Mr. Erik Panzer, Dr. Norman Schaeffler, Dr. Matthew Zeiger, , Dr. Pavlos Vlachos, Dr. Dimitri Stamos, Mr. Christopher Moore, Mr. Luis Chalmetta, and Mr. Andy Mathes. Each of you contributed in some way to my experience and education at Virginia Tech.

The support of the office of Naval Research, under grant numbers ONR N00014-93-1-0264, and N00014-96-1-0941, Edwin Rood, monitor, is gratefully acknowledged.

Martin J. Donnelly

June 2006
Blacksburg, Virginia

Table of Contents

List of Figures

List of Tables

CHAPTER 1

Introduction and Literature Review

Problem Statement

The interest of current study is primarily driven by the free surface signatures of a ship's wake which is present a long time after the ship has passed. These free surface signatures can be detected by synthetic aperture radar (SAR). A typical SAR image is shown in Figure 1. This image is comprised of the Kelvin waves, a turbulent momentum wake, and large vortical structures. Understanding of the surface signature is dependent on understanding of these large vortical structures and how they interact with the free surface to generate a slowly decaying wake.

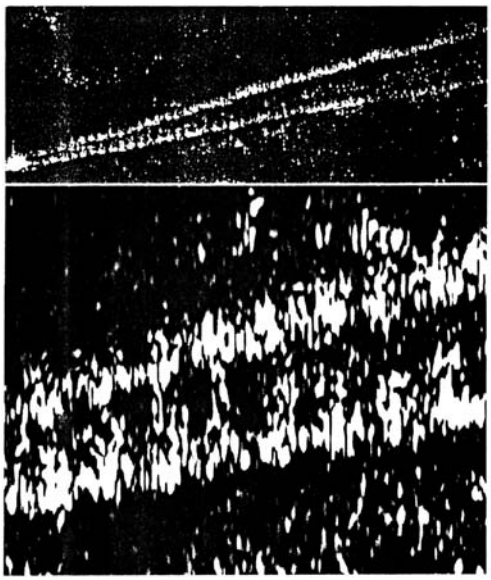

Figure 1. (top) Synthetic Aperture Radar image of a Ship Wake, (bottom) close up view of above revealing free surface signatures (Lyden et al 1988)

The interaction of spanwise vortical structures with both solid boundaries and free surfaces were investigated. A variety of experimental configurations were studied, including

- a vortex pair propagating towards a solid boundary
- a spanwise vortex interacting with a turbulent boundary layer
- the interaction of a spanwise vortex, free shear layer and a free surface

Why Spanwise Vortices?

The flow in the proximity of a ship hull is fully turbulent and can have large quasi-coherent vortical structures interacting with it. Free surface, wave-induced separation bubbles break down into vortical structures, which downstream of reattachment can mix with the turbulent boundary layer. It is believed that these spanwise vortices (rollers), that is large vortical structures drifting with the boundary layer, with their axes normal or nearly normal to the stream present a great challenge in the understanding of these flow fields. The imposed vortical flows in this study are nominally two-dimensional but in reality, significant three-dimensional motions emerge. These three-dimensional motions which result in vorticity transport mechanisms can be depicted schematically in Figure 2. The most obvious mechanism of this vorticity transport is mechanism a, that is free- surface, wave-induced separation bubbles. The large vortical structure can add energy to the boundary layer and create additional mixing. Three-dimensional mechanisms, b and c, are known to arise for these types of

interaction problem. Mechanism c in which these rollers give rise to axial motions could be of importance near the free surface. In mechanism b a turning of vorticity to form streamers could be possible, and has been observed by other researchers. This mechanism could generate flow situations similar to vortices whose axis is parallel to the free surface.

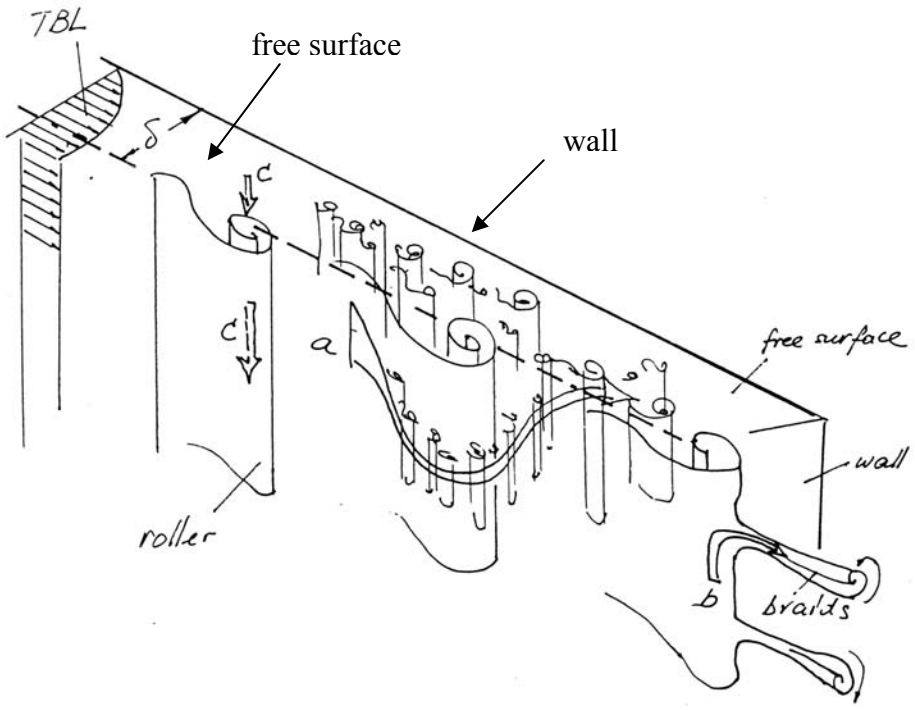

Figure 2. Schematic of Spanwise Vortices Interacting with a Turbulent Boundary Layer

This study sheds some light on these flow features which comprise the flow around the hull of a ship and in its wake.

Literature Review

A Vortex Pair Propagating Towards a Solid Boundary

Many investigators have studied the behavior of a pair of vortices in the vicinity of a wall. In some of these studies the emphasis is on the ground effects on aircraft tip vortices. Pioneering contributions can be found in the works of Dee and Nicholas (1968), Harvey and Perry(1971), and Ciffone and Pedley (1978). Quite a few papers on this problem have appeared more recently Zheng and Ash (1991), Zheng and Ash (1993), Robins and Delisi (1993), Ash and Zheng (1994).

Inviscid analysis of the flow of pairs of vortices approaching a solid wall (Barker and Crow 1977) indicate that when the vortices approach the wall, they move away from each in a parabolic path. In real life, single or pairs of vortices start moving away from the wall in a process that resembles "rebounding." Saffman (1979) clearly pointed out that this is a viscous effect. Orlandi (1990) describes the rebounding process in greater detail. The fundamental work on this problem is reviewed by Doligalski et al. (1994). The present group Luton et al. (1995) obtained a numerical solution of laminar vortex wall interaction and most recently, Corjon and Poinsot (1997) examined the effect of cross flow.

Most of the work described above is analytical. The methods of the early experimental contributions were not very sophisticated and as a result, the data obtained were rather limited. Limited experimental information is available documenting the

development of secondary vortices and their interaction with the primary vortices. In this study we report on results obtained with a high-speed digital video camera and laser-Doppler velocimetry (LDV). Both methods allow us to document the temporal development of the entire velocity field.

The Interaction of Rolling Vortices with a Turbulent Boundary Layer

In a variety of engineering applications one encounters the interaction of coherent vortical structures with a turbulent boundary layer. Vortical structures comparable in size or larger than the thickness of the boundary layer could be generated downstream of obstructions which induce separation. Dynamic motions of solid surfaces with sharp edges like propeller blades or impeller fins generate free shear layers which roll up and form vortical structures. Such structures again may interact with a turbulent boundary layer.

Broadly speaking, studies of the interactions of vortices with a turbulent boundary layer can be grouped into two categories: (i) those which focus on the effect of the externally imposed vortical structure on the turbulent boundary layer and (ii) those which explore the effect of the turbulent boundary layer on the organization of the vortex. This distinction is usually dictated by the interest in a specific engineering application. The problem of course is highly nonlinear and the two effects are strongly coupled. In this dissertation information is presented on the temporal development of both the turbulence characteristics and the organized character of the imposed vortex.

The effects of a variety of disturbances imposed on a turbulent boundary layer have been investigated in the past. A long line of investigators introduced axial vortices ("streamers") in turbulent boundary layers. One of the initial contributions is due to Shabaka et al. (1985). A more recent example is the work of Littell and Eaton (1991) who generated a disturbance by rapidly pitching a half delta wing. Three-dimensional disturbances can also be introduced locally. Makita et al. (1989) create artificial horseshoe vortices in their turbulent boundary layer. Disturbances can also be introduced into a uniform spanwise direction to create structures with spanwise vorticity. Such vortical structures are often referred to as rollers. Rollers can be generated by pitching airfoils in a free stream or by periodically lifting spanwise fences out of a wall. A number of investigators have employed pitching fences, to study the structure of unsteady separation (Francis et al. (1979), Reisenthal et al. (1985), Consigny et al. (1984), and Nagib et al. (1985)). In another line of work, disturbances were created in a free stream in order to study their interactions with blades further downstream (Poling and Telionis (1986), Poling et al. (1988), Booth and Yu (1986), and Wilder et al. (1990)). More recently, investigations of rollers with turbulent boundary layers were carried out (Nelson et al. 1990, Kothmann and Pauley 1992 and Macrorie and Pauley 1992). It is believed that the present contribution resembles mostly the latter category.

Nelson et al. (1990) lift a fence from the floor of a flat plate on which a turbulent boundary layer has developed. They then measure periodic velocity fields by ensemble averaging LDV data. Pauley and his co-workers instead pitch a small airfoil upstream of

the leading edge of a flat plate and allow the disturbances to enter the boundary layer which grows downstream.

In the present effort a disturbance is created in a manner very similar to the method employed by Nelson et al. (1990) who employ a fence with a chordlength half the thickness of the boundary layer. As a result their vortices are fully embedded in the turbulent boundary layer. A very interesting result for this choice of parameters is that the vortex disintegrates very quickly and completely disappears a few chordlengths downstream of the fence. In the present research we confirm the findings of Nelson et al. for vortices on the order of the boundary layer thickness. Additional experiments are performed for vortical structures two and three times the size of the boundary layer. These vortices propagate much further downstream and can contribute significant amounts of energy to the turbulent boundary layer.

The Interaction of a Spanwise Vortex, Shear Layers and a Free Surface

The interaction of vorticity and a free surface is one of the very few fluid mechanics phenomena which remained unexplored until very recently. Sarpkaya (1986) identified the basic elements of the free surface disturbances generated by a pair of stationary vortices parallel to the free stream. Bernal and Kwon (1989) provided the first convincing demonstration that a vortex tube will disconnect in the vicinity of the surface and reconnect to the surface. A number of problems involving the interaction of discrete vortical structures with a free surface have been investigated. Typical problems studied include:

- a pair or a single vortex with axis parallel to the free surface (Sarpkaya et al. 1988, Sarpkaya and Suthon 1990,1991)
- a jet with its axis parallel to the free surface (Anthony and Willmarth 1992)
- a pair of parallel linear vortices drifting towards the free surface (Marcus and Berger 1989, Willmarth et al. 1989, Willert and Gharib 1994)

The most interesting feature of such flows, vortex reconnection with a free surface can best be demonstrated and studied by the interaction of a vortex ring rising towards the surface (Bernal and Kwon 1989, Gharib et al 1992, Gharib 1994). Extensive numerical calculations of these problems have also been carried out (Ohring and Lugt 1989, Yu and Trygvasson 1990, Dommermuth and Yue 1990, Swean et al. 1991).

The interaction of turbulence in the form of turbulent boundary layers (Komori et al. 1982, Lam and Banarjee 1988, Rashidi and Banarjee1988, Swean et al. 1989, Longo et al. 1993, Stern et al. 1994)and isotropic grid turbulence (Banarjee 1994, Pan and Banarjee (1994), Gharib et al. 1994) have also been investigated.

A crucial element in the physics of the vorticity-free surface interaction is that vorticity can actually escape from the flowfield through the free surface. Rood (1994) indicates how the vorticity component normal to the surface can be balanced by surface tangential acceleration and thus removed from the field

Literature Review Update

Three significant contributions have been made to this area of research since the original literature review was completed in 1999.

Reed and Milgram (2002) published a review of ship wakes and their radar images in the Annual Review of Fluid Mechanics. Due to classification limitations this work does not reveal for how long surface ship wakes are visible before decaying into normal ocean wave images. The work does elaborate on the complexity of surface ship wakes, which contain high-Froude number processes such as large surface waves, breaking waves, high concentration of bubbles, and often unknown surface tension properties. The most visible or highly reflective region of the ship wake primarily consists of short wave components and concentrations of high surfactants. The authors do not provide insight into the underlying flow phenomenon that allows these wakes to propagate significant distances downstream.

Dabiri (2002) and Dooley (2005) conducted very similar investigations in which a splitter plate generates a vertical shear layer which interacts with the free surface. The splitter plate has a sharp trailing edge, spans the water channel test section from floor to free-surface, and is sufficiently long to generate an upstream turbulent boundary layer on both sides of the plate. Dabiri (2002) focuses primarily on how free surface disturbances correlate to near-free surface turbulence. This investigation makes use of a free surface gradient detector simultaneously sampled with a planar digital particle image velocimetry image. Dooley (2005) utilizes a stereo digital particle image velocimetry system which

allows for the measurement of all three velocity components. The primary focus is the analysis of the velocity fields in the frequency domain. Both author's results reveal the presence of a free surface layer in which surface normal velocity fluctuations decrease while surface parallel velocity fluctuations increase. Dabiri (2002) reveals the presence of a kink in surface parallel vorticity as a pre-cursor to reconnection with the free surface. Dooley (2005) concludes that streamwise velocity fluctuations observed at all depths are a result of a long-wavelength lateral oscillation in the mean flow pattern which only takes place near the free-surface.

Author's Contribution

In this dissertation we consider a coherent vortex embedded in either a fully developed turbulent shear layer, or turbulent boundary layer interacting with the free surface. In earlier studies, both experimental and numerical, assumptions or provisions are made to keep the free surface disturbances small or nonexistent. This is not a limitation placed on the present study and large surface depressions are seen. The data taken in these experiments should lead to a greater understanding of high-Froude-number vortex/free surface interactions. It is hoped that this analysis will also aid in the development of numerical techniques aimed at tackling these large-surface-depression high-Froude-number cases.

Experimental Investigation:

Experimental Setups

A variety of experimental setups have been used in an attempt to elucidate some of the more important aspects of vortex interactions with solid boundaries and free surfaces.

A Vortex Pair Impinging on a Solid Boundary

A pair of flaps, shown in Figure 3, is actuated by a stepping motor to generate a counter-rotating pair of vortices. Motions are monitored using a digital rotary encoder to make sure that the motions are repeatable. The flaps are 8 inches in length, 3 inches in width, and are bounded by a plexiglass floor and ceiling. The flaps are placed at an initial angle of 27.5 degrees and are pitched at a variety of angular velocities to 90 degrees. The ability to control the flap pitching rate allows this setup to generate a range of vortex strengths, quantified by a Reynolds number based on circulation ($Re_\Gamma = \Gamma/\nu$).

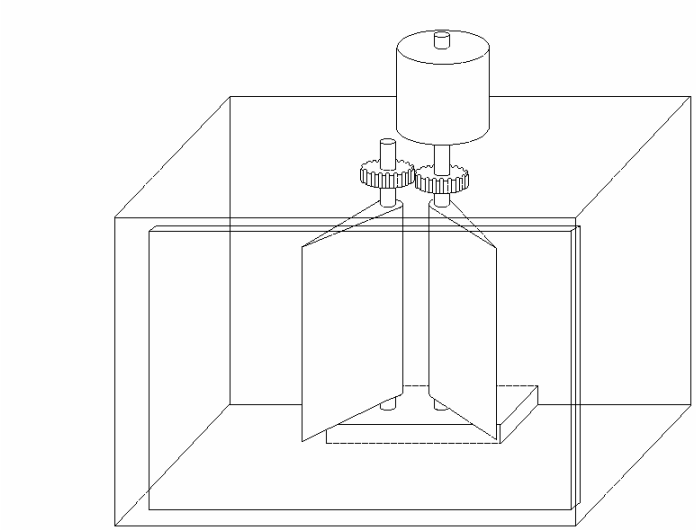

Figure 3. Schematic of Experimental Setup

At this point a pair of vortices is shed at a distance of 5 inches from a solid boundary and propagates towards the wall due to their mutual interaction. A top view of the experimental setup shown in Figure 4 shows initial and final flap positions along with distance to the wall non-dimensionalized by the flap length. This entire setup was installed in a tank of water, which was placed on mounting legs to allow optical access from beneath.

Particle flow visualizations and ensemble-averaged laser Doppler Velocimetry (LDV) measurements are taken at the centerline of the flaps. For these LDV measurements the fiber-optic-based system is used. The probe is mounted on a two-dimensional traverse allowing for a plane of the flow field to be reconstructed. The ensemble averaging procedure requires a set of time records to be taken at each point of interest in the flowfield. This set of time records is then averaged to produce a single

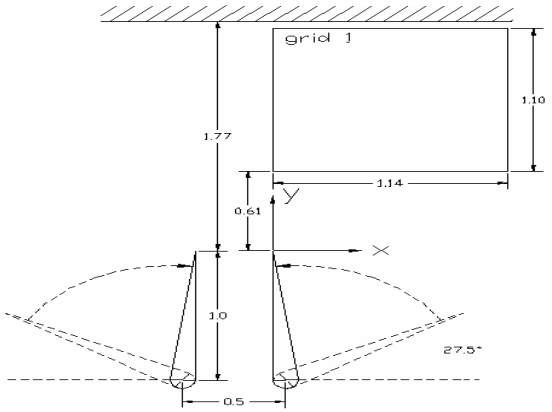

Figure 4. Top schematic of flaps and data acquisition grid 1

time record for each point of the flow field. As the flap motions trigger each of these time records, a two-dimensional grid of the time developing flow field can be generated. As the ensemble averaging procedure calculates a mean or average time record, velocity fluctuations for each time record in the data set can also be calculated. Although these quantities were not calculated for this setup they will prove to be useful for subsequent vortex interaction setups.

Particle flow visualizations revealed that for flap pitch rates less than 2 rad/sec the vortex trajectory closely resembles the parabolic nature of the inviscid analysis. For higher pitch rates both vortex rebound and meandering can be observed. Three planes of LDV measurements are acquired, each measuring a grid located further along the wall. One of the measurement grids taken is shown in Figure 4. Additional planes were necessary, as the initial effort did not capture separation at the wall, which subsequently rolls up into a secondary vortex.

A sample velocity vector plot can be seen in Figure 5. This plot corresponds to a flap pitch rate of $\omega = 2.36$ rad/sec. From these velocity vector plots streamlines

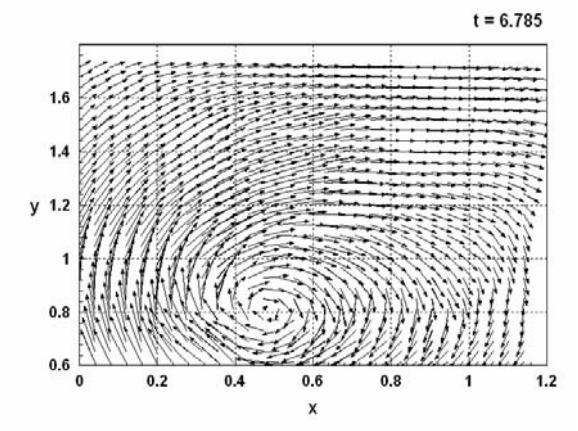

Figure 5. Velocity Vectors, ω = 2.356 rad/sec, t = 6.785

calculated by allowing massless particles to propagate through the flowfield. A sample streamline plot can be seen in Figure 6, which corresponds to velocity vector plot in Figure 5. Vorticity has also been calculated for this flowfield and a sample plot corresponding to the two previous plots is shown in Figure 7.

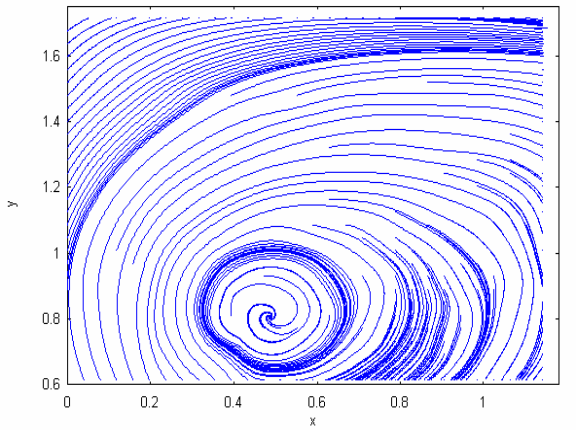

Figure 6. Instantaneous streamlines ω = 2.356 rad/sec, t = 6.785

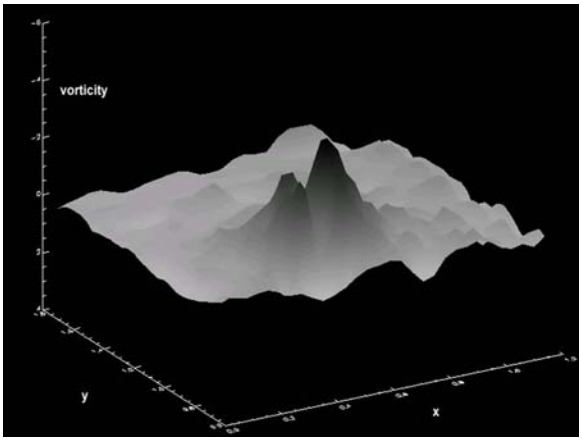

Figure 7. Vorticity Surfaces ω = 2.356 rad/sec, t = 6.785

The Interaction of Rolling Vortices with a Turbulent Boundary Layer

Measurements were conducted in the 1'x1' water tunnel on vortex/turbulent boundary layer interactions. These data sets provide a reference for subsequent measurements in which a free surface was introduced to the problem.

A turbulent boundary layer was allowed to develop on a flat plate installed in the test section of the original ESM water tunnel. An articulated fence 60 cm from the leading edge pitches out of a cavity in the plate to generate a vortex. As the fence is lowered into the cavity the vortical structure is swept downstream and allowed to interact with the turbulent boundary layer. A schematic of this setup can be seen in Figure 8. Three fences were used with chordlengths equal to 12.7, 25.4, and 38.1 mm. Using different fence sizes allowed for the development of vortical structures which were on the order of, twice, and three times the thickness of the boundary layer. A DC motor connected was connected to the fence via a four bar linkage system and controlled by the

computer. The angular position of the fence was monitored with a optical encoder mounted in front of an angular display.

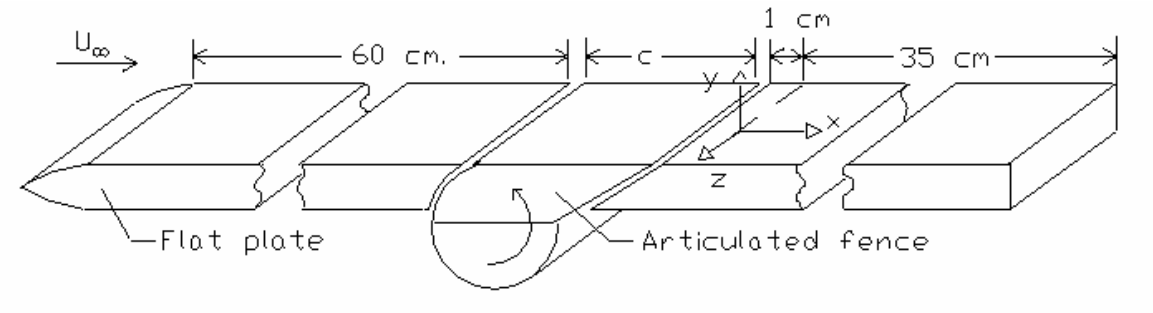

Figure 8. Schematic of Experimental Setup for Vortex Flat Plate Boundary Layer Interactions

The component-based LDV system was first used to verify presence of a turbulent boundary layer by comparing with known data. The boundary layer was allowed to naturally transition to a turbulent state. In hindsight the boundary layer should have been tripped to fix the transition location and avoid any effect this fluctuation made have had on the measurement domain. The LDV system was then used to take velocity field measurements at the centerline of the plate. The mirror delivery system and focusing lens were mounted on a traversing table and vertical traversing scale to allow the measurement volume to be moved through a two-dimensional grid. Again, the motion of the fence triggers velocity measurements so that an ensemble averaging procedure may be used. This procedure allowed for both calculations of mean velocity time records and their fluctuating components. The fluctuating components of the velocity were then used to calculate a two-dimensional time history of the turbulent kinetic energy.

Preliminary attempts were made at flow visualization with a gravity fed dye injection system. To obtain any useful images, the flow speed had to be reduced until the boundary layer became laminar. The dye injection port was located in the articulated fence. A few instantaneous frames of the visualization can be seen in Figure 9. The vortex is observed to roll up behind the fence. As the fence returns into the cavity, the vortex propagates downstream. Within three chordlengths downstream the dye begins to diffuse.

A sample plot of velocity vectors with color vorticity contours is shown in Figure 10. These data are for the 12.7 mm fence which generates a vortical structure approximately the same size as the boundary layer. This vortex is seen to quickly disintegrate without significant changes to the turbulence levels in the boundary layer. A plot of the two-dimensional turbulent kinetic energy is shown in Figure 11. This plot is for the 38.1 mm fence which generates a vortical structure three times as large as the boundary layer. A significant increase of two-dimensional turbulent kinetic energy is observed for this case.

Fig. 5. Flow visualization of vortex interaction

Figure 9. Flow visualization of boundary layer vortex interaction

Analysis of this entire data set may lead to understanding of one of the vorticity transport mechanisms within the boundary layer. Turbulent structures from within the boundary layer can be picked up by this vortical structure and deposited downstream, perhaps even deeper into the boundary layer, resulting in additional mixing. The presence of his large vortical structure could also lead to increased turbulence levels due to free-stream energy being fed into the boundary layer.

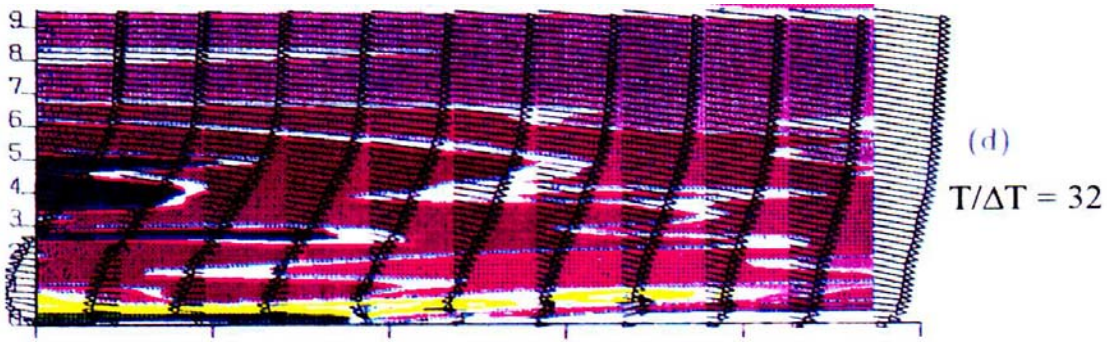

Figure 10. Velocity vectors superimposed over vorticity contours for fence size c = 12.7 mm, non-dimensional time T/ΔT = 32.

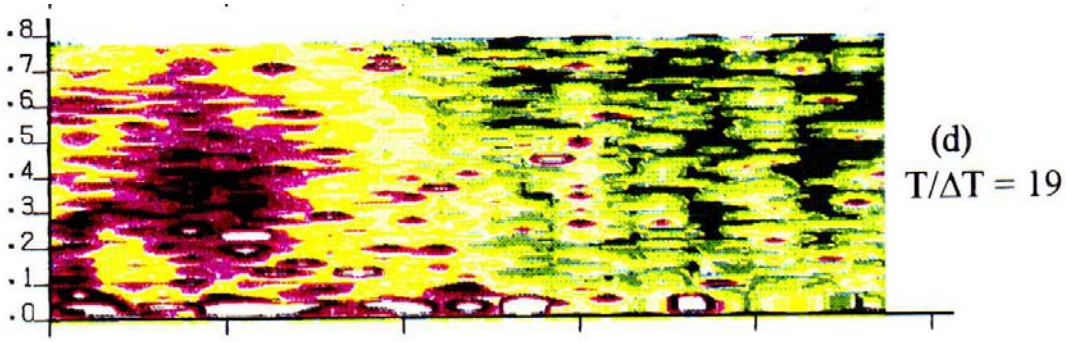

Figure 11. Two-dimensional Turbulent Kinetic Energy Contours for fence size c = 38.1 mm, non-dimensional time T/ ΔT = 19.

The Interaction of a Spanwise Vortex, Free Shear Layer, and a Free Surface

A flat plate was installed in the test section parallel to the freestream and piercing, or normal to the free surface, as shown in Figure 12. At the downstream edge of the plate a flap is attached to a cylindrical rod, which in turn is attached to a stepping motor.

With this setup the flap can be quickly rotated out into the developed boundary layer to generate a vortex with its axis normal to the free surface. The flap is slowly

returned in order to avoid any additional disturbances. The vortex is swept downstream, and interacts with the free shear layer emanating from the plate and the free surface. In order not to generate unwanted free surface disturbances, the span of the flap is 0.75 inches below the free surface. The edge vortex generated by the motion of the flap quickly reconnects with the free surface.

Video taken of the vortex propagating downstream shows that a free surface depression develops within three flap lengths downstream of the plate. This depression grows to a maximum before decaying. This entire process takes approximately 15 flap lengths downstream from the edge of the surface piercing plate.

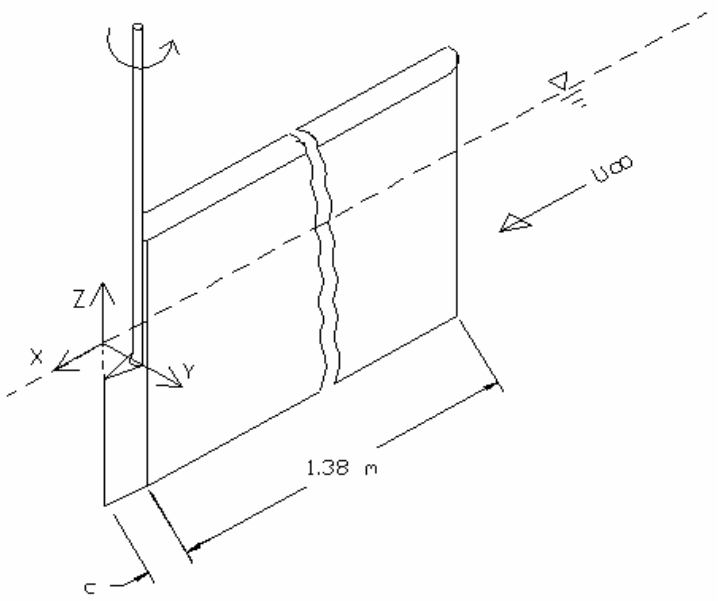

Figure 12. Schematic of Trailing Edge Vortex Experimental Setup

An LDV analysis of this vortex reconnection was performed using the component based LDV system. Lines of LDV data were collected at five downstream locations,

labeled x = 2C, 4C, 6C, 8C, and 10C, (C, chordlength of the flap = 1.5 inches) and shown in Figure 13, and five distinct elevations below the free surface. Lines instead of grids of data were acquired for this setup as an attempt was made to retake these measurements from the side of the water tunnel. By acquiring two-dimensional velocity data from both the bottom of the water tunnel and the side a three dimensional velocity vector can be reconstructed. Precise placement and traversing of the measurement volume are required for this approach to be successful.

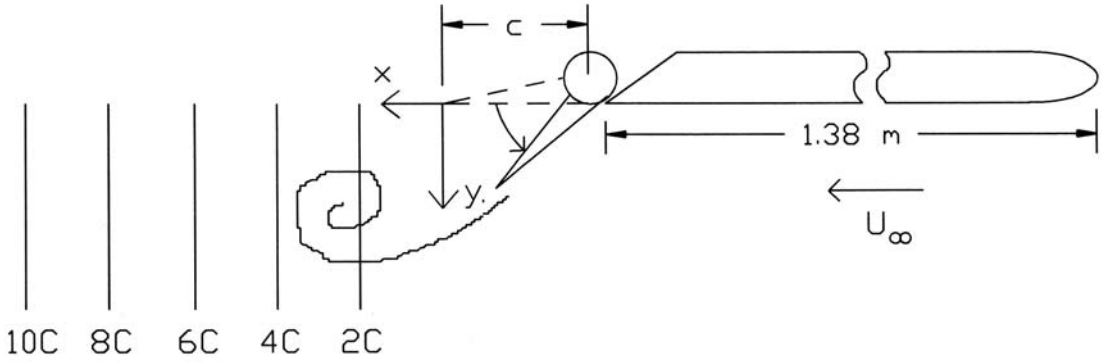

Figure 13. Top View of Experimental Setup with Data Acquisition Locations Labeled

Again data is ensemble averaged for multiple motions of the flap in order to measure mean time dependent velocities as well as fluctuating components. As several ensembles were being discarded during the data acquisition or averaging process it was decided to add additional validation to the data acquisition process. A translucent screen was positioned over the area of maximum free surface depression. A parallel light source beneath the tunnel projected an image of the depression and accompanying free surface disturbances onto the screen. At the same time velocity data acquisition was occurring

this image was captured and digitized by a frame grabber. A threshold was then applied to this gray-scale image leaving any significant free surface disturbances as black and everything else white. A centroid is then calculated from the black areas. Any black area not connected to the area containing the centroid is eliminated from the calculation and the centroid is recalculated. This iterative process determined the centroid of the image of the vortex depression. See Figure 14 for a sample of the images from this iterative process. Comparison of this centroid location to a predetermined average location allowed for additional validation of each time record acquired. The addition of this process eliminated any ensembles of the motion from being discarded.

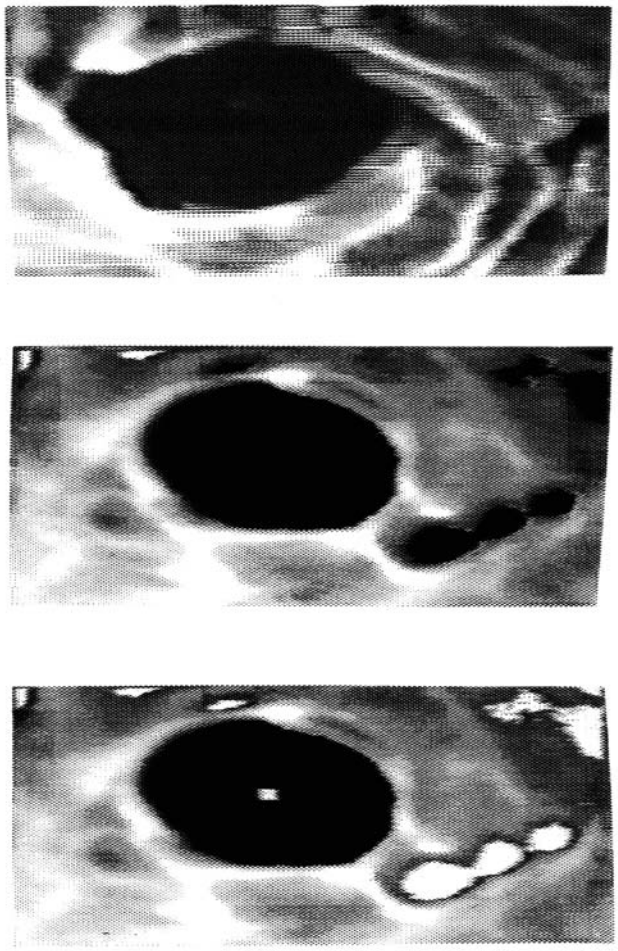

Figure 14. Shadowgraph Image of Vortex Location with Image Processing to determine Centroid Location

A schematic of the entire experimental setup is shown in Figure 16. This schematic gives the reader a better understanding of the location of the shadowgraph screen and LDV system beneath the test section measuring two components of velocity parallel to the free surface.

A plot of velocity vector data for three different elevations is shown in Figure 15. Two dimensional velocity fields are produced from single lines of data by first subtracting the freestream value of velocity. This creates a vector field which is more descriptive of the vortical motion and more clearly indicates the position of the vortex core. Then plotting consecutive instants of time records along a spatial axis. This representation is only accurate if there is not a significant alteration of the vortex. This assumption is not valid for the interaction of a vortex with a free shear layer but is still used here in order to gain insight into the flow-field. Data presented in this serves to allow the reader to visualize temporal variation of the velocity vectors where the horizontal axis is time increasing from right to left.

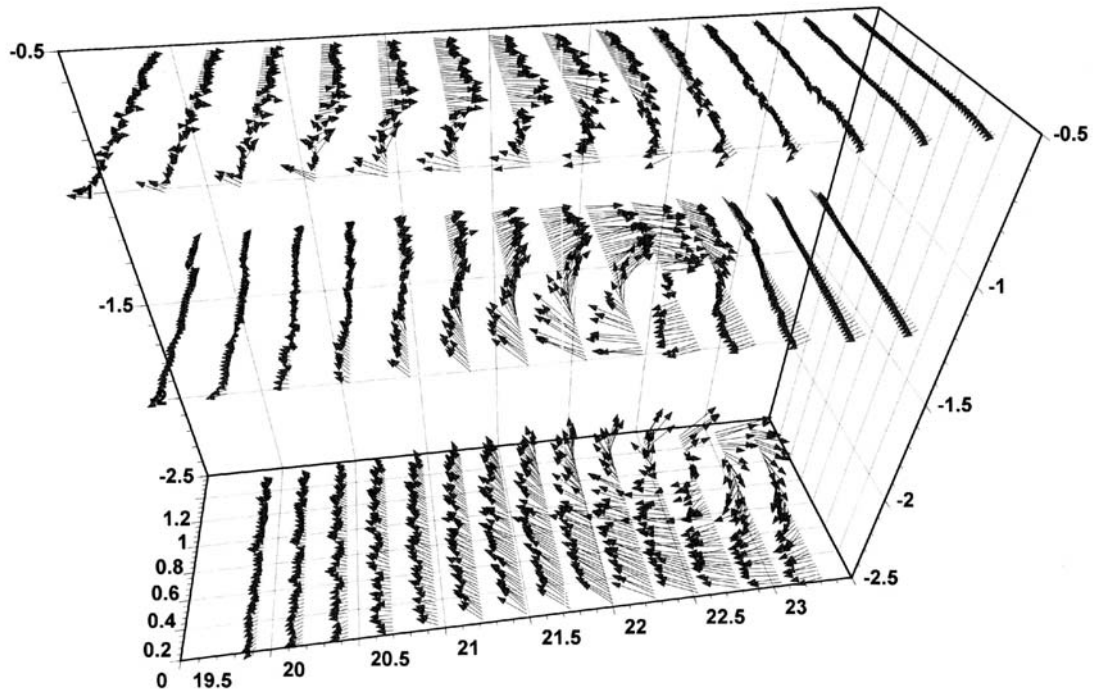

Figure 15. Three dimensional representation of trailing edge vortex, 2-D vector fields produced by propagating lines of data in time.

RMS values of the fluctuations of the velocity components were also recorded. These results could be the effect of the large surface depressions generated by the vortex reconnection changing the effect of the free surface or the depth of the free surface layer. Further investigation of these results will be necessary to explain these results.

Velocity measurements were taken using two different two-component laser Doppler velocimetry systems (LDV) and a particle image velocimetry (PIV) system. Both of these methods use optical means to measure the velocity of tracer particles suspended in the fluid. It is the non-intrusive nature of these techniques which is of importance to this study. A mechanical measurement probe in the flow could disturb the development of the vortical structures we are attempting to measure. A brief description of the measurement systems, the water tunnel facilities used, and the experimental setups investigated is provided here.

Instrumentation and Experimental Techniques

Component-based laser Doppler velocimetry system

The first of two laser Doppler velocimetry systems used in this study is a component-based, mirror delivered system. A 60 mW He-Ne laser with a wavelength, λ = 632.8 nm, is used as the light source. The system consists of an optics train which includes a beam collimator, two polarization axis rotators, a pair of prism-type beam splitters, two Bragg cells, beam steering wedges, a single photodetector, and a beam expansion unit with a 2.27 expansion ratio. The optics train splits the single input beam

into three separate beams of equal intensity, same polarity, but shifted in frequency by the Bragg cells. A schematic sketch of the components is shown in Figure 16.

The system can measure two components of velocity by sharing one of the beams to generate two distinct fringe patterns. The three laser beams are delivered to the test section via a pair of optical mirrors ($\lambda/20$) and focused into a measurement volume by a 250 mm f/4 lens. The mirrors and focusing lens are mounted on an automated, two-dimensional traversing mechanism. This setup allowed for the automated measurements of two-dimensional grids at the centerline of the water tunnel test section. As only a single photodetector is used in this system the frequency shifting allows for electronic down mixing of the two measured frequency (velocity) signals. This now down-mixed or separated frequency signal, which is proportional to the velocity, is provided to two TSI frequency counters. The frequency counters report a voltage proportional to the frequency of the input signal. Silicon carbide seeding particles (TSI Model 10081) were used as tracer particles. These particles have an irregular shape with a mean diameter of 1.5 μm, a density of 3.2 g/cm^3, and a refractive index of 2.65. In addition to this system two TSI frequency counters were used to measure the now down-mixed or separated frequency signal from the photodetector.

Fiber-Optic Based laser Doppler velocimetry system

The second of the two laser Doppler velocimetry systems used in this research is also a component-based system but differs in that the laser beams are delivered to the test section with a fiber-optic probe. Focusing of the beams into a measurement volume is

done with a 100 mm-focusing lens, which is part of the probe. This short focal length limits the usefulness of this probe in the larger water tunnel facility. However, the fiber-optic delivery system provides for much greater flexibility in placing and traversing the measurement volume. A 3.5 W Argon Ion laser is used as the light source for this system. The additional power is necessary for this system as the beam is split into two colors, blue and green. Also, significant power losses can occur when the beams are coupled with their fibers. This system uses 4 beams, 2 different colored pairs to measure two components of velocity. Color filters and two photo-detectors measure the back-scattered light from the measurement volume. The same TSI frequency counters and seeding particles as above are used with this system.

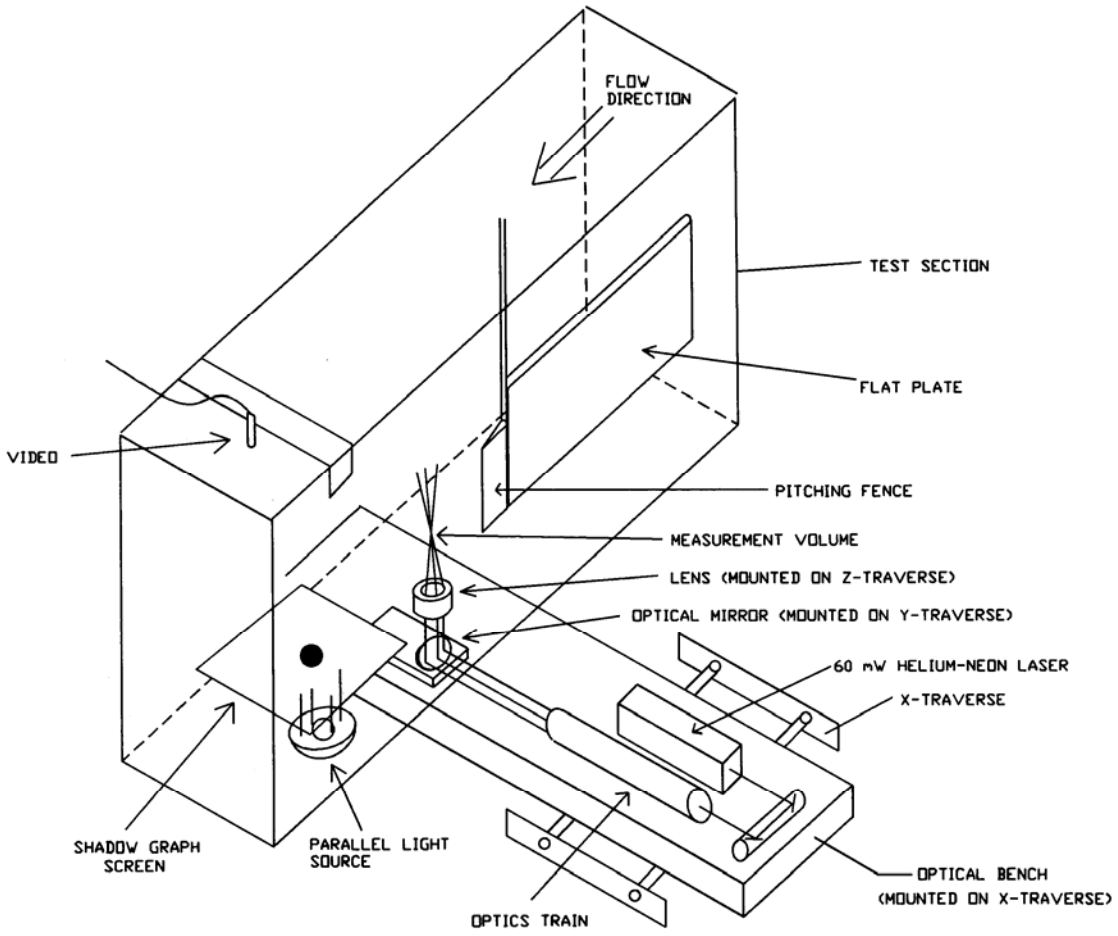

Figure 16. Schematic of laser Doppler velocimetry system and shadow-graph validation

LDV Signal Processing

Both down-mixed signals resulting from the original photomultiplier signal are sent to two TSI counters, Models 1980 and 1990. Signal processing by the counters was performed in non-coincidence 8-cycle mode. This mode required that a particle traverse at least eight fringes of the measurement volume (of the 16 possible) to be validated. The counters have a voltage output which is proportional to the measured frequency. The

constant of proportionality is a function of the panel settings on the counters. Both counter output voltages are connected to the PC-based data acquisition system.

Typically, LDV seeding must be added to the flow in order to achieve appropriate data rates. For the present research, silicon carbide seeding was used. Silicon carbide has a density of 3.2 g/cm^3, a refractive index of 2.65 and a mean diameter of 1.5 μm. Some settling of the seeding occurred, so reseeding of the water tunnel was carried out about every twelve hours, or when the data rate decreased to a point such that reseeding was necessary. Since each set of data took approximately twenty-four hours to acquire, at least one reseeding took place during acquisition of each dataset. The seeding was performed at a location downstream of the model as the model was resetting to the initial position, thus minimizing the effect on the experiment.

Table 1 Laser Beam and Measurement Volume Specifications for the TSI LDV System Employed in the ESM Water Tunnel

Effective Beam Diameter – $D_{e^{-2}}$ Exiting Laser: 1.25 ± 0.1 mm After Beam Expander: 2.838 mm	Lens 1: 250 mm Focal Length, Used from Bottom of Tunnel	Lens 2: 350 mm Focal Length, Used from Side of Tunnel
Convergence Half-Angle, κ	**4.05°**	**2.89°**
Fringe Spacing, $d_f = \frac{\lambda}{2 \cdot \sin\kappa}$	**4.45 μm**	**6.273 μm**
$d_{e^{-2}} = \frac{4\lambda f}{\pi D_{e^{-2}}}$ (f = lens focal length)	**71.0 μm**	**99.4 μm**

Measurement Volume Diameter, $d_m = \frac{d_{e^{-2}}}{\cos\kappa}$	**71.2 μm**	**99.5 μm**
Measurement Volume Length, $l_m = \frac{d_{e^{-2}}}{\sin\kappa}$	**1.006 mm**	**1.970 mm**
Number of Fringes	**16**	**16**

The laser and optics train are mounted on an optical bench, which is in turn mounted on a large traversing mechanism, allowing motion parallel to the axis of the test section. On the optical bench are mounted mirrors and the focusing lens needed to direct the beams emanating from the beam expander into the test section. One mirror is mounted on another traverse which allows for horizontal motion perpendicular to the axis of the test section. A third traverse rides on the y-traverse, and carries the focusing lens (plus an additional mirror if the alignment of the system is from the side of the test section). This latter traverse allows vertical motion perpendicular to the test section axis. All of these traverses are driven by stepping motors. Position feedback from each traverse is provided by a Linear Variable Differential Transducer (LVDT). The accuracy of the LVDT's and the resolution of the stepping motor/lead screw combinations result in the location of the measurement volume being known accurately to 0.06 mm (60 μm), much less than the length of the measurement volume.

Uncertainty Analysis for the Velocity Measured with the LDV System

The velocity that corresponds to the frequency output from the LDV data acquisition system may be found from

$$V = f\frac{\lambda}{2\cdot\sin\kappa} \qquad (1.1)$$

where f is the measured Doppler frequency, λ is the wavelength of the laser light and κ is the half-angle of the two incident beams that generate the measurement volume. For a He-Ne laser, the wavelength of the coherent light is 632.8 nm. Kline & McKlintock [1954] presented a method for error propagation in calculated quantities. This method is now generally accepted by scientists and engineers as the most appropriate way to propagate error through calculated quantities. If there are n measured quantities x_1, x_2…, x_n with errors δx_1, δx_2…, δx_n then the error associated with a function of these quantities, $y(x_1, x_2,\ldots, x_n)$ is given by

$$\delta y = \left\{ \left[\left(\frac{\partial y}{\partial x_1} \right) \delta x_1 \right]^2 + \left[\left(\frac{\partial y}{\partial x_{21}} \right) \delta x_2 \right]^2 + \ldots + \left[\left(\frac{\partial y}{\partial x_n} \right) \delta x_n \right]^2 \right\}^{\frac{1}{2}} \qquad (1.2)$$

Applying this method to equation 1.1, and assuming that the error in the known wavelength is negligible, we find that

$$\delta V = \left\{ \left[\left(\frac{\lambda}{2 \cdot \sin\kappa} \right) \delta f \right]^2 + \left[\left(-\frac{f\lambda\cos\kappa}{2 \cdot \sin^2\kappa} \right) \delta\kappa \right]^2 \right\}^{\frac{1}{2}} = \left\{ \left[\frac{V}{f} \delta f \right]^2 + \left[\frac{V}{\tan\kappa} \delta\kappa \right]^2 \right\}^{\frac{1}{2}} \qquad (1.3)$$

The uncertainty in the frequency measurement is due to the combination of errors arising from the TSI counters and the data acquisition system. Wilder [1992] determined that the worst-case uncertainty in the frequency measurement due to this system is $\delta f = 0.01 f$. The velocity is calculated based on the focal length of the lens and the beam spacing.

The alignment mask used with the TSI system allows the beams to be located accurately within one-half beam diameter (1.42 mm) of the correct location. This difference, when considered in combination with the focal length of the lenses, results in an error of $\delta\kappa = 0.229° = 0.057\kappa$ for the 250 mm focal-length lens, and $\delta\kappa = 0.164° = 0.057\kappa$ for the 350 mm focal-length lens. Substituting the values for $\delta\kappa$ and δf into equation 2.3, it is found that the uncertainty in the measured velocity for both the 250 mm focal-length and the 350 mm focal-length lenses are essentially equal at $\delta V = 0.058V$.

Particle Image Velocimetry system

The final velocity measurement technique used in this study is a particle image velocimetry system (PIV). A particle image velocimetry system consists of a laser sheet and an image-recording device. Two consecutive images taken of a seeded flow field illuminated with the laser sheet apart can be processed to return the velocity field, if the time between the two instances is known.

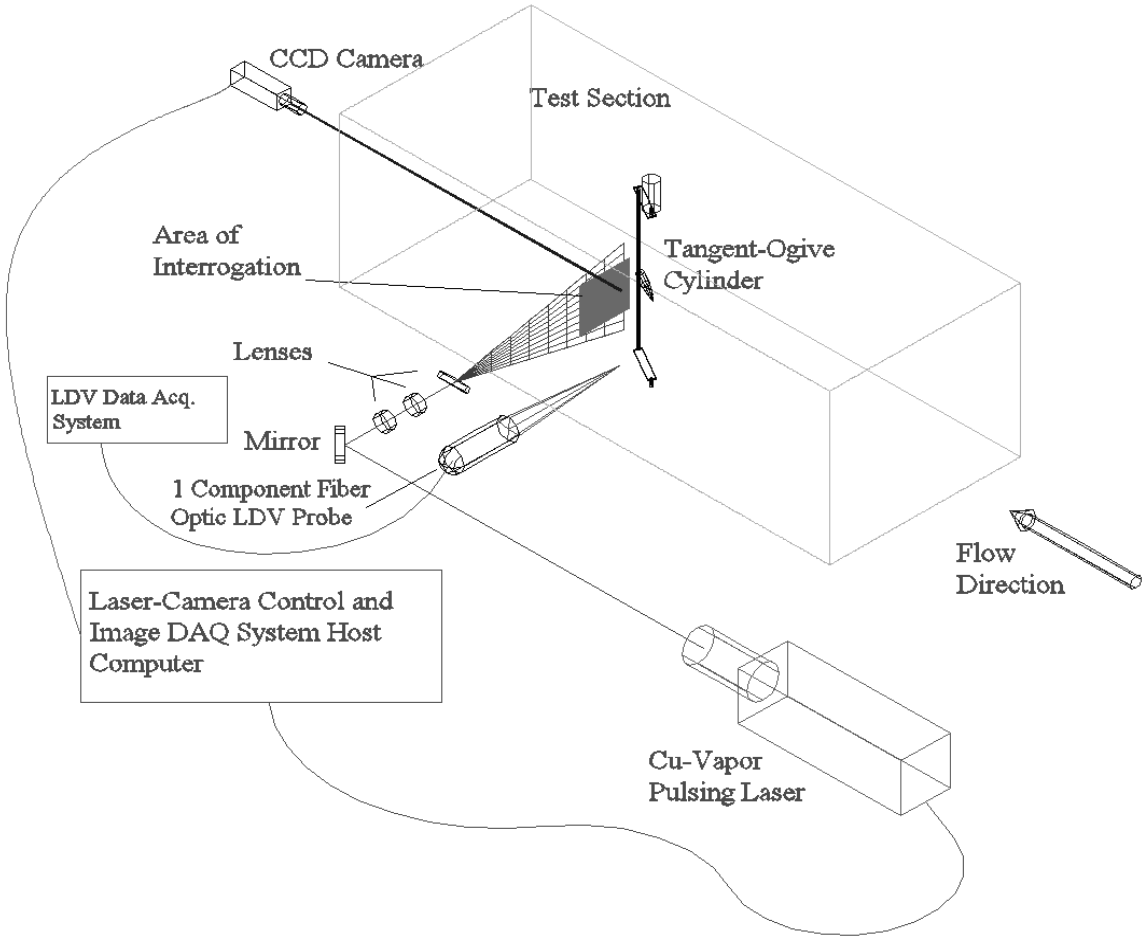

Figure 17. PIV Setup in the ESM Water Tunnel.

A schematic sketch of the PIV system is shown in Figure 17. The light source used for this system is a 45 W pulsed copper vapor laser (ACL45), delivering 5-7 mJ/pulse, purchased from Oxford Lasers. Two optical mirrors specially coated for the wavelength of the copper vapor laser are used to steer the beam towards the sheet forming optics. The specially coated optical mirrors were purchased for the beam delivery system when it was determined that the laser sheet had insufficient power to illuminate the seeding particles. The sheet forming optics consists of two achromatic, or bonded focusing lenses and a cylindrical lens. The focal lengths of the focusing lens are f

= 500 mm and 25 mm, with diameters of 50 mm and 25 mm respectively. Achromatic lenses are used due to the high energy density of the focused laser beam. By placing the focusing lenses a distance apart equal to the sum of their focal lengths a columnar laser beam with a 20:1 reduction of the original 45 mm beam diameter is produced. The positions of the focusing lenses are sometimes adjusted to generate a thinner laser sheet at the area of interest. This method should only be used when the measurement domain is small so that the effect of divergence or change in thickness of the laser sheet is minimal. The last component of the beam forming optics is a cylindrical lens. Several lenses each with different divergence angles are being used in this research.

The image recording device in this system is a high-speed CCD digital video camera. The CCD array has a resolution of 256x256 pixels and the camera has an adjustable frame rate up to 1000 Hz. The use of a digital video camera allows this system to record time-developing flow fields. Image acquisition and laser pulsing are synchronized using a timing card constructed for this purpose. A commercial PIV analysis package, Visiflow, is used to batch process the acquired sequence of images into a velocity field. This package also allows for calculation of vorticity and streamlines in the flowfield.

Uncertainty Analysis for Velocities Measured with PIV

The present DPIV system implementation is limited to the investigation of low-speed liquid flows. This limitation results from two hardware considerations. The minimum possible time interval between two consecutive frames is 1 ms while the

moderate pixel resolution of the digital camera limits the maximum field of view. Because of the desired number of independent velocity vectors per frame (32 in each direction), the maximum in-plane displacement between two consecutive frames is constrained to 8 pixels or less. The uncertainty of the velocity estimation can be quantified as:

$$\left(\frac{\sigma_u}{u^2}\right)^2 = \left(\frac{\sigma_{\Delta X}}{\Delta X^2}\right)^2 + \left(\frac{\sigma_{dt}}{dt^2}\right)^2 \qquad (1.4)$$

Where σ denotes the uncertainty of the subscripted quantity. For such low velocities and by using a digital interrogation procedure the uncertainty σ_{dt} is negligible. Thus the only error source will be introduced by the displacement estimation. Assuming a typical particle image diameter of 2 pixels in order to optimize the correlation peak detection algorithm, the uncertainty of the velocity estimation is on the order of 1% of the maximum resolvable velocity.

The uncertainty in the average fluctuations in the velocity components can be determined by using the fact that the statistical uncertainty of the estimation of a fluctuating quantity is inversely proportional to the square root of the number of samples used. Therefore, for a typical experiment with 2000 time records, the uncertainty of the estimation of U_{rms} or V_{rms} is on the order of 2% of the mean value. However, in the case of the in plane turbulent kinetic energy one has to consider the fact that there is no contribution to the estimation of the third velocity component.

Flow Visualization Techniques

A variety of flow visualization techniques and devices have been constructed and used during this research effort. These techniques have included a gravity fed dye injection system, hydrogen bubble visualizations using laser sheets, and particle flow visualizations.

Facilities:

Facilities used in this research include two water tunnels which were both located in the Engineering Science and Mechanics Fluids Lab. The original facility was built in 1976 by the Engineering Science and Mechanics Department with the support of the Army Research Office. This tunnel is a 570- gallon closed-circuit facility with the return located above the test section thereby pressurizing the test section. The settling chamber has a 6:1 two-dimensional contraction ratio and contains, flow straighteners, screens and honeycombs and a set of guide vanes in the divergence to the settling chamber to improve flow quality. A centrifugal pump powered by a 2 h.p., variable-speed DC motor provided free-stream velocities in the test section from 45 cm/s to 1.5 m/sec. Lower velocities, down to 10 cm/s could be obtained by closing a butterfly valve upstream of the pump. Measurements taken in the test section during testing showed upstream turbulence levels to be approximately 1%. These values were very much dependent on the cleanliness of the water in the facility. The test section in this facility consisted of a removable plexiglass box 2 feet in length and 1 foot square. All measurements taken in the facility were taken with the model surface at the centerline of the tunnel.

The original facility was replaced in 1995 with a larger water tunnel purchased from Engineering Laboratory Design. This water tunnel is shown in Figure 18. The facility is fabricated of fiberglass-reinforced plastic and clear acrylic plexiglass is used for the test section and downstream viewing window. The return in this facility is below the test section, allowing it to be run with a free surface. The larger facility when completely filled contains 1500 gallons of water and can be run at freestream speeds from 10 cm/s to 1 m/s. The flow is driven by a 4500 GPM, 20 HP axial flow pump. The settling chamber contains a set of screens each with a finer mesh for turbulence reduction and flow straightening and is followed by a three-dimensional contraction with a 6:1 ratio. The test section is 6 feet in length and 2 feet square. Testing performed initially showed turbulence levels to be a maximum of 4%. The impeller was then replaced due to the fact that it was cavitating at higher speeds. Subsequent testing of turbulence levels in the test section indicated that the turbulence level was reduced to below 1%. A variety of experimental setups have been tested in this tunnel and some will be discussed in the main body of the dissertation or in the appendices.

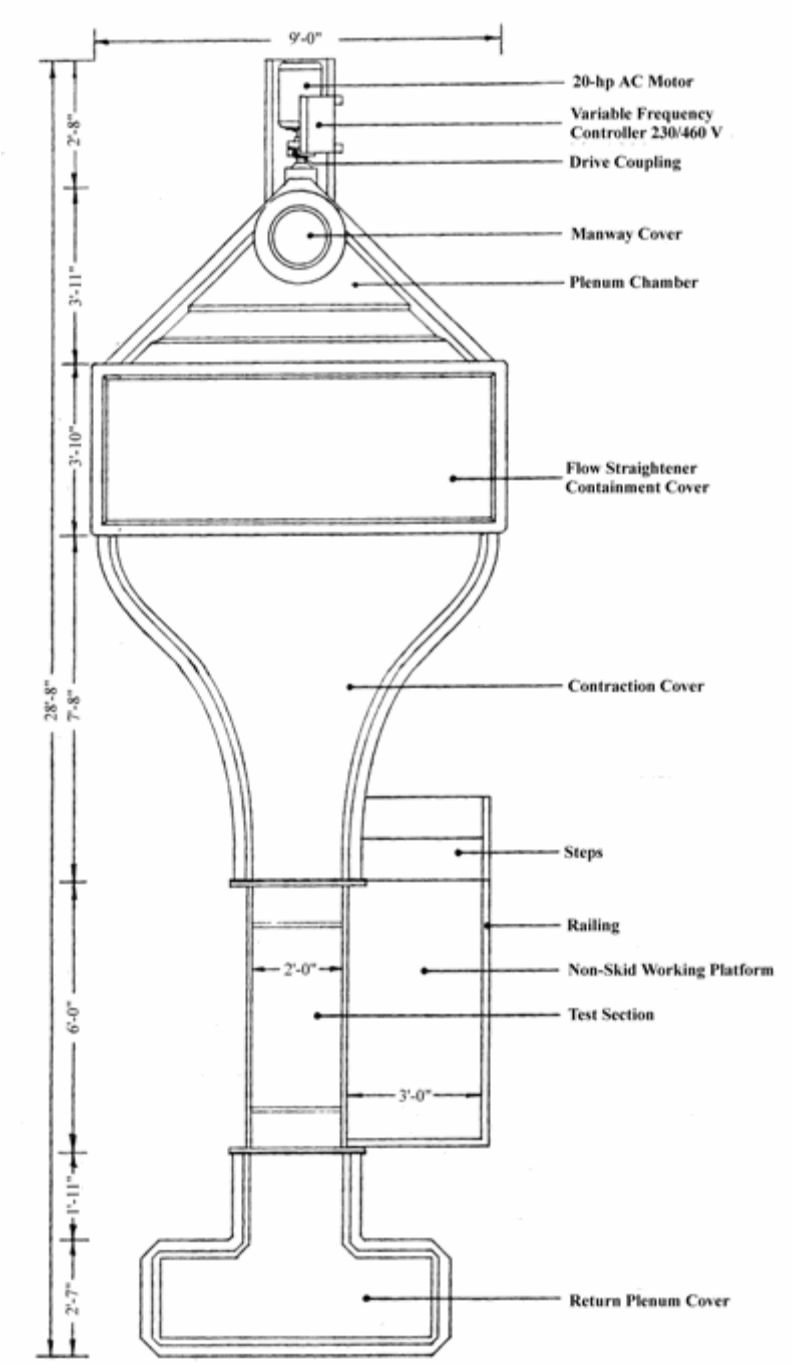

Figure 18. The Engineering Science and Mechanics Fluid Mechanics Laboratory water tunnel.

Structure of this Dissertation

This dissertation is based on three papers with the author of the dissertation as a first author. The topic of these papers is essentially the topic of the dissertation. Each is concerned with different aspects of the interaction of coherent vortices generated by moving sharp edges. In Chapter 2 we present the interaction of two such vortices that approach a solid surface in a direction normal to it. They then turn and follow trajectories parallel to the wall. But in this case there is no mean flow, and therefore no significant boundary layer. In the following two chapters we examine the interaction of vortices with developed boundary layers, with thickness the order of magnitude of the diameter of the core of the vortex. In Chapter 3, we study the interaction of vortices with a wall boundary layer, and in Chapter 4, we present data for vortices that are released in the wake of a flat plate. This is essentially the interaction of a coherent vortex with a free shear layer. In the latter chapter we also examine the effects of a free surface.

Chapter 2, A Vortex Pair Impinging on a Solid Boundary, was originally included in the proceedings of the AIAA annual winter meeting held in Reno, NV, 1998.

Donnelly, M J.., Vlachos, P., and Telionis, D. P., "A Vortex Pair Impinging on a Solid Boundary," *AIAA Aerospace Sciences Meeting*, Reno, Nevada, AIAA Paper No. 98-0673.

Chapter 3, The Interaction of Rolling Vortices with a Turbulent Boundary Layer, was published in the Journal of Fluids Engineering, December 1995.

Donnelly, M.J., Rediniotis, O.K., Ragab, S.A., Telionis D.P., "The Interaction of Rolling Vortices with a Trubulent Boundary Layer," Journal of Fluids Engineering, Volume 117, Number 4, pp 564-570, December 1995.

Chapter 4, The Three-Dimensional Character of the Interaction of Large Rollers with a Free Surface, was original presented at an ASME summer meeting and later published as part of the ASME Fluids Engineering Division proceedings.

Donnelly, M. J., Rediniotis, O. K., and Telionis, D. P., "The Three-Dimensional Character of the Interaction of Large Rollers with a Free Surface," *ASME Fluids Engineering Division*, FED-vol. 217, pp. 191-198, 1995

During his years at VA Tech, the author of this dissertation has worked on many other projects. His collaboration with other members of the fluid mechanics laboratory has resulted in many other publications. He has thus co-authored another six papers. All nine of these papers are listed in Appendix A. All these papers have been presented at various conferences. One of these papers has appeared in the ASME Journal of Fluids Engineering. Another two have been submitted for publications in archival journals.

On one of these papers which are not included in the main body of the dissertation, the author was the first author. But the topic was not directly linked to the dissertation, and thus was omitted from the present document. In the other four papers, the present author has made contributions that are outlined in the Appendices, but his name did not appear as a first author. Three of these papers with content closely linked to the topic of this dissertation are included in the Appendices.

References

Ash, R., and Zheng, Z., "Cross Wind Effects on Turbulent Aircraft Wake Vortices Near the Ground," AIAA Paper 94-2381, June 1994.

Banerjee, S. "Upwellings, Downdrafts, and Whirlpools: Dominant Structures in Free Surface Turbulence," *Applied Mechanics Review*, Volume 47, No. 6, Part 2, June (1994).

Barker, S. and Crow, S., "The Motion of Two-Dimensional Vortex Pairs in a Ground Effect," Journal of Fluid Mechanics, Vol. 82, No. 4, 1977, pp. 659-671.

Bernal, L.P., Hirsa, A., Kwon, J.T., and Willmarth, W.W. "On the Interaction of Vortex Rings and Pairs with a Free Surfacefor Varying Amounts of Surface Active Agent," *Physics of Fluids*, Volume 1, No. 12, (1989), pp. 2001-2004.

Bernal, L.P., and Scherer, J. "Free-Surface Turbulent Flows," AIAA Paper No. 97-1111.

Ciffone, D.L., and Pedley, B., "Measured Wake-Vortex Characteristics of Aircraft in Ground Effect,' AIAA Paper 78-109. Huntsville, AL, Jan 16-18, 1978.

Corjon, A., and Poinsot, T., "Behavior of Wake Vortices Near Ground," AIAA Journal, Vol. 35, No. 5, 1997, pp. 849-855.

Cutler, A., and Bradshaw, P. "Vortex/Boundary Layer Interactions," AIAA Paper No. 89-0083.

Dabiri, Dana, "On the Interaction of a Vertical Shear Layer with a free surface," Journal of Fluid Mechanics, vol. 480, pp. 217-232, (2003).

Dee, F., and Nicholas, O., "Flight Measurements of Wing Tip Vortex Motion Near the Ground," Royal Aircraft Establishment, TR 68007, London, 1968.

Doligalski, T., Smith, C., and Walker, J., "Vortex Interactions with Walls," Annual Review of Fluid Mechanics, Vol. 26, 1994, pp. 573-616.

Dommermuth, D.G., and Mui, R.C.Y. "Numerical Simulation of Free-Surface Turbulence," *Applied Mechanics Review*, Volume 47, No. 6, Part 2, June (1994).

Dommeruth, D.G., and Yue, D.K.P. "A Numerical Study of Three-Dimensional Viscous Interactions of Vortices with a Free Surface," *Proceedings of the Eighteenth Symposium on Naval Hydrodynamics*, Ann Arbor, Michigan, (1990).

Dooley, B.S., "Stereo Digital Particle Image Velocimetry Investigation of a Free Surface Mixing Layer," Ph.D. Dissertation, California Institute of Technology, (2005).

Esmaili, H., and Piomelli, U. "Large-Eddy Simulation of Turbulent Boundary Layers with Embedded Streamwise Vortices," AIAA Paper No. 92-0552.

Feyedelem, M.S., and Sarpkaya, T. "Free and Near-Free-Surface Swirling Turbulent Jets," AIAA Paper No. 97-0438.

Gharib, M. "Some Aspects of Near-Surface Vortices," *Applied Mechanics Review*, Volume 47, No. 6, Part 2, June (1994).

Gharib, M., Dabiri, D., and Zhang, X. "Interaction of Small-Scale Turbulence with a Free Surface," FED-Volume 181, Free-Surface Turbulence, ASME (1994).

Gharib, M., and Weigand, A. "Experimental Studies of Vortex Disconnection and Connection at a Free Surface," *Journal of Fluid Mechanics,* Volume 321 (1996), pp. 59-86.

Gharib, M., Weigand, A., Willert, C., and Liepmann, D., "Experimental Studies of Vortex Reconnection to a Free Surface: A Physical Flow Model," *Proceedings of the Nineteenth Symposium on Naval Hydrodynamics*, Seoul, Korea , August (1992).

Harvey, J., and Perry, F., "Flowfield Produced by Trailing Vortices in the Vicinity of the Ground," AIAA Journal, Vol. 9, No. 8, 1971, pp. 1659, 1660.

Kothmann, B.D., and Pauley, W.R. "Interaction of Unsteady, Turbulent, Vortical Structures with a Turbulent Boundary Layer," AIAA Paper No. 92-0060.

Liepmann, D., and Gharib, M. "The Vorticity and Entrainment Dynamics of Near-Surface Jets," FED-Volume 181, Free-Surface Turbulence, ASME (1994).

Littell, H.S., and Eaton, J.K. "Unsteady Flowfield Behind a Vortex Generator Rapidly Pitched to Angle of Attack," *AIAA Journal*, Volume 29, No. 4, April (1991).

Luton, J.A. *Numerical Simulations of Vortices Near Free and Solid Surfaces.* Virginia Tech. (1996).

Luton, J.A., Ragab, S.A., and Telionis, D.P. "Interaction of Spanwise Vortices with a Boundary Layer," AIAA Paper N. 94-2377.

Macrorie, M., and Pauley, W.R. "Experimental Development of Spanwise Vortex Models with Streamwise Decay due to Wall Interaction," AIAA Paper No. 92-2688.

Makita, H., Sassa, K., Abe, M., and Itabashi, A. "Decay Process of a Manipulated Large-Scale Horseshoe Vortex in a Turbulent Boundary Layer," *AIAA Journal*, Volume 27, No. 2, February (1989).

Mangiavacchi, N., Gundlapalli, R., and Akhavan, R. "Dynamics of a Turbulent Jet Interacting with a Free Surface," FED-Volume 181, Free-Surface Turbulence, ASME (1994).

Marcus, D.L., and Berger, S.A. "The Interaction Between a Counter-Rotating Vortex Pair in Vertical Ascent and a Free Surface," *Physics of Fluids*, Volume 1, No. 12, December (1989).

Marshall, J.S. "Buckling of a Columnar Vortex," *Physics of Fluids*, Volume 4, No. 12, December (1992).
#. Marshall, J.S. "A General Theory of Curved Vortices with Circular Cross-Section and Variable Core Area," *Journal of Fluid Mechanics*, Volume 229, (1991), pp. 311-338.

Mei, R. "Velocity Fudelity of Flow Tracer Particles," *Experiments in Fluids*, Volume 22 (1996), pp. 1-13.

Montividas, R.E., Acharya, M., and Metwally, M.H. "Reactive Control of an Unsteady Separating Flow," *AIAA Journal*, Volume 30, No. 4, (1991).

Nelson, C.F., Koga, D.J., and Eaton, J.K. "Unsteady, Separated Flow Behind an Oscillating, Two-Dimensional Spoiler," *AIAA Journal*, Volume 28 (1990), pp. 845-852.

Ohring, S., and Lugt, H.J. "Interaction of a Viscous Vortex Pair with a Free Surface," *Journal of Fluid Mechanics*, Volume 227, (1991), pp. 47-70.

Orlandi, P., "Rebound of Vortex Dipole," Physics of Fluids, Vol. 2, No. 9, 1990, pp. 1429-1436.

Pan, Y., and Banarjee, S. "Attached Vortices and Two-Dimensional Aspects of Free-Surface Turbulence," FED-Volume 181, Free-Surface Turbulence, ASME (1994).

Pasin, M., and Tabakoff, W. "Laser Measurements of Unsteady Flow Field in a Radial Turbine Guide Vanes," AIAA Paper No. 92-0394.

Peace, A.J., and Riley, N., "A viscous vortex pair in ground effect,' Journal of Fluid Mechanics, Vol. 129, 1983, pp 409-426.

Reed, A.M., and Milgram, J.H., "Ship Wakes and their Radar Images," Annual Review of Fluid Mechanics, Vol. 34: 469-502, January 2002.

Ragab, S.A., Sheen, S.C., and Sreedhar, M. "An Investigation of Finite Difference Methods for Large-Eddy Simulation of a Mixing Layer," AIAA Paper No. 92-0554.

Rashidi, M., and Banerjee, S. "Turbulence Structure in Free-Surface Channel Flows,' *Physics of Fluids*, Volume 31, No. 9, September (1988).

Robins, R. and Delisi, D., "Potential Hazard of Aircraft Wake Vortices in Ground Effect with Crosswind," Journal of Aircraft, Vol. 30, No. 2, 1993, pp. 201-206.

Rood, E.P. "Interpreting Vortex Interactions with a Free Surface," *Journal of Fluids Engineering*, Volume 116, March (1994), pp. 91-93.

Rood, E.P. "Myths, math, and Physics of Free-Surface Vorticity," Applied Mechnics Review, Volume 47, No. 6, Part 2, June (1994).

Saffman, P., "The Approach of a Vortex Pair to a Plane Surface in Inviscid Fluid," Journal of Fluid Mechanics, Vol. 92, 1979, pp. 497-503.

Sarpkaya, T. "Three-Dimensional Interactions of Vortices with a Free Surface," AIAA Paper No. 92-0059.

Sarpkaya, T. "Vorticity, Free Surface and Surfactants." *Annual Review of Fluid Mechanics*, Volume 28 (1996), pp. 83-128.

Sarpkaya, T., Magee, M., and Merrill, C. "Vortices, Free-Surface and Turbulence," FED-Volume 181, Free-Surface Turbulence, ASME (1994).

Sarpkaya, T., Merrill, C., Carroll, J. "Coherent Structures in Vortex/Free-Surface Interaction," AIAA Paper No. 94-0530.

Sarpkaya, T., and Neubert, D. "Interaction of a Streamwise Vortex with a Free Surface," AIAA Paper No. 93-0556.

Shabaka, I.M.M.A., Metha, R.D., and Bradshaw, P. "Longitudinal Vortices Imbedded in Turbulent Boundary Layers. Part 1. Single Vortex," *Journal of Fluid Mechanics*, Volume 133, (1983), pp. 37-57.

Shizawa, T., and Eaton, J.K. "Interaction of a Longitudinal Vortex with a Three-Dimensional Turbulent Boundary Layer," *AIAA Journal*, Volume 30, No. 5, May (1992).

Simpson, R.L. "Three-Dimensional Turbulent Boundary Layers and Separation," AIAA Paper No. 95-0226.

Smith, R.H., Durgin, W.W., and Johari, H. "The Direct Measurement of Circulation in Free Surface Vortices," AIAA Paper No. 95-0104.

Stahl, H.P., and Stultz, K. "Free-Surface Deformation Measurement," AIAA Paper No. 97-xxxx.

Stern, F., Parthasarathy, R., Huang, H.P., and Longo, J. "Effects of Waves and Free Surface on Turbulence in the Boundary Layer of a Surface Piercing Flat Plate," FED-Volume 181, Free-Surface Turbulence, ASME (1994).

Tamburino, A., and Gulliver, J.S. "Free-Surface Turbulence Measurements in an Open-Channel Flow," FED-Volume 181, Free-Surface Turbulence, ASME (1994).

Tryggvason, G. "Deformation of a Free Surface as a Result of Vortical Flows," Letters, *Physics of Fluids*, Volume 31, No. 5, May (1988).

Tryggvason, G. "Numerical Interaction of Vortex Collision with a Free-Surface," ONR Free Surface Vorticity Workshop, (1991).

Walker, D.T., and Chen, C.Y. "Evaluation of Algebraic Stress Modeling in Free Surface Jet Flows," FED-Volume 181, Free-Surface Turbulence, ASME (1994).

Weigand, A. "Simultaneous Mapping of the Velocity and Deformation Field at a Free Surface," *Experiments in Fluids*, Volume 20 (1996), pp. 358-364.

Weigand, A., and Gharib, M. "Turbulent Vortex Ring/Free Surface Interaction," FED-Volume 181, Free-Surface Turbulence, ASME (1994).

Wendt, B.J., Greber, I., and Hingst, W.R. "The Structure and Development of Streamwise Vortex Arrays Embedded in a Turbulent Boundary Layer," AIAA Paper No. 92-0551.

Wilder, M.C. *Airfoil-Vortex Interaction and the Wake of an Oscillating Airfoil,* Virginia Tech, (1993).

Wilder, M.C., and Mathioulakis, D.S., Poling, D.R., Telionis, D.P., "The Formation and Internal Structure of Coherent Vortices in the Wake of a Pitching Airfoil," Journal of Fluids and Structures, Vol. 10, pp. 1-15, 1996

Yeh, H. "Vorticity Conditions at a Fluid-Fluid Interface," Presented at 1993 Free-Surface Turbulence Workshop. California Institute of Technology, 1993.

Zheng, Z., and Ash, R., "Prediction of Turbulent Wake Vortex Near the Ground," Transitional and Turbulent Compressible Flows, edited by L. D. Krol and T. A. Zang, ASME Fluids Engineering Conf. (Washington, DC) ASME FED Vol. 151, American Society of Mechanical Engineers, New York, 1993, pp. 196-201.

Zheng, Z. and Ash, R., "Viscous Effects on a Vortex Wake in Ground Effect," FAA Proceedings of the Aircraft Wake Vortices Conference (Washington, DC), edited by J. N. Hallock, No. DOT/FAA/SD/92/1.1-1.2, 1991, pp. 31-1-31-30.

Abstracts

Banerjee, S., and Rashidi, M. “Interactions of Coherent Structures with Free Surfaces in Turbulent Channel Flows,” ONR Free Surface Vorticity Workshop, (1991).

Bernal, L.P. “Experimental Investigations of Vortex Reconnection at a Free Surface,” ONR Free Surface Vorticity Workshop, (1991).

Dommermuth, D.G., Liepmann, D., Wiegand, A., and Yue, D.K.P. “The Interaction of Vortices with Walls and Free Surfaces: A Comparison Between Numerical Simulations and Experimental Measurements,” ONR Free Surface Vorticity Workshop, (1991).

Lugt, H.J., and Ohring, S. “The Oblique Ascent of a Viscous Vortex Pair Toward a Deformable Free Surface,” ONR Free-Surface Vorticity Workshop (1991).

Sarpkaya, T. “Structure of Scars and Striations,” Workshop on Scientific Research on Vortex/Free Surface Interactions, February (1991).

CHAPTER 2

A Vortex Pair Impinging on a Solid Boundary

Abstract

An experimental investigation is conducted which considers the interaction of a vortex pair propagating towards a solid boundary. This problem holds significance in several engineering applications including investigations into trailing wing tip vortices and their interaction with the ground. Data are acquired with both a high-speed digital video camera and a laser Doppler velocimetry system (LDV). The digital video camera is used to capture the development and trajectory of one of the primary vortices for a variety of pitch rates. The flow field is assumed to be symmetric and only half of it is investigated. The LDV system measures two components of velocity in a plane at the center of the vortex generating flaps. Grids of data were acquired for three pitch rates and a variety of locations. It is determined that the initial vortex trajectory is consistent with an inviscid analysis of this problem. Upon development of a secondary vortex, due to separation at the wall, the primary vortex is seen to meander and even stall.

Nomenclature

L = flap length

ω = flap pitch rate (rad/sec)

U* = dimensional velocity ($L\omega$)

t* = dimensional time

t = non-dimensional time ($t^*\omega$)

x* = dimensional length

x = non-dimensional length (x^*/L)

y* = dimensional length

y = non-dimensional length (y^*/L)

Introduction

Vortices interacting with solid surfaces are often encountered in engineering applications and in nature. The problems of interest are as varied as coherent vortices interacting and altering the character of a turbulent boundary layer, or wing tip vortices interacting with the ground and with other aircraft that follow. The length scales in such problems are different and yet it appears that the physics of the phenomena are very similar.

Many investigators have studied the behavior of a pair of vortices in the vicinity of a wall. In some of these studies the emphasis is on the ground effects on aircraft tip vortices. Pioneering contributions can be found in the works of Harvey and Perry [1] and Dee and Nicholas [2]. Quite a few papers on this problem have appeared more recently [3-7].

Inviscid analysis of the flow of pairs of vortices approaching a solid wall [8] indicate that when the vortices approach the wall, they move away from each other but continue to get closer to the wall. In real life, single or pairs of vortices start moving away from the wall in a process that resembles "rebounding." Saffman [9] clearly pointed out that this is a viscous effect. Orlandi [11] describes the rebounding process in greater detail. The fundamental work on this problem is reviewed by Doligalski et al. [11]. Luton et al [13] obtained a numerical solution of laminar vortex wall interaction and most recently, Corjon and Poinsot [14] examined the effect of cross flow.

Most of the work described above is analytical. The methods of the early experimental contributions were not very sophisticated and as a result, the data obtained were rather limited. No experimental information is available documenting the development of secondary vortices and their interaction with the primary vortices. In this chapter, we report on results obtained with a high-speed digital video camera and laser-Doppler velocimetry (LDV). Both methods will allow us to document the temporal development of the entire velocity field.

Facilities and Instrumentation

The research presented here was conducted in the test section of the Engineering Science and Mechanics water tunnel. The water tunnel was used only as a large tank of water in which to mount the experimental hardware, as there was zero mean flow. It was determined that the flow settled faster between measurements due to the large domain around the model.

As shown in Figure 2.1, a pair of actuated flaps, 8 inches in length by 3 inches in width, is used to generate a counter rotating pair of vortices approximately 5 inches from a solid boundary. Through their mutual interaction, these vortices propagate towards the wall. The flaps can be pitched at any chosen angular velocity to generate a variety of Reynolds numbers based on the circulation of the vortex ($Re_\Gamma = \Gamma/\nu$).

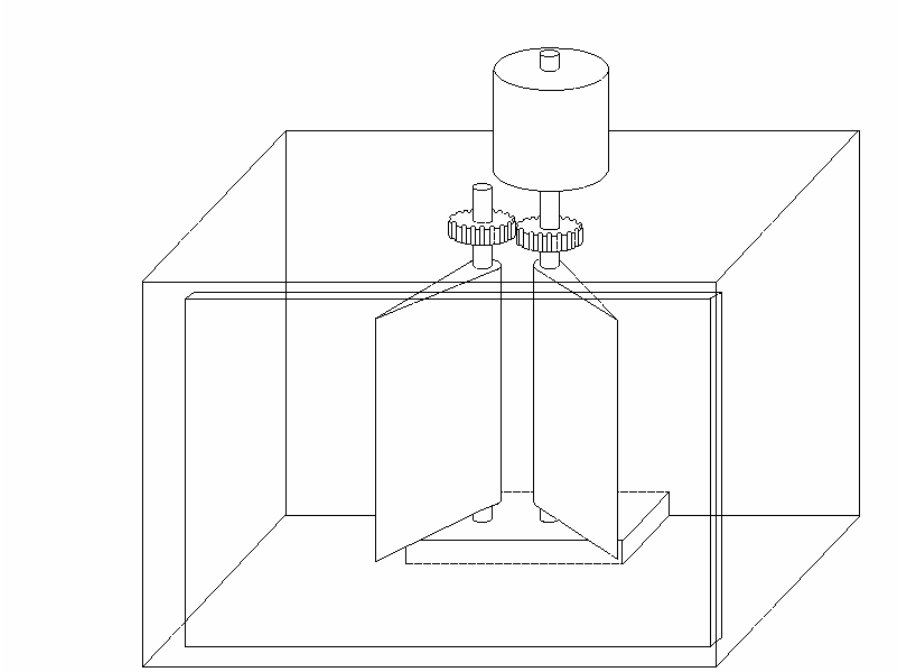

Figure 2.1. View of Experimental Setup

The flaps were parked at an angle of 27.5 degrees with respect to the line joining their axis. They were then swept swiftly until they were normal to this line and therefore parallel to themselves. The distance between the flap axes was equal to one half chords as shown in Figure 2.2. The purpose of this design was the following: It was found that if the distance between the axes was very small, then the rotation of the two flaps essentially created a jet by squeezing the fluid between the two flaps. Even with the distance chosen, some jet-like flow was present which was welcome, because it gave an initial velocity towards the wall to the two vortices thus generated.

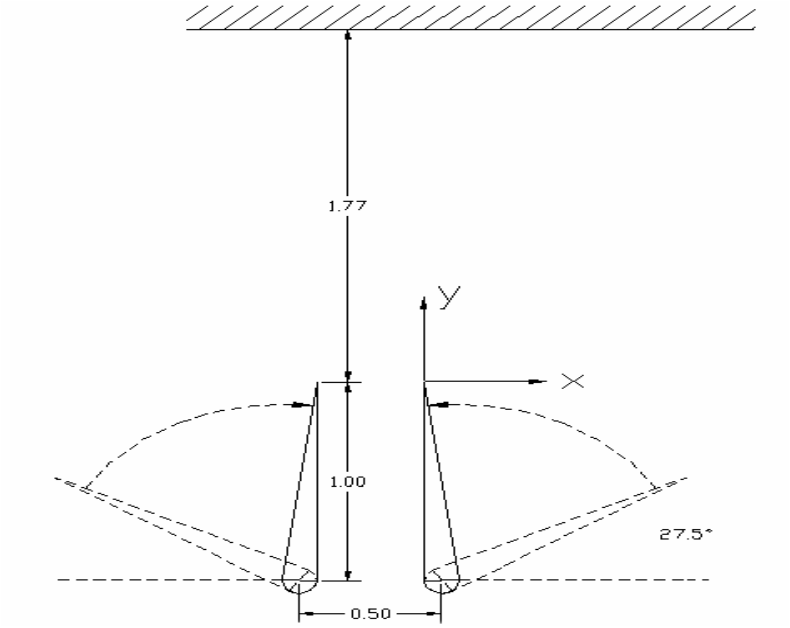

Figure 2.2. Top View of Experimental Setup

Data are acquired with both a high-speed digital video camera and a two-component fiber optic Argon-Ion laser Doppler velocimetry (LDV) system. Use of the LDV system allows for quantitative measurements of ensemble-averaged velocities in a two-dimensional plane, while the digital video camera allows for flow visualization and analysis of the developing flow field, seeded with tracer particles.

Data Analysis

Flow visualizations were obtained for pitch rates from 1.18 rad/sec to 3.142 rad/sec. This would result in a variety of vortex strengths and Re_Γ. These results once obtained were edge-enhanced in order to visually determine the vortex core location versus time. This would allow for an analysis of the vortex trajectories.

The laser Doppler velocimetry data were first smoothed using cubic splines. The smoothing of the data allows for a calculation of both instantaneous streamlines and vorticity contours. All of the data are then nondimensionalized. Lengths are nondimensionalized using the flap chord (L), and velocities by the flap chord times the pitch rate (ωL).

Instantaneous streamlines are calculated by assuming the flow is steady at a given instant in time and allowing massless particles to propagate through the measured velocity field. Velocity values within the field are approximated by first-order Taylor series expansions about the nearest grid point. The time over which the particles are allowed to propagate is chosen commiserate with the maximum velocity in the field, so that the maximum distance propagated does not exceed half a grid point.

Vorticity is calculated with second-order, centered finite differences of nondimensional velocity components on the interior grid points. Points on the measurement domain boundary are calculated with second order forward and backward differences.

Results and Discussion

The pair of vortices generated by the motion of the flaps propels itself towards the wall. This can be explained easily in terms of the Biot-Savart formula. Two counter-rotating vortices with circulation, Γ, at a distance d apart induce on each other a velocity equal to

$$V = \Gamma/(2\pi d)$$

In the proximity of a wall, the motion of two ideal vortices can be modeled by adding the mirror images of the pair. Again due to induced velocity, the vortices then tend to move parallel to the wall and apart from each other. This is indeed the case as will be described later. However the vortices under investigation here are far from ideal.

Ideal vortices have all of their vorticity concentrated at their center. The vortices generated by the pitching of a flap have a finite core, i.e. their vorticity is distributed over a finite area about their center. This was known as the "viscous core", but Wilder et al.[15] pointed out that vorticity is distributed in this way simply because of the rolling of the vortex sheet which is essentially an inviscid mechanism. The significance here is that even with the very low Reynolds numbers of the present test, the phenomena we study are dynamically similar to the interaction of vortices generated at much larger Reynolds numbers because the ratio of the vortex core radii to the length scale of the geometry matches that of any realistic problem, as for example the interaction of aircraft wing-tip vortices with the ground.

The wall was placed 1.77 chords away from the axes of the flaps. Flow visualizations were obtained in a domain defined in Figure 2.3. This domain was chosen in order to examine more carefully the interaction with the wall.

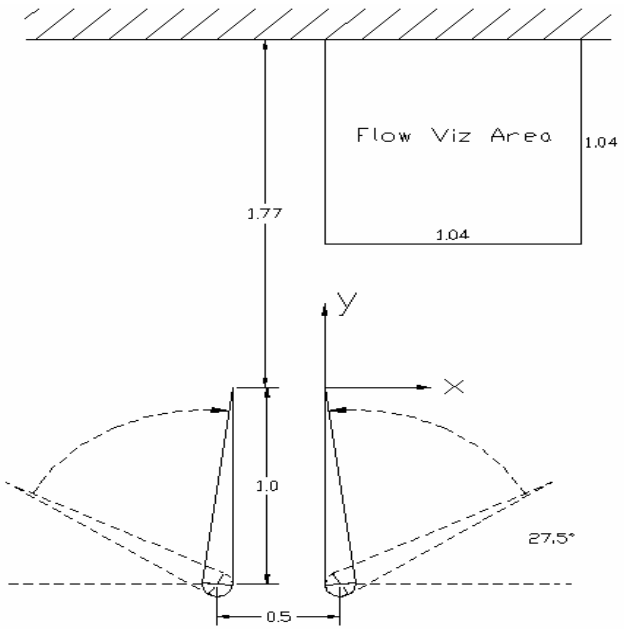

Figure 2.3. Top schematic of flaps and flow visualization area

An example of a sample image obtained by the digital video camera is presented in Figure 2.4. A sequence of these images documents the trajectory of the primary vortex. Each image obtained was edge-enhanced, so that the vortex core location could more easily be identified. An example of this edge enhancement filter is shown in Figure 2.5. Of interest in this image is the initial development of a secondary vortex in the upper right corner of the image. This secondary vortex is known to be the result of separation of the boundary layer induced by the cross flow of the primary vortex. When the adverse pressure gradient in this region is sufficiently strong, a separation bubble forms containing the opposite sense of vorticity as the primary vortex. This is nothing but the vorticity released along the point of separation of the boundary layer. It is this secondary vortex which is known to change the trajectory of the primary vortex from its inviscid path. As documented by Harvey and Perry [1] these changes include the rebound of the primary vortex away from the solid boundary and even an arrest of the horizontal motion of the primary vortex.

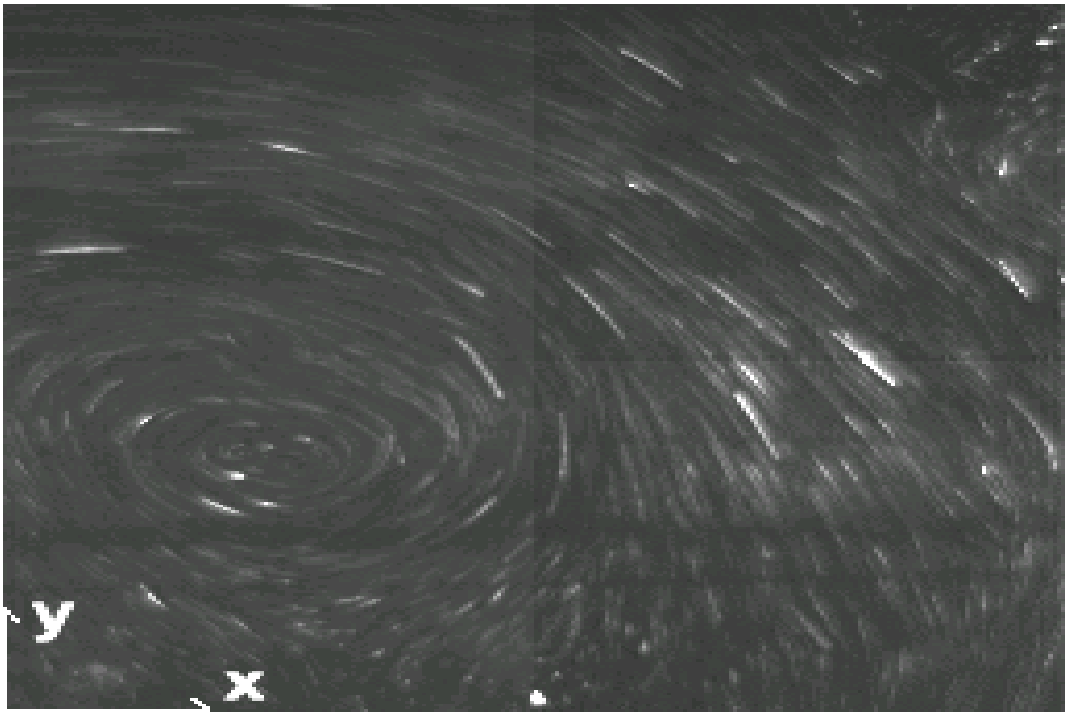

Figure 2.4. Sample flow visualization image for ω = 2.827 rad/sec, t = 6.36

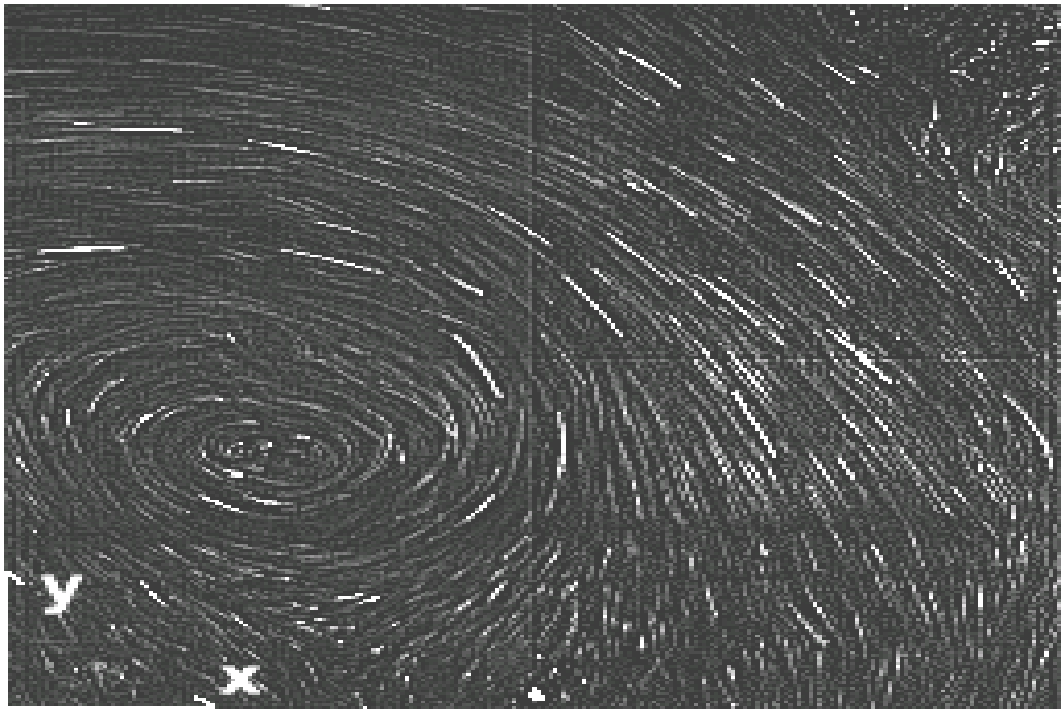

Figure 2.5. Edge enhanced image used to determine vortex center location, ω = 2.827 rad/sec, t = 6.36

The vortex trajectory information is detailed in Figure 2.6. Although the data are somewhat scattered, due to the inherent error in visually determining the core location and the differences in starting position due to development of the primary vortex, a careful analysis reveals some of the points discussed earlier. For pitch rates less than 1.963 rad/sec, the trajectory resembles the parabolic nature of an inviscisd analysis. It is determined that the strength of the primary vortex for these cases is insufficient to result in separation and development of a secondary vortex. For higher pitch rates, or specifically $\omega = 3.142$ rad/sec, an initial rebound of the core can be seen followed by a motion back towards the wall. This meander of the vortex trajectory could be a result of the secondary vortex spiralling around the primary vortex. Unfortunately, the flow visualization area was not large enough or not recorded for a sufficient length of time to document either the development of this secondary vortex or this proposed spiralling.

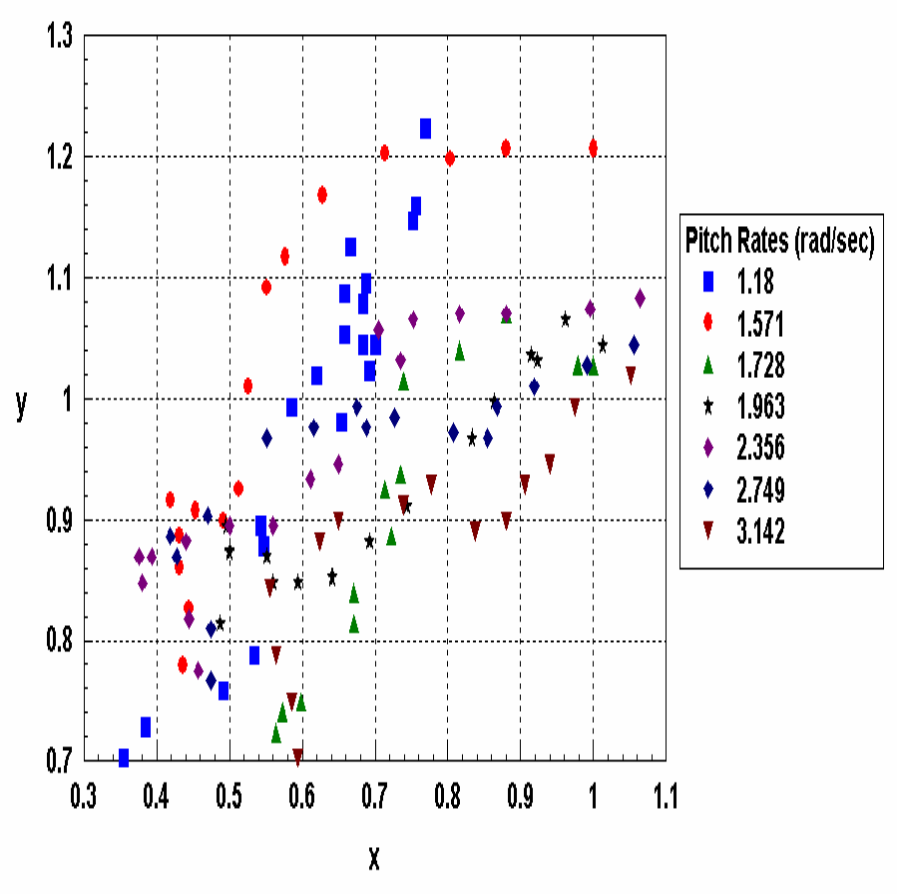

Figure 2.6. Vortex trajectories determined from flow visualizations

The location of the initial plane of laser Doppler velocimetry data taken is presented in Figure 2.7. This plane and subsequent LDV data grids suffer from the same problem as the flow visualization images, in that they fail to capture the development of the secondary vortex and its subsequent trajectory.

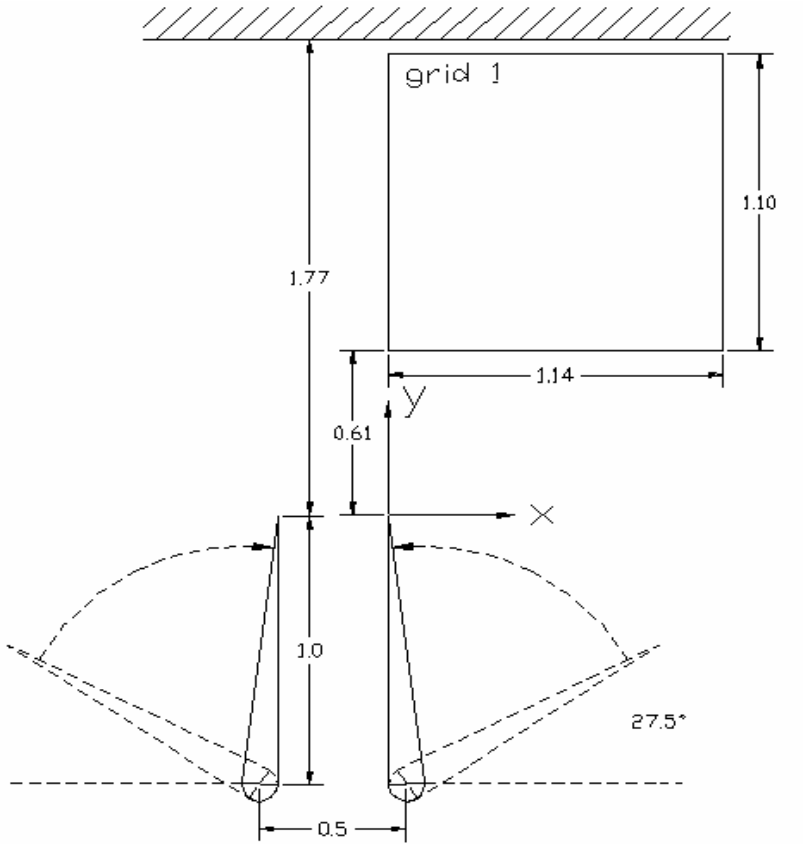

Figure 2.7. Top schematic of flaps and data acquisition grid 1

Figures 2.8 through 2.12 document the temporal development of the primary vortex with nondimensional velocity vectors. Figures 2.13 through 2.17 document the same nondimensional instances in time with instantaneous streamlines. Both of these figures reveal a primary vortex trajectory very similar to documented inviscid trajectories. For x less than 1, the path remains parallel to the wall.

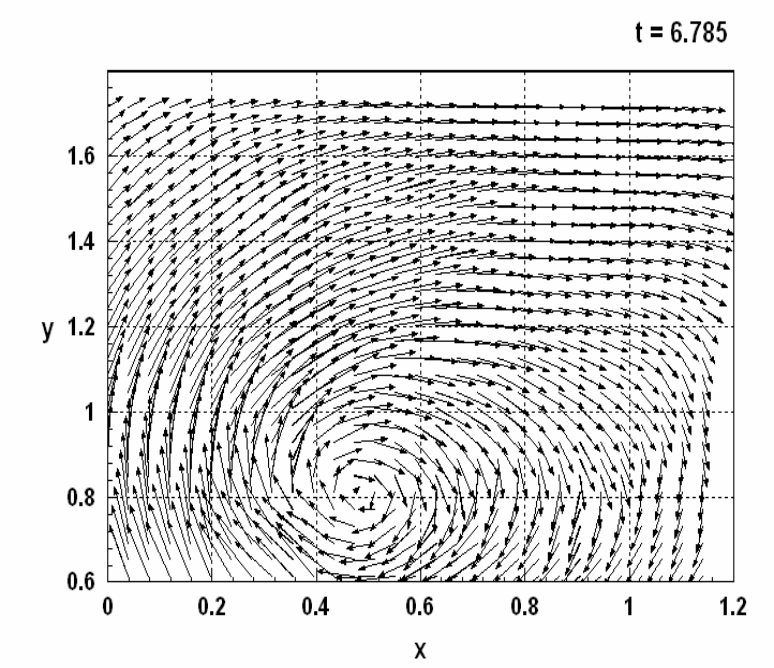

Figure 2.8. Velocity Vectors, ω = 2.356 rad/sec, t = 6.785

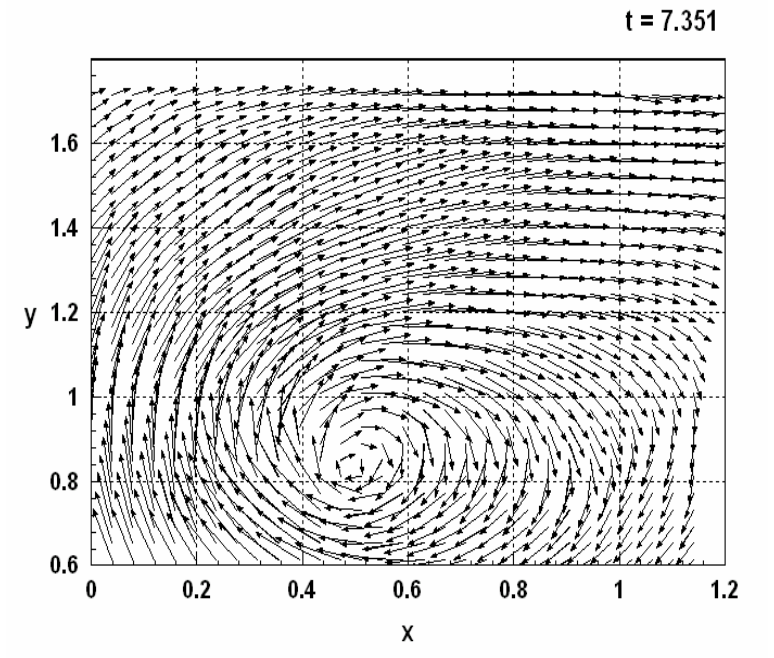

Figure 2.9. Velocity Vectors, ω = 2.356 rad/sec, t = 7.351

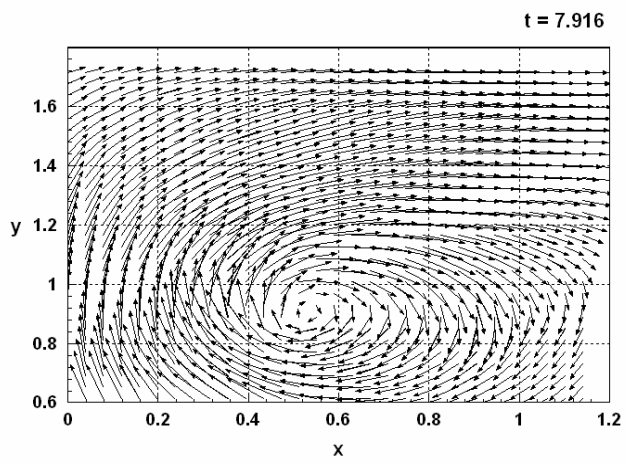

Figure 2.10. Velocity Vectors, ω = 2.356 rad/sec, t = 7.916

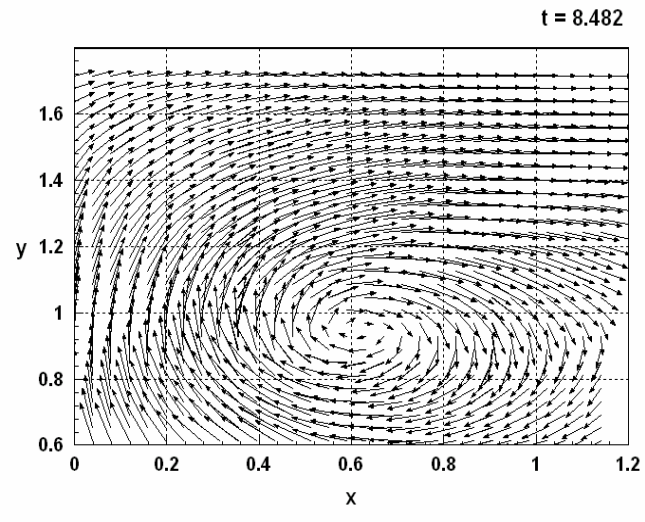

Figure 2.11. Velocity Vectors, ω = 2.356 rad/sec, t = 8.482

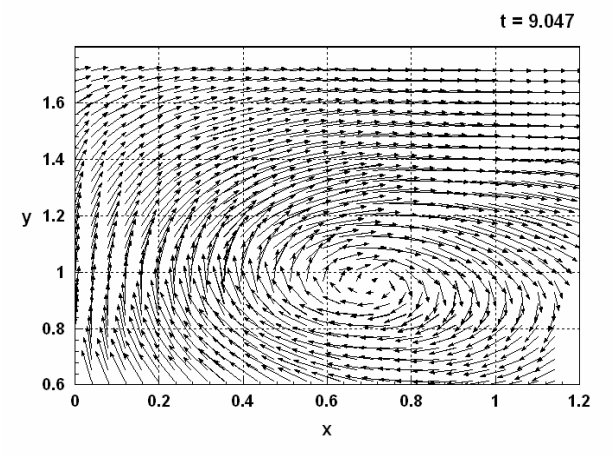

Figure 2.12. Velocity Vectors, ω = 2.356 rad/sec, t = 9.047

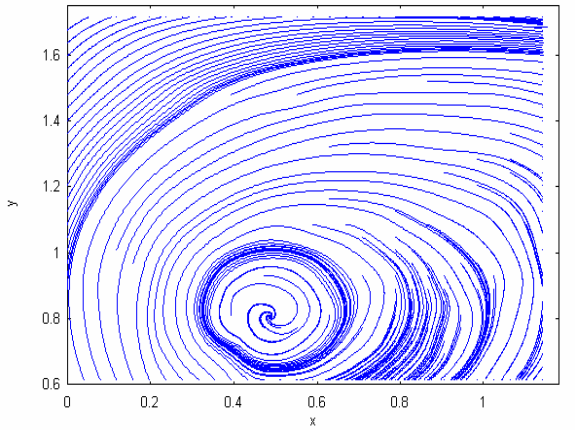

Figure 2.13. Instantaneous streamlines ω = 2.356 rad/sec, t = 6.785

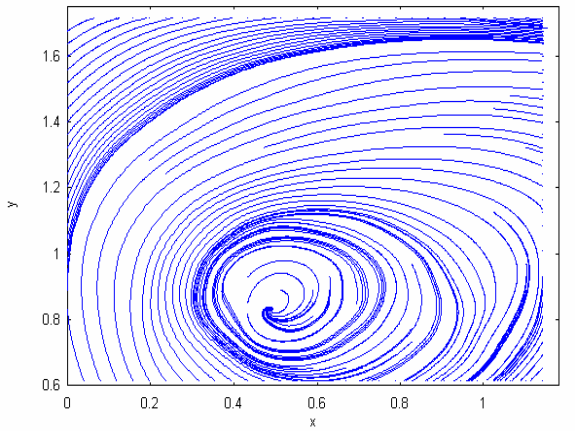

Figure 2.14. Instantaneous streamlines ω = 2.356 rad/sec, t = 7.351

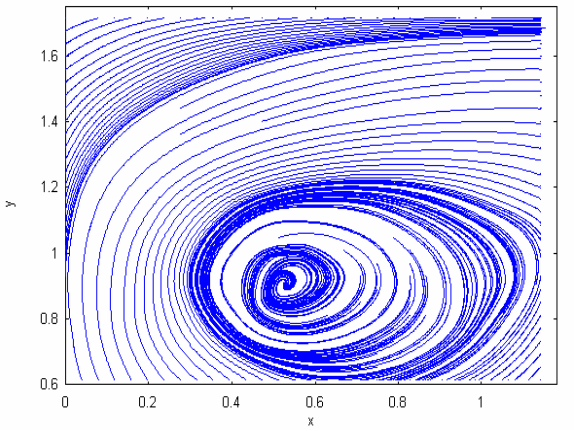

Figure 2.15. Instantaneous streamlines ω = 2.356 rad/sec, t = 7.916

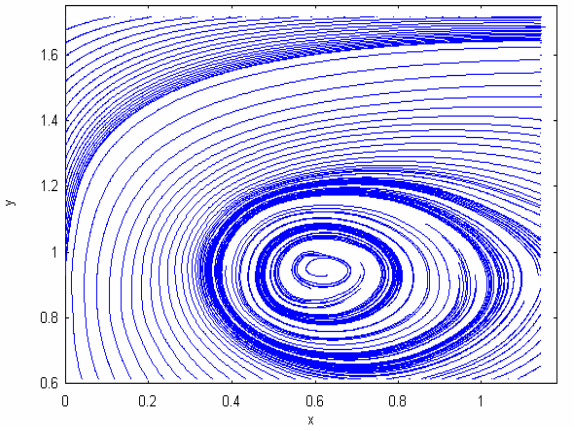

Figure 2.16. Instantaneous streamlines ω = 2.356 rad/sec, t = 8.482

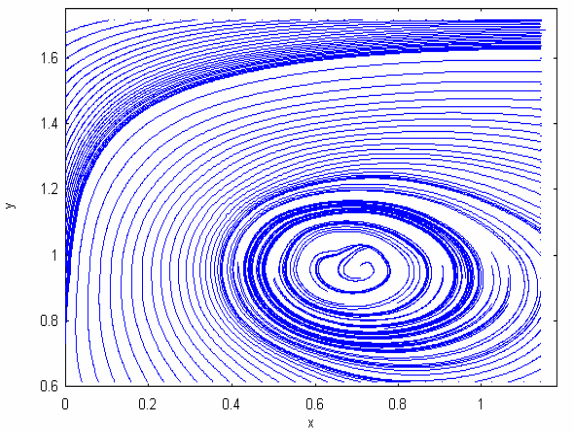

Figure 2.17. Instantaneous streamlines ω = 2.356 rad/sec, t = 9.047

Figure 2.18 through 2.22 document the vorticity levels for the same time instances and pitch rate as Figures 2.13 through 2.17. Again the vortex trajectory is seen to remain parallel to the wall. These plots also show a reduction in peak values of vorticity for the primary vortex indicating diffusion. Multiple localized peaks in the vorticity surface can be attributed to both erroneous vectors in the velocity field and finite or limited resolution of the LDV measurements.

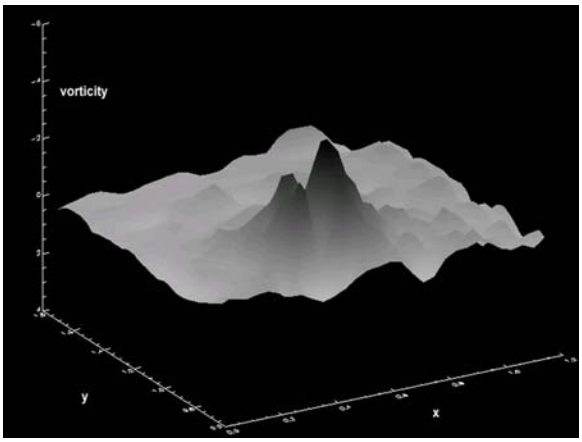

Figure 2.18. Vorticity Surfaces ω = 2.356 rad/sec, t = 6.785

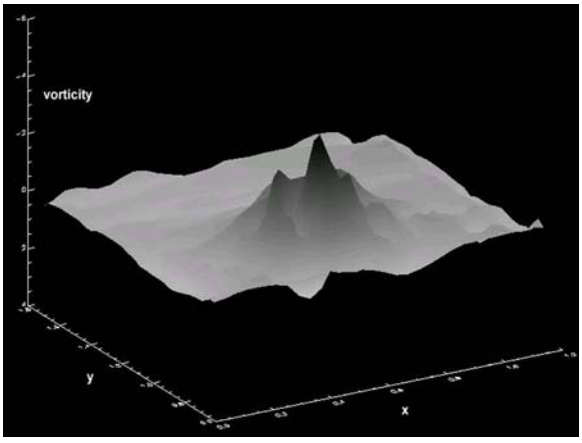

Figure 2.19. Vorticity Surfaces ω = 2.356 rad/sec, t = 7.351

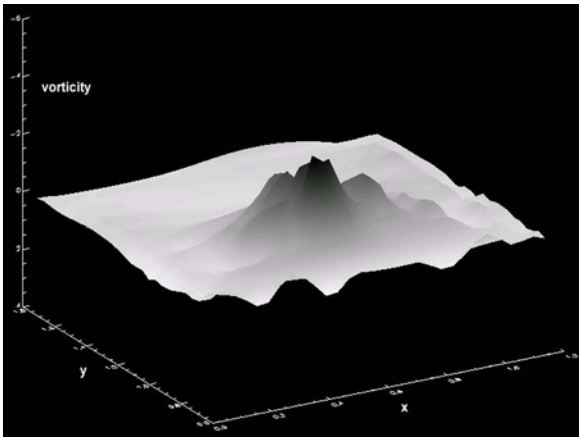

Figure 2.20. Vorticity Surfaces ω = 2.356 rad/sec, t = 7.916

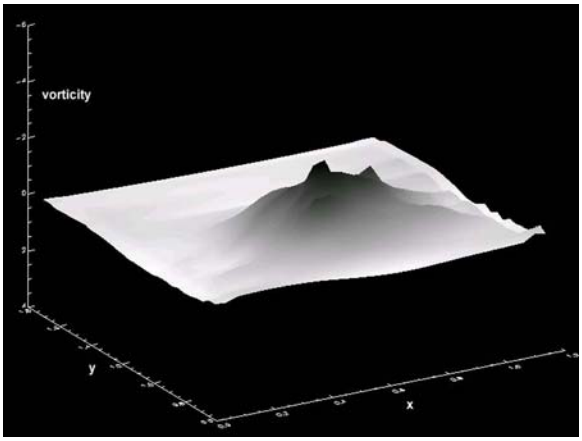

Figure 2.21. Vorticity Surfaces ω = 2.356 rad/sec, t = 8.482

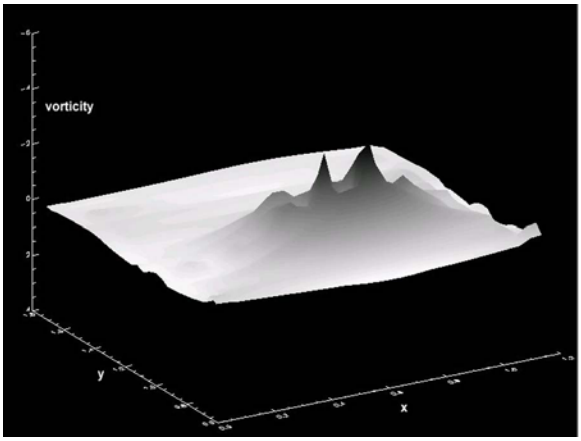

Figure 2.22. Vorticity Surfaces ω = 2.356 rad/sec, t = 9.047

Figure 2.23 documents the second grid of LDV data taken. The lack of evidence of secondary vorticity led the authors to both increase the pitch rate to 2.67 rad/sec and widen the field of acquisition to x = 2.2.

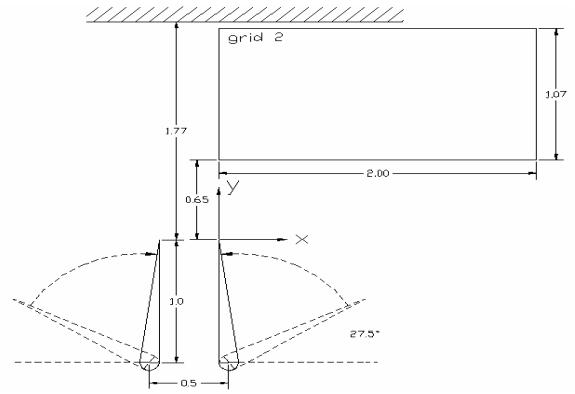

Figure 2.23. Top schematic of flaps and data acquisition grid 2

Figures 2.24 through 2.28 use instantaneous streamlines to document the trajectory of the primary vortex. Although a secondary vortex is not visualized evidence of its presence can be seen. The primary vortex is seen to meander, or initially rebound away from the wall, hesitate, then start moving back towards the wall. This analysis is in agreement with flow visualization information discussed earlier. This meandering is evidence of the existence of a secondary vortex and its effect on the primary vortex.

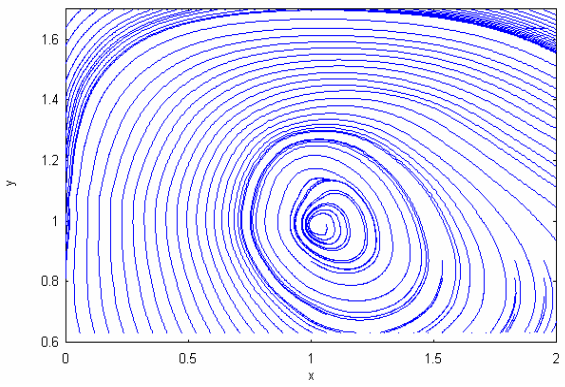

Figure 2.24. Instantaneous streamlines ω = 2.67 rad/sec, t = 10.894

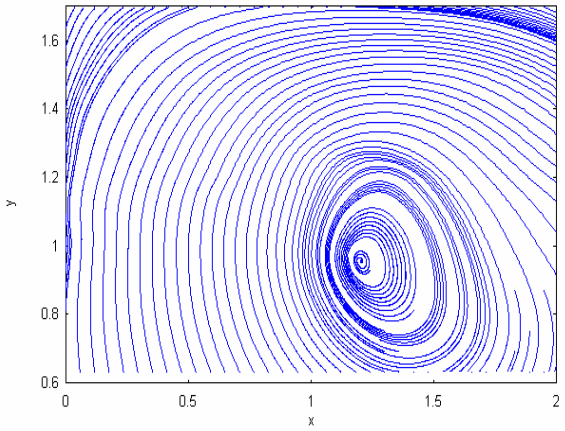

Figure 2.25. Instantaneous streamlines ω = 2.67 rad/sec, t = 12.175

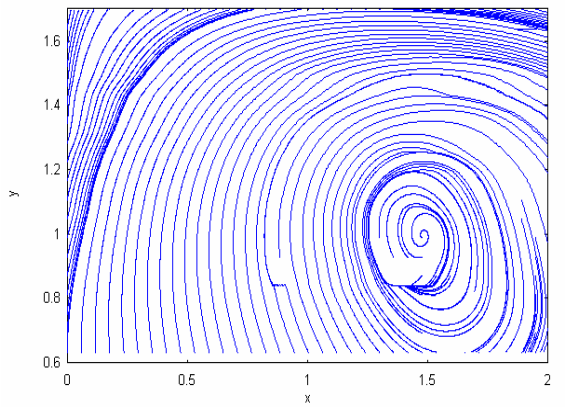

Figure 2.26. Instantaneous streamlines ω = 2.67 rad/sec, t = 13.457

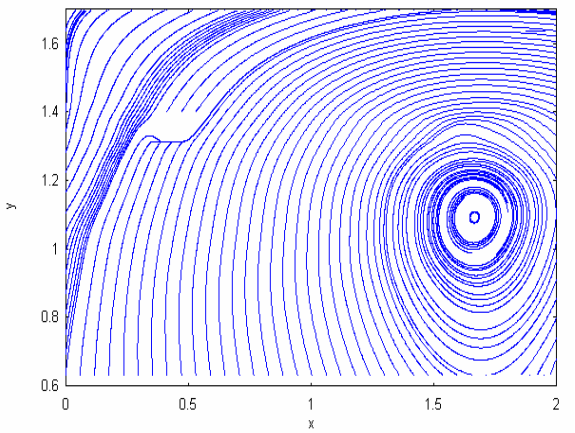

Figure 2.27. Instantaneous streamlines ω = 2.67 rad/sec, t = 14.738

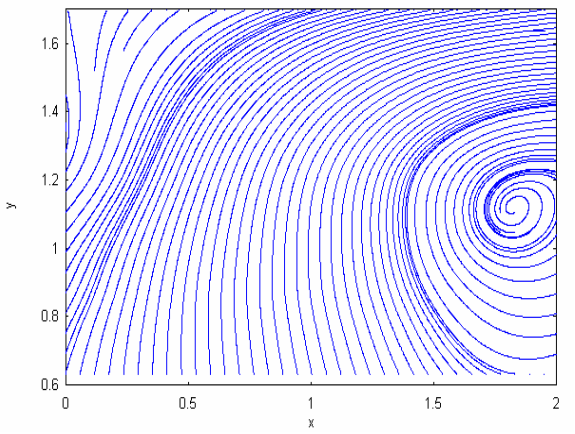

Figure 2.28. Instantaneous streamlines ω = 2.67 rad/sec, t = 16.020

Figures 2.29 through 2.33 are vorticity contours for the same pitch rate and time instances documented in Figures 2.24 through 2.28. Again the meandering of the primary vortex trajectory can be seen. As discussed earlier for LDV data grid 1 the peak value of vorticity is seen to decay indicating diffusion of the primary vortex as it interacts with the secondary vortex.

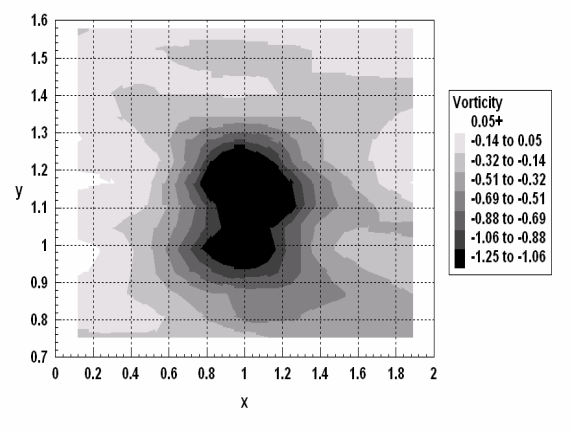

Figure 2.29. Vorticity Contours ω = 2.67 rad/sec, t = 10.894

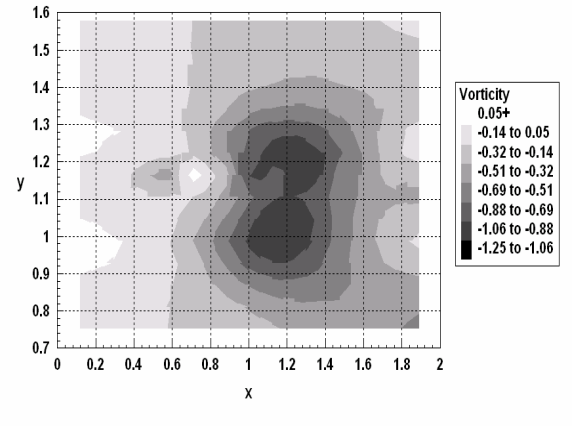

Figure 2.30. Vorticity Contours ω = 2.67 rad/sec, t = 12.175

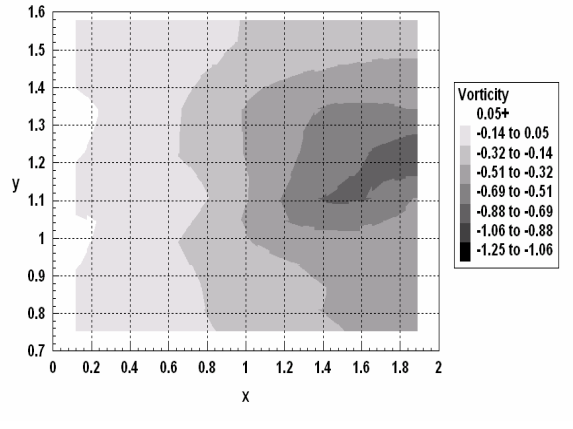

Figure 2.31. Vorticity Contours ω = 2.67 rad/sec, t = 13.457

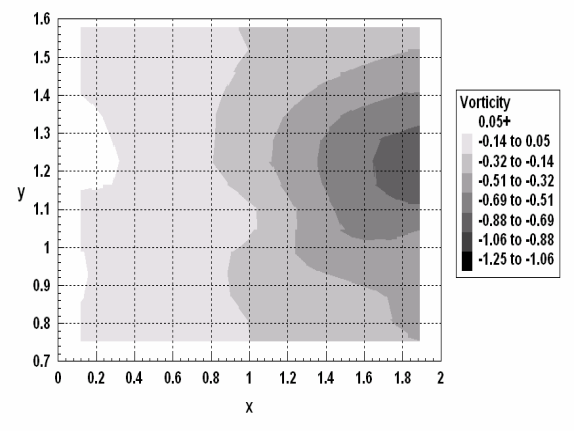

Figure 2.32. Vorticity Contours ω = 2.67 rad/sec, t = 14.738

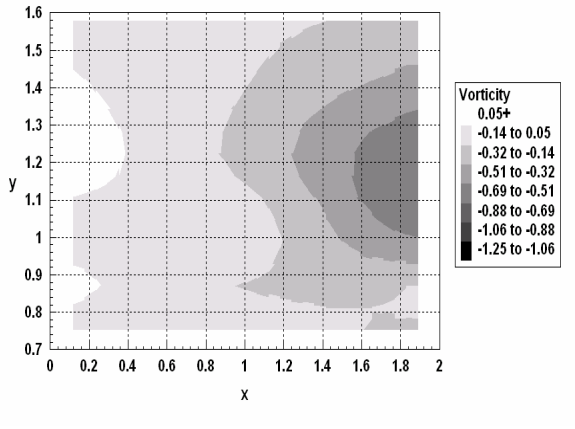

Figure 2.33. Vorticity Contours ω = 2.67 rad/sec, t = 16.020

Again the authors moved the data acquisition grid further in the x direction in an attempt to locate and visualize the secondary vortex. The pitch rate was returned to 2.356 rad/sec, equal to the first LDV data set presented. This grid is presented in Figure 2.34.

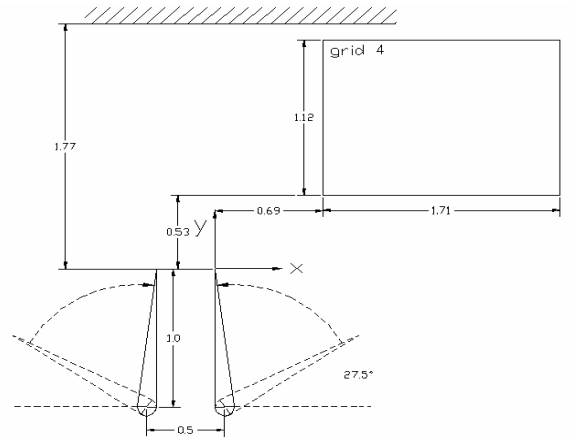

Figure 2. 34. Top schematic of flaps and data acquisition grid 4

Again the plots of instantaneous streamlines are used to search the field for the presence of a secondary vortex. These are presented in Figures 2.35 through 2.39. A study of earlier times in the development of the motion indicates the presence of a secondary vortex on the right side of the image. The secondary vorticity is lifted of the wall and appears to wrap around the primary vortex. This is in qualitative agreement with the findings of Luton et al [13].

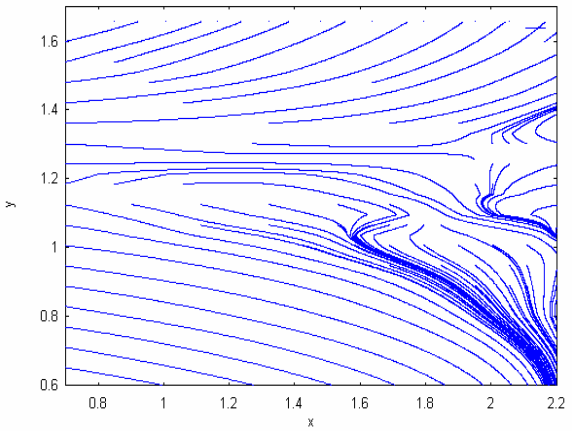

Figure 2.35. Instantaneous streamlines ω = 2.356 rad/sec, t = 1.414

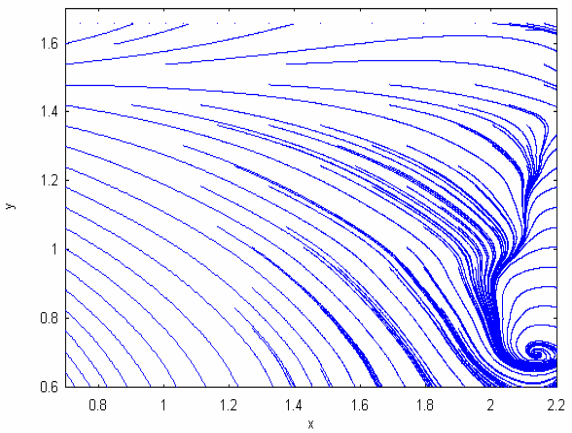

Figure 2.36. Instantaneous streamlines ω = 2.356 rad/sec, t = 2.827

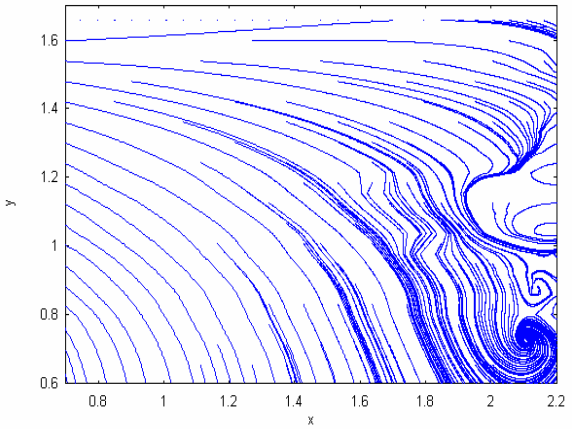

Figure 2.37. Instantaneous streamlines ω = 2.356 rad/sec, t = 3.534

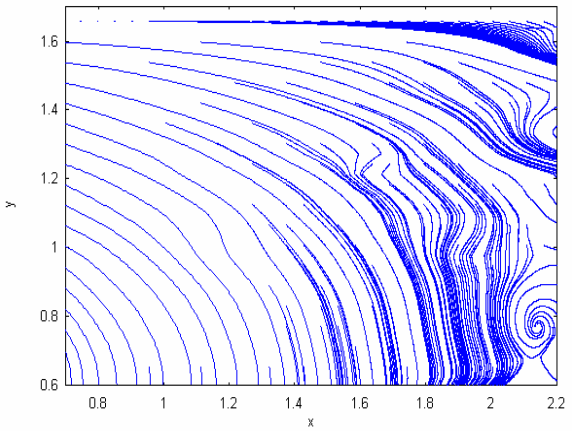

Figure 2.38. Instantaneous streamlines ω = 2.356 rad/sec, t = 4.241

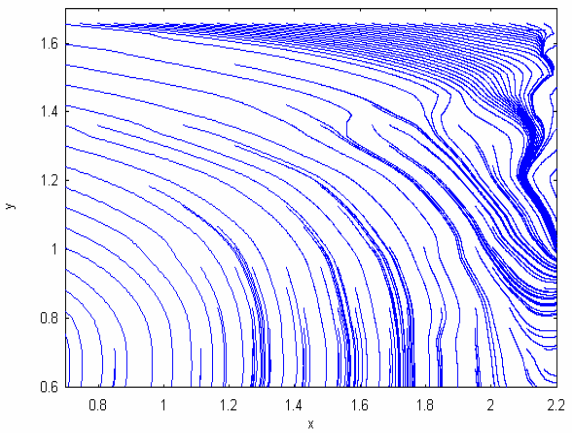

Figure 2.39. Instantaneous streamlines ω = 2.356 rad/sec, t = 4.948

Conclusions

Flow visualizations and subsequent plots of the primary vortex trajectories, for a variety of pitch rates, reveals that the development of secondary vorticity is dependent on initial vortex strength. For slower pitch rates the trajectory is similar to an inviscid analysis. For higher pitch rates vortex meandering can be seen indicating the presence of secondary vorticity. Laser Doppler velocimetry measurements over several grids support the conclusions of the flow visualization analysis. The primary vortex propagates parallel to the wall until reaching a nondimensional distance x = 1. At this point velocity vectors, instantaneous streamlines, and vorticity surfaces and contours reveal an initial movement away from the wall followed by a return towards the wall. Once the data acquisition grid was moved far enough in the x-direction actual evidence of secondary vorticity could be seen. This smaller secondary vortex was seen to quickly roll up and move out of the field of measurement around the primary vortex. The authors plan on continuing this investigation and documenting both the trajectories of the primary and secondary vortex as they interact.

Acknowledgements

The support of the office of Naval Research, under grant number ONR N00014-96-1-0941, Edwin Rood, monitor, is gratefully acknowledged.

References

1. Harvey, J., and Perry, F., "Flowfield Produced by Trailing Vortices in the Vicinity of the Ground," AIAA Journal, Vol. 9, No. 8, 1971, pp. 1659, 1660.

2. Dee, F., and Nicholas, O., "Flight Measurements of Wing Tip Vortex Motion Near the Ground," Royal Aircraft Establishment, TR 68007, London, 1968.

3. Zheng, Z. and Ash, R., "Viscous Effects on a Vortex Wake in Ground Effect," FAA Proceedings of the Aircraft Wake Vortices Conference (Washington, DC), edited by J. N. Hallock, No. DOT/FAA/SD/92/1.1-1.2, 1991, pp. 31-1-31-30.

4. Zheng, Z., and Ash, R., "Prediction of Turbulent Wake Vortex Near the Ground," Transitional and Turbulent Compressible Flows, edited by L. D. Krol and T. A. Zang, ASME Fluids Engineering Conf. (Washington, DC) ASME FED Vol. 151, American Society of Mechanical Engineers, New York, 1993, pp. 196-201.

5. Robins, R. and Delisi, D., "Potential Hazard of Aircraft Wake Vortices in Ground Effect with Crosswind," Journal of Aircraft, Vol. 30, No. 2, 1993, pp. 201-206.

6. Ash, R., and Zheng, Z., "Cross Wind Effects on Turbulent Aircraft Wake Vortices Near the Ground," AIAA Paper 94-2381, June 1994.

7. Ciffone, D.L., and Pedley, B., "Measured Wake-Vortex Characteristics of Aircraft in Ground Effect,' AIAA Paper 78-109. Huntsville, AL, Jan 16-18, 1978.

8. Barker, S. and Crow, S., "The Motion of Two-Dimensional Vortex Pairs in a Ground Effect," Journal of Fluid Mechanics, Vol. 82, No. 4, 1977, pp. 659-671.

9. Saffman, P., "The Approach of a Vortex Pair to a Plane Surface in Inviscid Fluid," Journal of Fluid Mechanics, Vol. 92, 1979, pp. 497-503.

10. Peace, A.J., and Riley, N., "A viscous vortex pair in ground effect,' Journal of Fluid Mechanics, Vol. 129, 1983, pp 409-426.

11. Orlandi, P., "Rebound of Vortex Dipole," Physics of Fluids, Vol. 2, No. 9, 1990, pp. 1429-1436.

12. Doligalski, T., Smith, C., and Walker, J., "Vortex Interactions with Walls," Annual Review of Fluid Mechanics, Vol. 26, 1994, pp. 573-616.

13. Luton, A., Ragab, S., and Telionis, D., “Interaction of Spanwise Vortices with a Boundary Layer,” Physics of Fluids, Vol. 2, Nov. 1995, pp. 2757-2765.

14. Corjon, A., and Poinsot, T., “Behavior of Wake Vortices Near Ground,” AIAA Journal, Vol. 35, No. 5, 1997, pp. 849-855.

15. Wilder, M.C., and Mathioulakis, D.S., Poling, D.R., Telionis, D.P., "The Formation and Internal Structure of Coherent Vortices in the Wake of a Pitching Airfoil," Journal of Fluids and Structures, Vol. 10, pp. 1-15, 1996.

CHAPTER 3

The Interaction of Rolling Vortices with a Turbulent Boundary Layer

Abstract

Laser-Doppler velocimetry is employed to measure the periodic field created by releasing spanwise vortices in a turbulent boundary layer. Phase-averaged vorticity and turbulence level contours are estimated and presented. It is found that vortices with diameter of the order of the boundary layer quickly diffuse and disappear while their turbulent kinetic energy spreads uniformly across the entire boundary layer. Larger vortices have a considerably longer life span and in turn feed more vorticity into the boundary layer.

Introduction

In a variety of engineering applications, one encounters the interaction of coherent vortical structures with a turbulent boundary layer. Vortical structures comparable in size or larger than the thickness of the boundary layer could be generated downstream of obstructions which induce separation. Dynamic motions of solid surfaces with sharp edges, like propeller blades or impeller fins generate free shear layers which roll up and form vortical structures. Such structures again may interact with a turbulent boundary layer.

Researchers are interested in the effects of vortical structures on the wall shear stress, the heat transfer, the turbulent characteristics of the boundary layer, or the interaction of the external structures with the natural organization of the boundary layer. In this chapter we will refer to such initially coherent vortical structures as ``vortices.'' These vortices are far from ideal, and

soon lose their coherence but one can easily trace their location. Ideal vortices are the vortices with a circumferential velocity component varying inversely with distance from their center, in a frame of reference attached to the center. There is no rigorous definition for the ``coherence'' of a vortex but many authors imply by this term a well-ordered distribution of vorticity, continuously decreasing from the center of the vortex.

Broadly speaking, studies of the interaction of vortices with a turbulent boundary layer can be grouped into two categories: (i) those which focus on the effect of the externally imposed vortical structure on the turbulent boundary layer and (ii) those which explore the effect of the turbulent boundary layer on the organization of the vortex. This distinction is usually dictated by the interest in a specific engineering application. The problem of course is highly nonlinear, and the two effects are strongly coupled. In the present chapter we present information on the temporal development of both the turbulence characteristics and the organized character of the disturbing vortex.

The effects of a variety of disturbances imposed on a turbulent boundary layer have been investigated in the past. A long line of investigators introduced axial vortices ("streamers"') in turbulent boundary layers. One of the initial contributions is due to Shabaka et al. (1985). A more recent example is the work of Littell and Eaton (1991) who generated a disturbance by rapidly pitching a half delta wing. Three-dimensional disturbances can also be introduced locally. Makita et al. (1989) create artificial horse-shoe vortices in their turbulent boundary layers. Disturbances can be introduced in a uniform spanwise direction to create structures with spanwise vorticity. Such vortical structures are commonly known as ``rollers.'' Rollers can be generated by pitching airfoils in a free stream or by periodically lifting span wise fences on a wall. A number of investigators have employed pitching fences to study the structure of

unsteady separation (Francis et al., 1979; Reisenthel et al., 1985; Consigny et al., 1984; Nagib et al., 1985). In another line of work, disturbances were created in a free stream in order to study their interaction with blades further downstream (Poling and Telionis, 1986; Poling et al., 1988; Booth and Yu, 1986; Wilder et al., 1990). More recently, careful investigations of the interaction of rollers with turbulent boundary layers were carried out (Nelson et al., 1990; Kothmann and Pouley, 1992; Macrorie and Pauley, 1992). The present contribution belongs to this category.

Nelson et al. (1990) lift a fence from the floor of a flat plate on which a turbulent boundary layer was developed. They then measure periodic velocity fields by ensemble averaging LDV data. Pauley and his co-workers (Kothmann and Pauley, 1992; Macrorie and Pauley, 1992) instead pitch a small airfoil upstream of the leading edge of a flat plate and allow the disturbances to enter the boundary layer which grows downstream. In the work reported here we create disturbance in a manner very similar to the one employed by Nelson et al. (1990).

Nelson et al. (1990) employ a fence with a chordlength approximately half of the boundary layer thickness. As a result their vortices are embedded in their boundary layers. A very interesting result for this choice of parameters is that the vortex disintegrates very quickly and completely disappears only a few chordlengths downstream of the fence. In this chapter we report on experiments conducted with fence chordlengths comparable with the boundary layer thickness and we confirm the fact that disturbances created in this way have a very short life span. We also report on vortices that are about twice and three times as large as the thickness of the boundary layer and provide evidence that such vortices can be sustained for longer distances downstream of the disturbing blade.

Shear flows developing away from solid surfaces have a nearly two-dimensional structure. On the other hand, turbulence in a boundary layer developing over a solid wall is

dominated by three-dimensional structures. The problem of interaction between an artificially created two-dimensional disturbance and a boundary layer is therefore a complex problem. In a future publication we will report on the three-dimensional character of such flows.

The Experimental Rig

A turbulent boundary layer was allowed to develop on a flat plate inserted in the test section of the Engineering Science and Mechanics (ESM) water tunnel. This facility has a test section of 25.4 cm × 30.5 cm and can provide flow speeds of up to 3 m/sec. at turbulence levels ranging from 0.6 to 1.5 percent. A detailed description of this facility and its calibration is included in Koromilas and Telionis (1980) and Mathioulakis and Telionis (1987). An articulated fence can be lifted 60 cm downstream of the leading edge of the plate to generate a local disturbance (Figure 3.1). The origin of the coordinate system, $x = 0$, was positioned on the plate, 10 mm downstream of the trailing edge of the fence.

Measurements were carried out with laser-Doppler velocimetry (LDV). A TSI, three-beam, two-component LDV system was employed. Two of the beams were shifted at 60 MHz and 40 MHz, respectively. It was thus possible to separate the two components by electronic filters and therefore employ only one photomultiplier. The original system described in Mathioulakis and Telionis (1987) was capable of obtaining two velocity components in planes parallel to the side walls of the tunnel. A system of coordinates was defined with its x-direction aligned with the freestream and the y direction normal to the plate, as shown in Figure 3.1. The design of the traversing system allowed traversing in the directions of x and y. This design was dictated by the need to study nominally two-dimensional flows. In the present effort we employ a modified system which allows traversing in the spanwise direction as well.

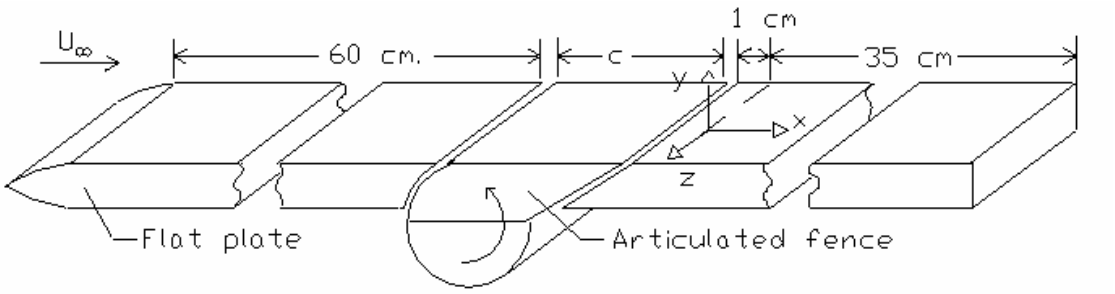

Figure 3.1. Schematic of Experimental Setup for Vortex Flat Plate Boundary Layer Interactions

A large optical bench and a more powerful laser (35 mW, Helium-Neon) are now employed. The TSI design was modified to mount the laser next to the train of optics instead of underneath it. The long side of the optical bench and therefore the direction of the optical beam was positioned normal to the axis of the test section, as discussed in Chapter 1, and in Figure 3.2. A mirror tower was again employed for traversing. The tower is now mounted on a precision sliding table to allow traversing in the spanwise direction. The position of the upper mirror of the tower is controlled by a lead screw, thus facilitating traversing in the *y* direction. A second set of mirror was also mounted on traversing brackets and the system allows the beams to be directed either from the side wall of the tunnel or from the ceiling of the tunnel. In this way, all three components of the velocity can be obtained, although not all simultaneously.

Traversing is achieved by two stepping motors and monitored by two linear variable differential transducers (LVDT). The latter provide an independent analog feedback to confirm the accurate positioning of the measuring volume. In this way, two-dimensional grids along planes *xy* or *yz* can be traversed. The accuracy in positioning the measuring volume is 0.05 mm. Phase referencing and instantaneous fence inclination information is obtained through optical methods. The optical encoder used has an accuracy of 0.1 deg.

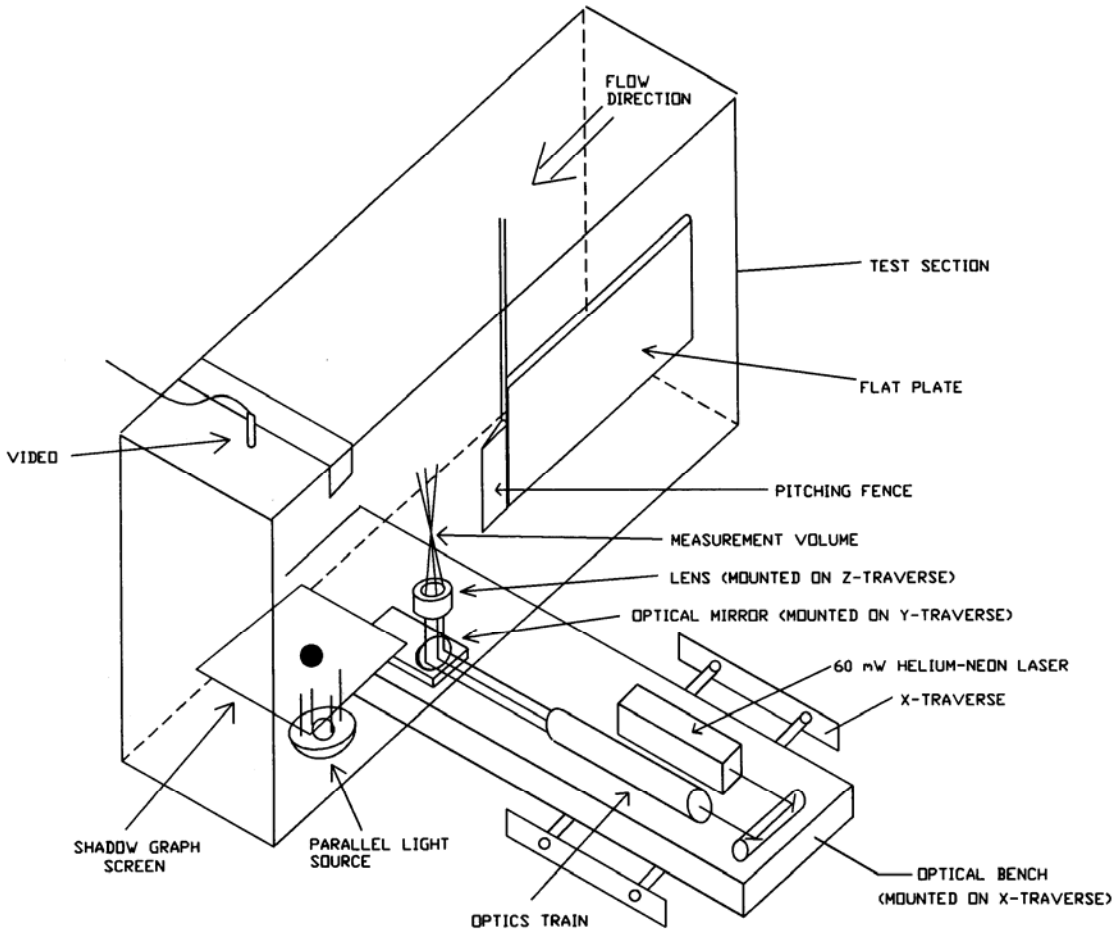

Figure 3.2. Schematic of laser Doppler velocimetry system and shadow-graph validation

The entire operation is controlled by two serially communicating laboratory computers which are programmed to operate the pitching mechanism and the stepping motors, collect the information on the instantaneous angle of the fence inclination, perform the LDV data acquisition, reduce the data and transfer them to a mainframe IBM 3090 for calculations and plotting. The entire data acquisition process is fully automated.

In our initial design, lifting of the fence generated a slot which prevented the formation of a wake downstream of the fence by a supplying fluid from the other side of the plate. The flow thus entering our field contained vorticity generated on the other side of the plate which has the opposite sign. It was decided that the real-life situation of large separated bubbles which are

convected with the flow can be better simulated if the fence lifts out of a cavity. This design is not without a disadvantage, because when the fence returns to its initial position, it ejects the fluid in the cavity, and thus imparts some momentum to the vortex generated by the fence. To minimize this effect, the cavity was filled with rubber foam.

Three fences were employed with chordlengths *c* equal to 12.7, 25.4, and 38.1 mm. The fences were pitched through a four-bar linkage by a motor which in turn was controlled by one of the laboratory computers. The schedule of their motion is shown in 3.3. The fences were lifted sharply to an angle of 28 deg and then returned to their initial position, flush with the plate, and remained there for a short period, in order to allow the flow to settle again to steady-state, turbulent boundary-layer flow.

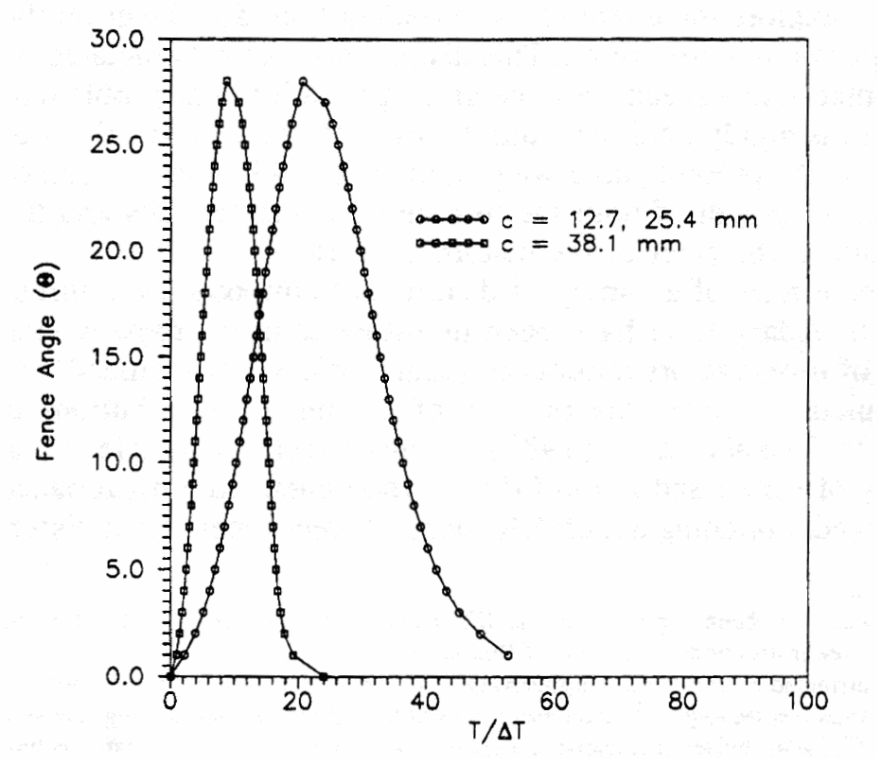

Figure 3.3. Time schedule of fence motion.

The period of the fence's motion was τ = 3.33 *s* which is equivalent to a dimensionless time of 925 if the momentum thickness, θ, and the freestream velocity were used for nondimensionalization. Dimensionless times $T/\Delta T$, where $\Delta T = \tau/100$, were defined and all the results are presented here in terms of this time parameter. In other words, the period is divided into one hundred time units. The fence returned to its initial position after at most 50 time units and remained flush with the plate for the duration of the period.

A LED (light-emitting diode) sensor was employed to provide a trigger. This allowed us to conditionally average the data. The average and RMS of the fluctuation of a quantity *g* was thus calculated according to

$$\overline{g}(t) = \frac{1}{N}\sum_{i=1}^{N} g_i(t) \tag{1}$$

$$g_{rms}(t) = \left[\frac{1}{N}\sum_{i=1}^{N}\left[g_1(t) - \overline{g}(t)\right]^2\right]^{1/2} \tag{2}$$

Where $g_i(t)$ is the *i*th realization. Note that the quantity $g_{rms}(t)$ is a statistical measure of the deviation of the quantity $g(t)$ from its average at a time *t*. We also obtained the ensemble average of the sum of the velocity component fluctuations. We were thus able to obtain the phase-averaged value of the turbulent kinetic energy

$$q(t) = \frac{1}{N}\sum_{i=1}^{N}\left[u_i'^2(t) + v_i'^2(t)\right] \tag{3}$$

where $u_i'(t)$ and $v_i'(t)$ are the fluctuations of the two components of the velocity. An example of waveforms obtained within a period by employing 5, 20, or 40 ensembles is shown in Figure 3.4. These data were obtained at x/c = 1.0 and y/δ = 0.5 behind the smallest fence. They indicate the scatter of the data and the character of the waveform produced by a pitching fence.

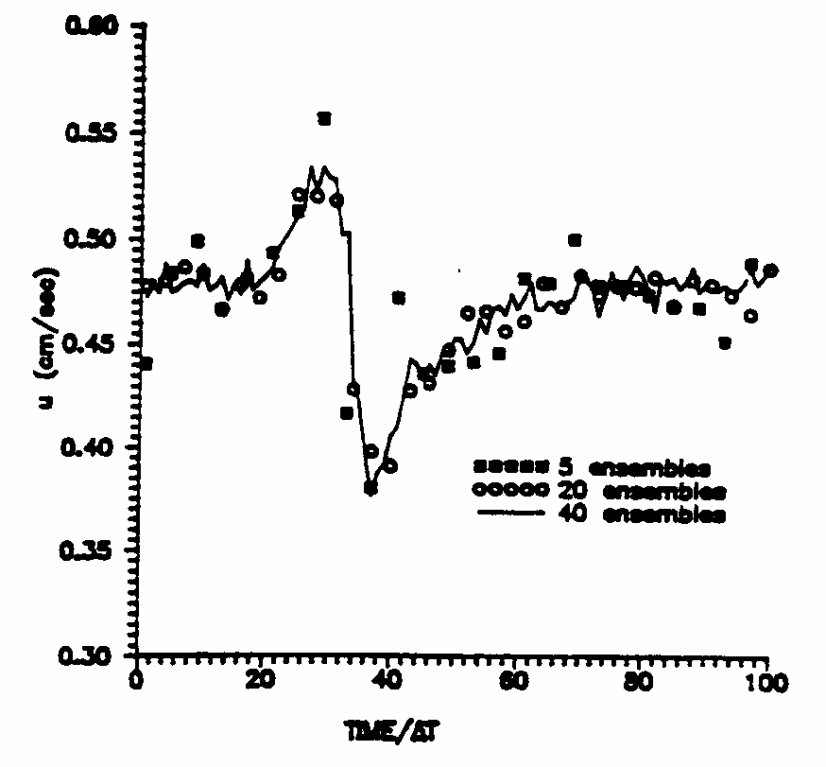

Figure 3.4. Effect of the number of ensembles per cycle on the waveform

Results and Discussion

Experiments were conducted at a free-stream velocity of 51 cm/s. The boundary layer was allowed to freely transition to a fully turbulent state. Data were obtained in the center plane of the tunnel and along normals to the plate. The boundary-layer thickness based on 99 percent recovery of the free-stream velocity and the momentum thickness were measured at $\delta = 14.0$ mm and $\theta = 1.837$ mm. The latter value corresponds to a Reynolds number of 913, while the Reynolds number based on the distance from the leading edge was $Re_L = U_\infty L/\upsilon = 2.98 \times 10^5$. In order to confirm the canonical nature of the turbulent boundary layer, the boundary layer thickness was calculated according to the empirical formula (White, 1984)

$$\frac{\delta}{x} = \frac{0.16}{\mathrm{Re}_x^{1/7}} \tag{4}$$

where $\bar{x}$ is the distance from the leading edge of the plate. At the origin of measurements, this yields a boundary layer thickness of 14.6 mm, which is very near the measured value of 14.0 mm. The quantities $\bar{u}$, u_{rms}, and v_{rms} were obtained for steady flow and compared to earlier measurements to confirm the reliability of the method (not displayed here due to lack of space). The same quantities averaged over cycles of the disturbance imposed display similar trends with those of undisturbed flow as shown in Figure 3.5, except that now the fluctuating components are approximately equal in magnitude, and the scatter is somewhat enhanced, requiring larger number of ensembles to arrive at converged profiles.

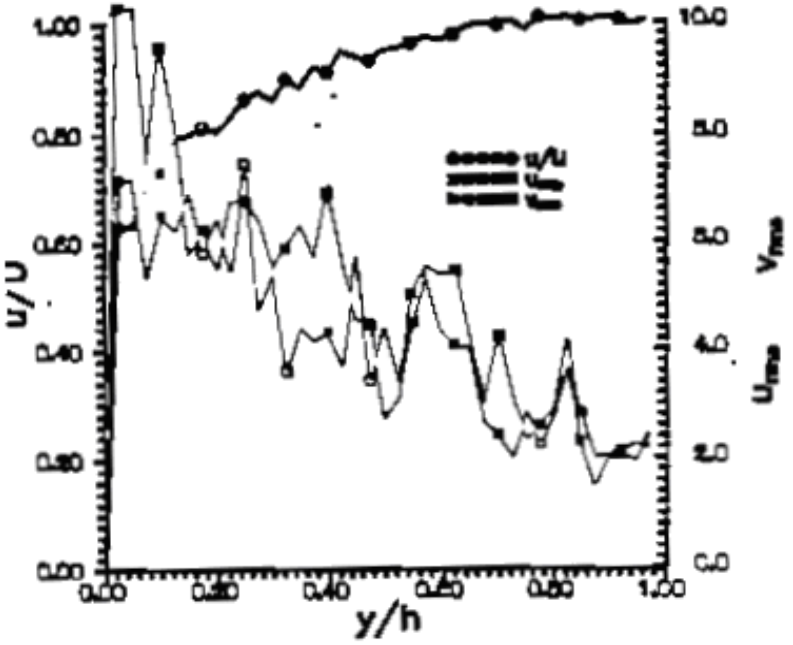

Figure 3.5. Mean velocity profile and fluctuating velocity components.

Data were obtained on 50 points along normals to the plate, along 10 stations for the 25.4 mm fence and 11 stations for the 12.7 mm and the 28.1 mm fences. The size of the fence and the approximate size of the vortical disturbance are of the same order. All distances were normalized with the chordlength of the fence. These data correspond to the same oncoming

turbulent boundary layer. The thickness of the boundary layer is therefore different if expressed in terms of the chord lengths of the plates.

Vorticity was calculated in terms of the measured velocity components. For an undisturbed boundary layer, the term *du/dy* is much larger than the term *dv/dx*. However, in the present case, this assumption is no longer valid in the presence of a large vortical disturbance. Our spacing is very fine in the *y* direction, so the term *du/dy* can be accurately calculated, but the estimation of the term *dv/d*x may involve considerable error. We estimated that the error in the calculation of vorticity may be as high as 30 percent of its corresponding maximum value. Nevertheless, we believe that vorticity thus calculated offers insight into the physics of the problem and for this reason, in the following figures we superimposed vorticity contours on the velocity vector fields.

Some understanding of the phenomena under consideration was gained by flow visualization. This was accomplished simply by releasing dye a little upstream of the plate. For very low speeds, the boundary layer was laminar and the dye streak was well defined. The motion of the dye was captured in a video tape. In Figure 3.6 we display a few instantaneous frames of visualization which indicate that a strong and tightly coiled vortex develops behind the fence. The vortex is then released but the dye, and quickly loses its coherence a few chordlengths downstream of the plate. It is not clear from the visualization if this is due to turbulence or to the fact that the vortex itself disintegrates.

Figure 3.6. Flow visualization of boundary layer vortex interaction

In Figure 3.7 we present ensemble-averaged velocity vectors downstream of the 12.7 mm fence, corresponding to seven phase angles or equivalently seven instants within the period of the motion. Superposed on these fields are vorticity contours. The boundary layer thickness in terms of dimensionless units based on the chord of the fence is approximately equal to 1.1. The height of the frame of data therefore is a little less than the thickness of the boundary layer. At the beginning of the phenomenon, not shown here, the disturbance has not yet entered the domain of observation. The field corresponds to the undisturbed turbulent boundary layer.

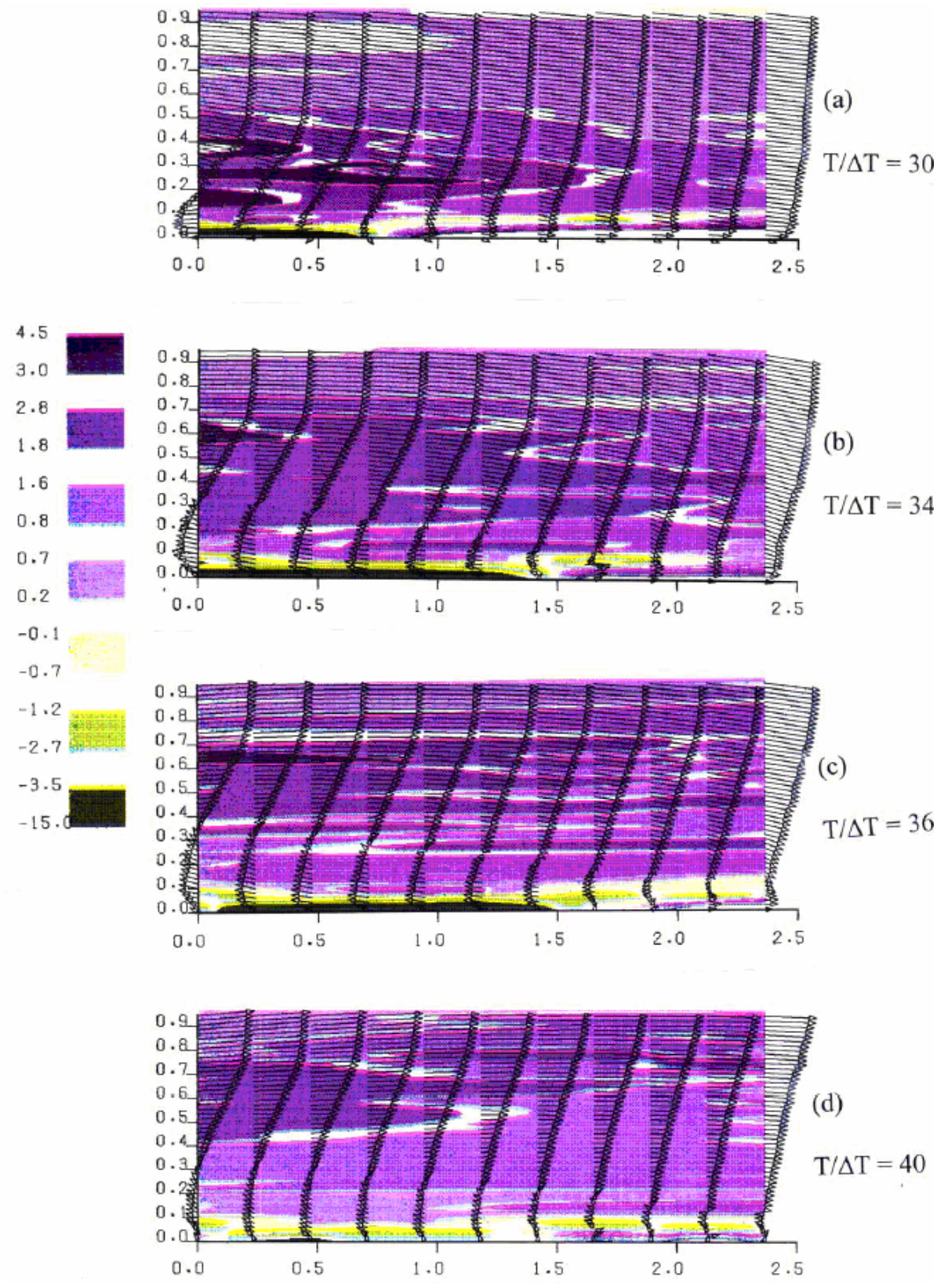

Figure 3.7. Velocity vectors and vorticity contours for C=12.7 mm at different times

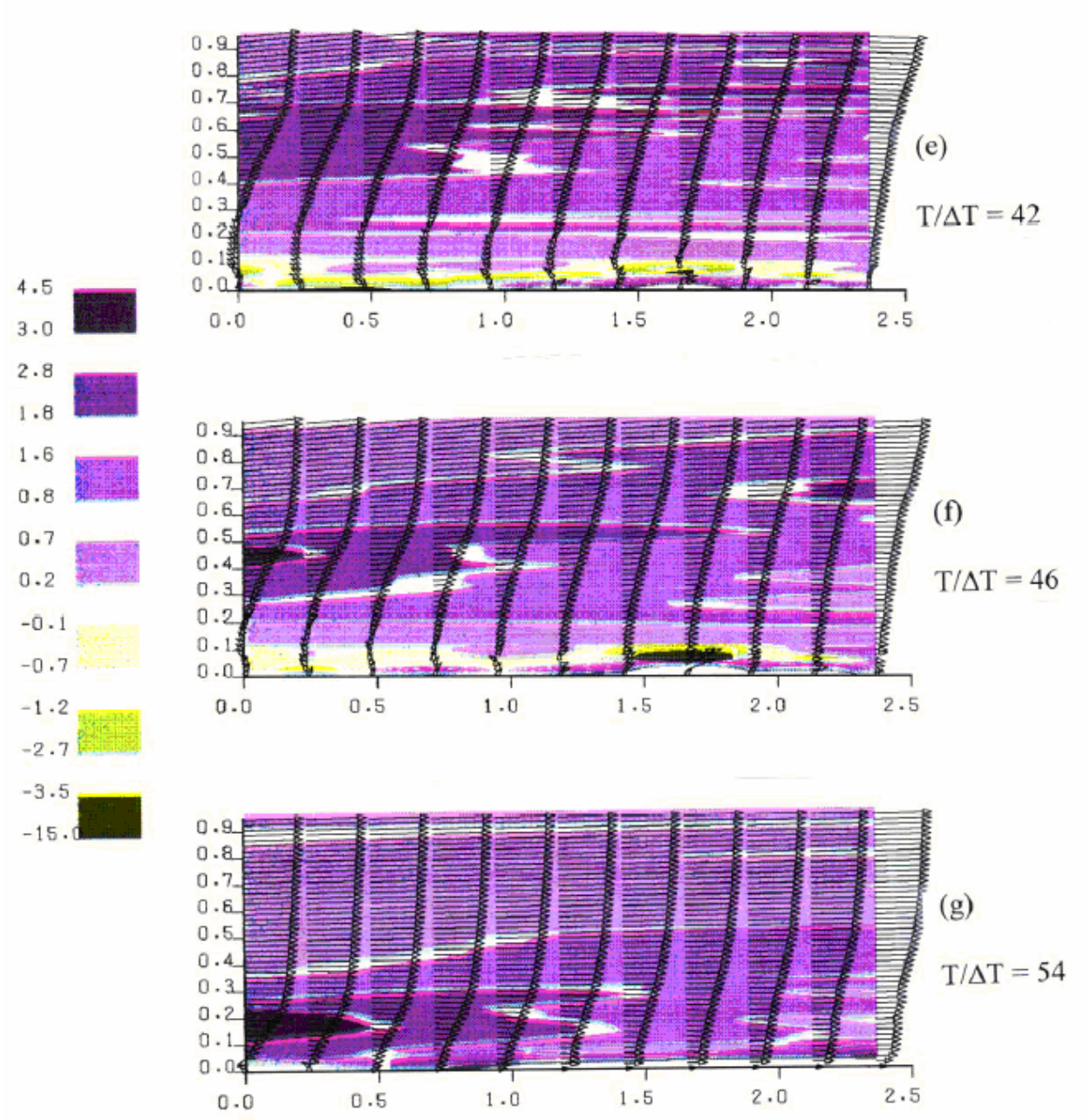

Figure 3.7. Continued

In Figure 3.7(a) the presence of the vortex is evident from the larger magnitude of vorticity as well as the appearance of reversed flow. Figure 3.7(a) corresponds to a dimensionless time of 30 for which the projected height of the fence is about 20 percent of its maximum. Note that vorticity of the opposite sense is present right next to the wall. In Figure 3.7(b) and (c) we observe that the vortex is moving more clearly into the domain of observation and the opposite

sign velocity is more evident. At this time, the disturbance on the velocity field has propagated over the entire domain of observation. However, the region with elevated vorticity does not propagate any further. On the other hand, vorticity of the opposite sign is creeping downstream at the bottom of the boundary layer. In the frame 3.7(d), which corresponds to time 40, we observe that the vorticity disturbance has practically disappeared but the reverse flow region is well-defined and extends beyond the domain of observation.

A good indication of the location of the center of the disturbance is the slope of the velocity vectors on the upper region of the domain of measurement. In the undisturbed flow, the directions of the velocity vectors are very nearly parallel to the wall. As the vortex enters this domain, the velocity vectors above its center slope upward and downward, upstream and downstream of its center, respectively. Figure 3.7 thus indicates that the vortex practically disintegrates by the time its center propagates to a dimensionless distance of about 1.0. The peak vorticity value is drastically reduced, the contours of vorticity are disconnected, disorganized and spread to an area much larger than originally occupied by the vortex. Moreover, flow reversal spreads to a considerable distance downstream and although the influence is weak, it covers the entire domain at $T/\Delta T = 46$.

At $T/\Delta T = 40$, the disturbance takes on the appearance of recirculating flow behind a backward facing step, because all velocity vectors are nearly parallel to the wall and the magnitude of the backward flow velocities is rather small. This is only reminiscent of the flow over an obstacle, because the projection of the fence normal to the wall by this time does not extend more than 0.05 units above the wall. In Figure 3.7(f) we observe that the velocity is further reduced along the entire field of measurement. This disturbance appears more like a dead-fluid region. And yet, the secondary vorticity survives intact and continues propagating

downstream. Apparently, the vortex disintegrates before it propagates more than one chordlength downstream of the fence. This is in qualitative agreement with the results of Nelson et al. (1990) who also examined the case of a vortex comparable in size with the thickness of the boundary layer.

Next we considered the case of a vortex approximately twice as large as the thickness of the boundary layer, generated by a fence with a chordlength equal to 25.4 mm. These results are not displayed here due to lack of space. A sequence of frames similar to Figure 3.7 indicates that the events are quite similar to the events with the small vortex. Vorticity is considerably dispersed and by the time $T/\Delta T$ = 38, vorticity contours do not indicate any coherence of a vortex. However, vorticity levels are considerably larger than the vorticity normally contained in a turbulent boundary layer.

Finally, we consider a fence with a chordlength of c = 38.1 mm. In the results presented in Figure 3.8, the boundary layer thickness corresponds to about 0.3 length units. The vortex now penetrates much further downstream into the domain of measurement. The net amount of vorticity decreases with time. The velocity vectors indicate that while on the left the flow is moving to the right all along the width of the domain, further downstream, there exists a recirculation region. The vortex therefore retains its character while convecting downstream. Notice also by comparison with Figure 3.7(e) that for the same time, the large vortex drifts much faster downstream than the small vortex, but its extent is constrained because the relative duration of the fence deployment is much shorter.

Only two components of the velocity were obtained here. Moreover, the data were conditionally averaged. It is therefore not possible to track the development of this three-dimensional vortical field in space and time. We offer here a physical picture of the phenomena

observed based only on the limited data and the analytical formulations that govern vorticity transport.

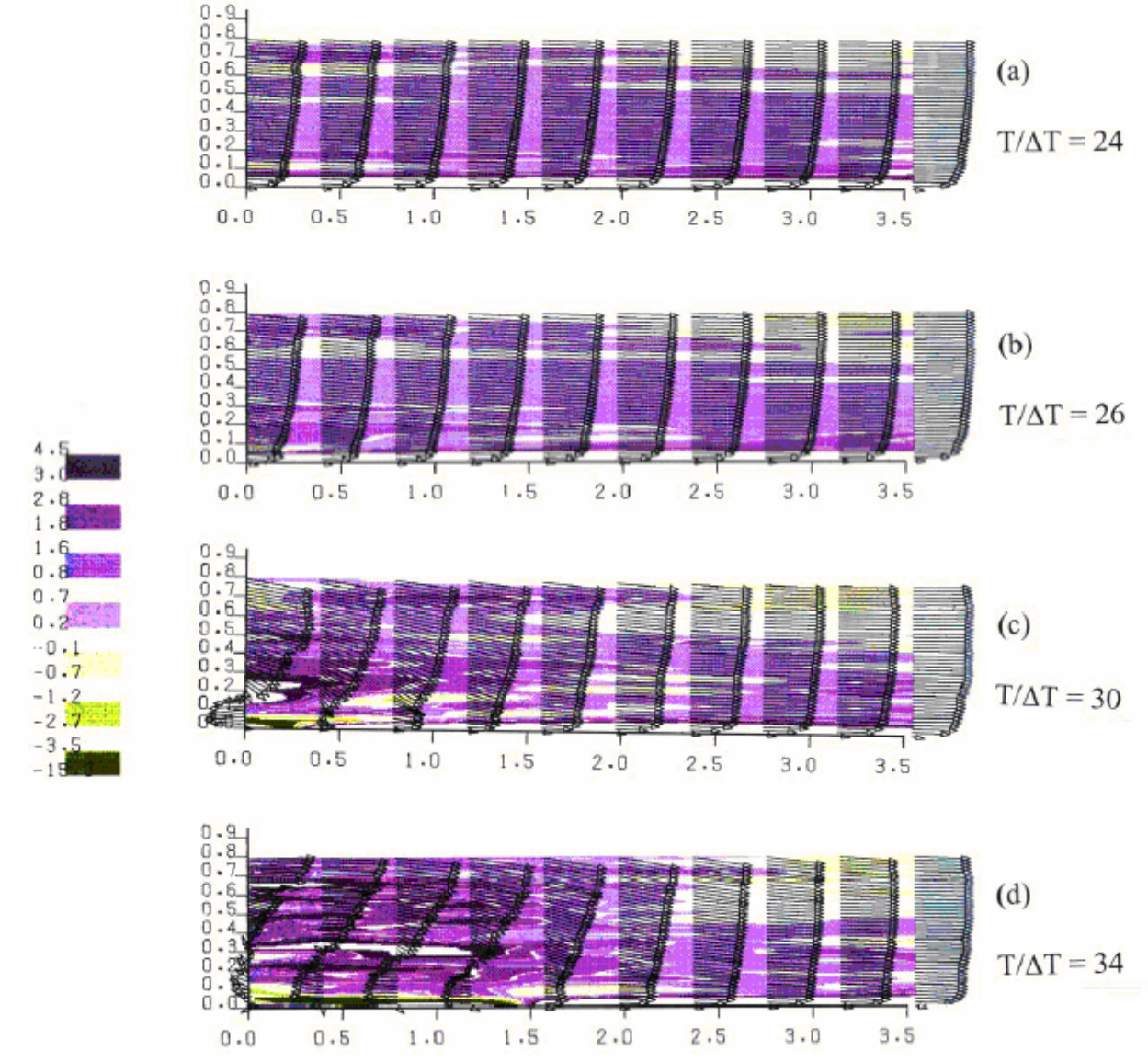

Figure 3.8. Velocity vectors and vorticity contours for C=38.1 mm at different times

The vorticity disturbance is created in our experiments in the form of straight vortex lines that are normal to the oncoming stream. The turbulent boundary layer though is dominated by random disturbances with a strong three-dimensional character which includes axial vorticity and locally swirling motions. As a result, the disturbance vortex lines which are convected with the

flow stretch locally in the downstream direction. This effect alone reduces the component of the vorticity which we measure.

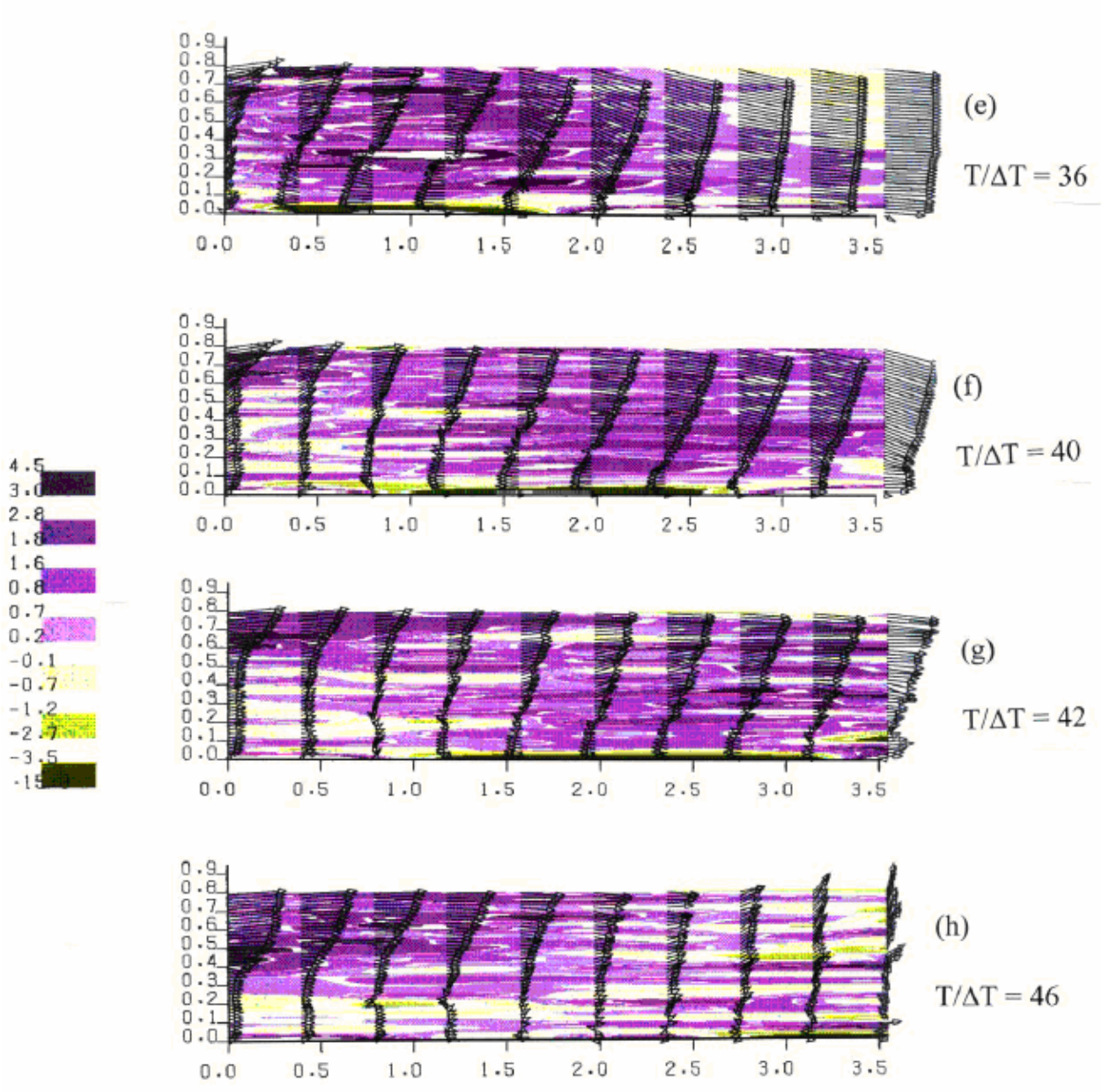

Figure 3.8. Continued

It is also possible that with great distortions of the vortex lines, vorticity disconnects and reconnects to form vortex rings (Kida and Takaoka, 1994) of which only cross-sections we capture by our measurement technique. These three-dimensional structures will bring vortex

filaments of opposite sense in close proximity and therefore will contribute to vorticity annihilation due to cross-diffusion by the mechanism described by Morton (1984) and later calculated by Kida et al. (1991). Turbulent diffusion is probably also responsible for the overall reduction of the measured levels of vorticity, because It transports vorticity outside the measuring domain, and also cascades it to smaller scales which are lost during our ensemble averaging procedure.

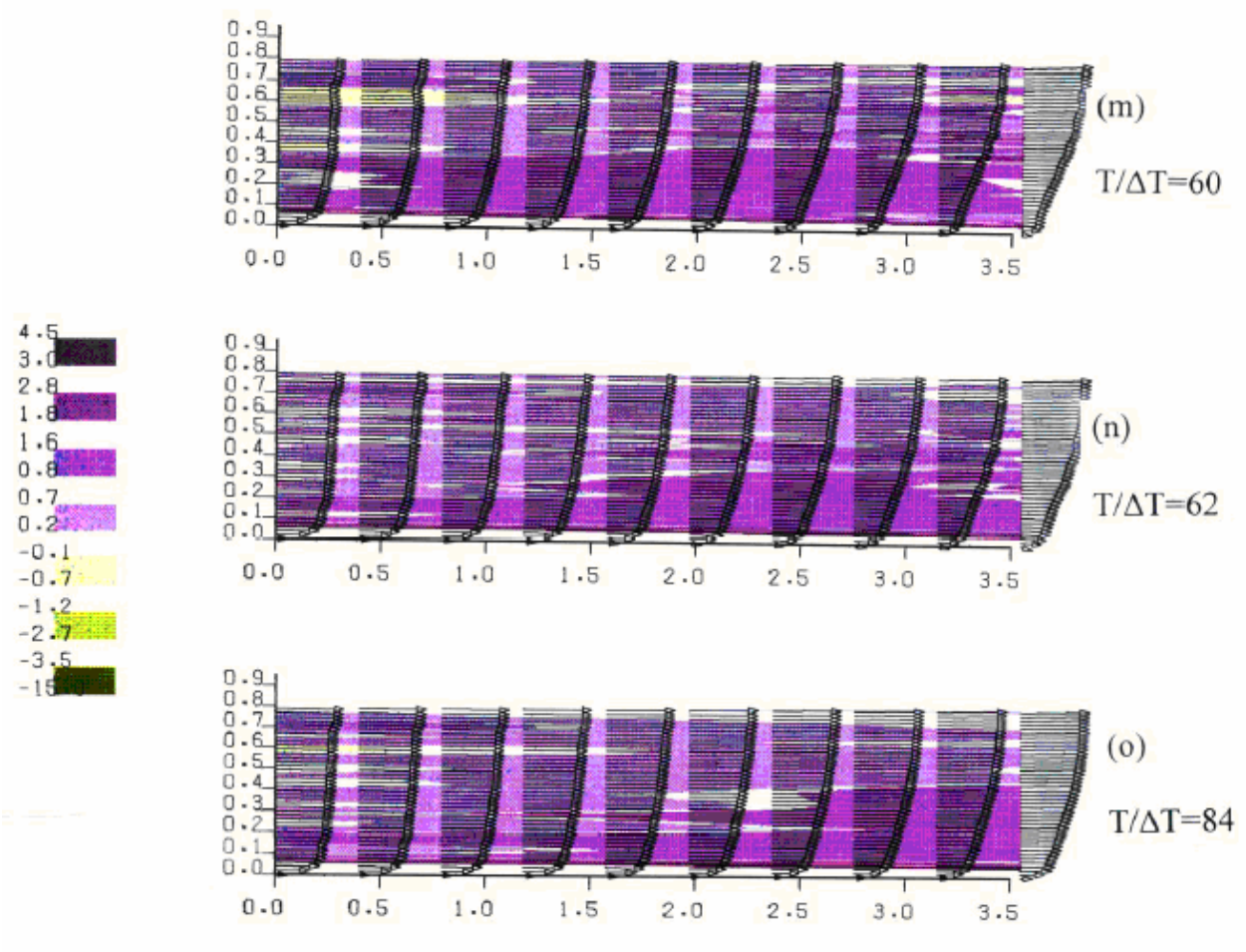

Figure 3.8. Continued

To examine more carefully the character of the disturbance, we plotted in Figures 3.9 through 3.11 the temporal variation of the *u*-component of the velocity at different elevations and *x*-stations.

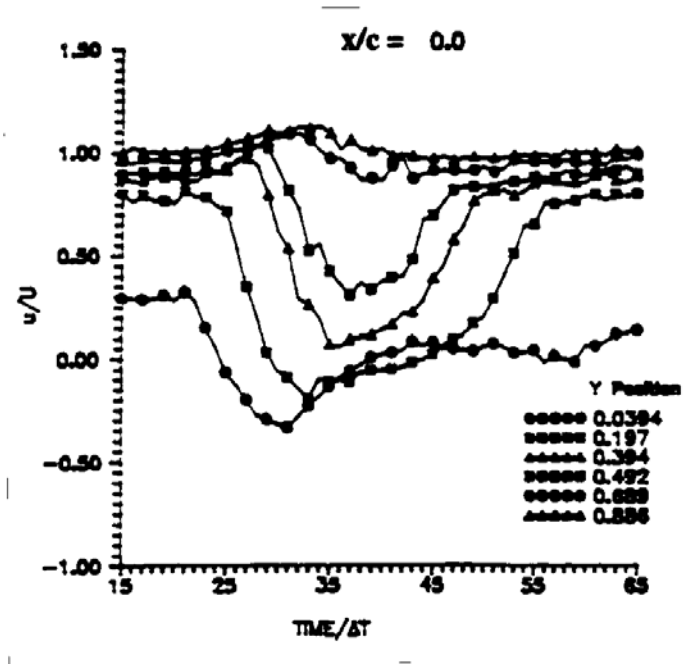

Figure 3.9. Temporal variation of the u-component of velocity at x/c=0 and different elevations, for a chordlength c=12.7 mm

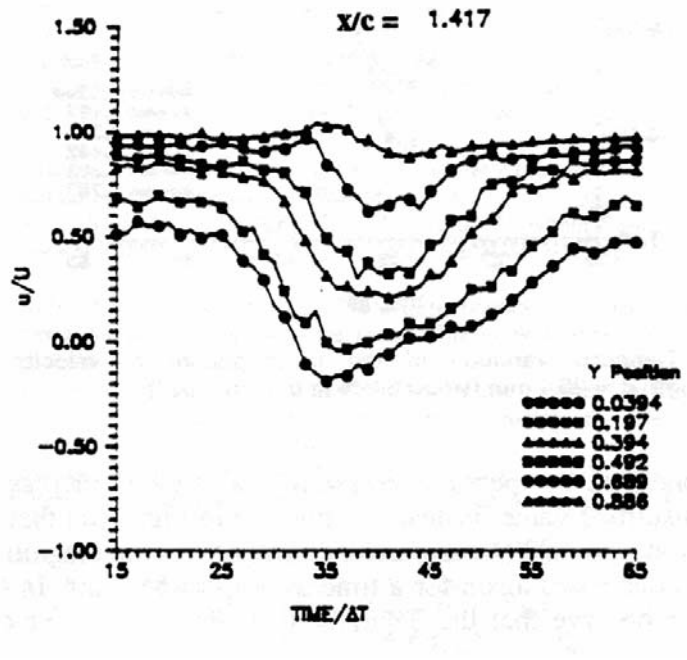

Figure 3.10. Temporal variation of the u-component of velocity at x/c=1.417 and different elevations, for a chordlength c=12.7 mm

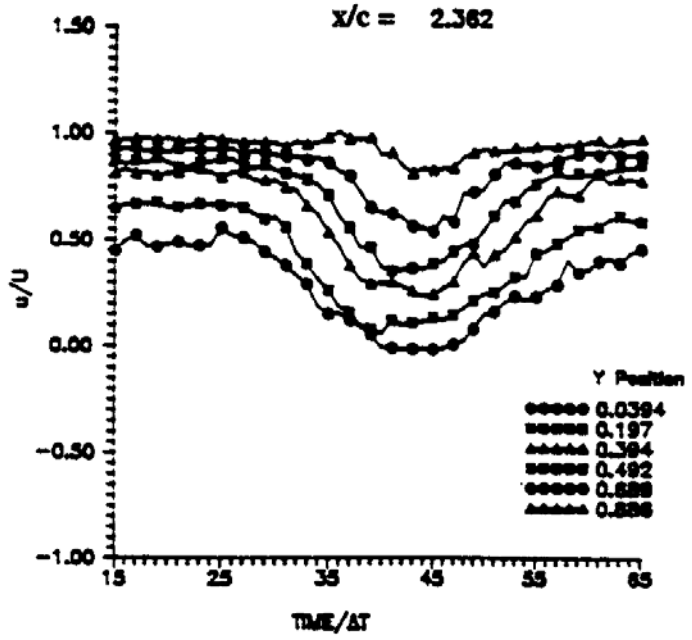

Figure 3.11. Temporal variation of the u-component of velocity at x/c=2.362 and different elevations, for a chordlength c=12.7 mm

If an ideal vortex is approaching a certain station, one would expect the velocity to increase above the center of the vortex and decrease below it. For an ideal vortex, the deviation from the undisturbed value should be the largest nearest the center. But if the vortex has a core with uniform vorticity, then within the core, the disturbance should be increasing with distance from the center. It appears from Figure 3.9 that the 12.7 mm fence creates a disturbance of the latter case, therefore a vortical core exists. In fact, we notice that the increase of the velocity at higher elevations is much smaller than the decrease of the velocity below it. Further downstream, at *x/c*= 1.417 the flow appears much more like a wake rather than a vortical disturbance. That is,

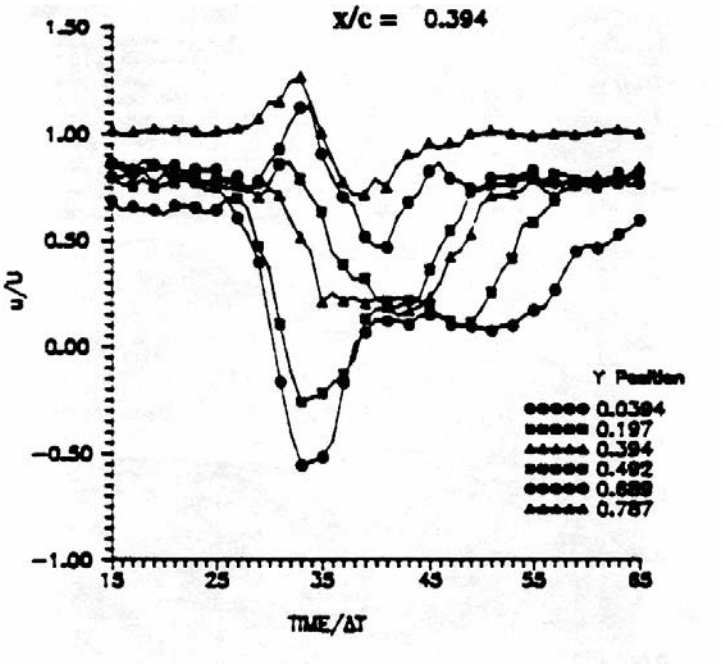

Figure 3.12. Temporal variation of the u-component of velocity at x/c=0.394and different elevations, for a chordlength c=38.1 mm

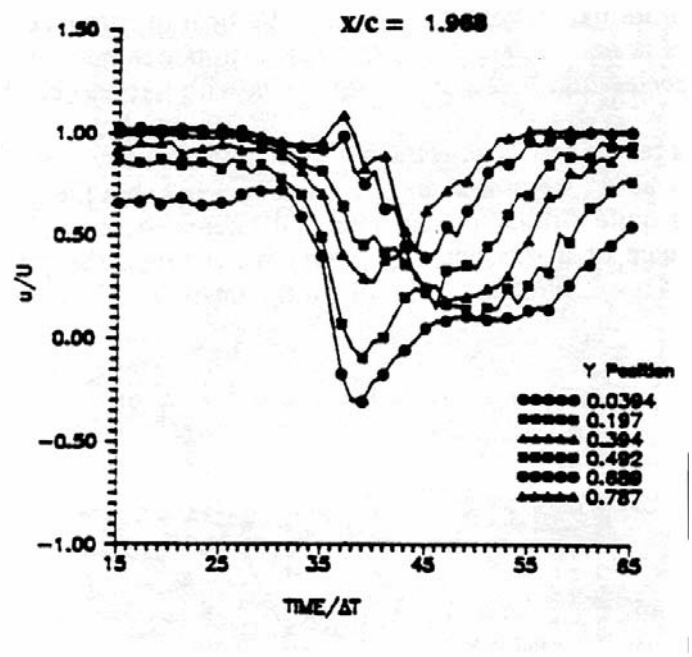

Figure 3.13. Temporal variation of the u-component of velocity at x/c=1.968 and different elevations, for a chordlength c=38-1 mm

there is no acceleration above the disturbance but considerable deceleration below it, in agreement with our earlier observation. A larger vortex displays a more pronounced increase of the velocity above its center as shown in Figure 3.12, but the general trend is quit similar in character. Of interest here is also the appearance of a secondary structure which trails the primary vortex. This is evident by the following behavior. At low elevations, one would expect a decrease followed by an increase to the undisturbed value. Instead we observe in Figure. 3.13 that the velocity at $y = 0.0394$ decreases first, regains some magnitude, but then decreases again for a time as long as 55 units. In Figure 3.13 we observe that the behavior is again reminiscent of a wake rather than a disturbing vortex. However, it is significant to note that now the velocity near the wall reverses its direction at distances much further downstream than in the case of the small fence.

Useful information is also contained in the temporal variation of turbulent kinetic energy. Turbulent kinetic energy contours were constructed and a few representative frames are presented in Figure 3.14. In the first frame we observe the levels of turbulent kinetic energy normally distributed in a steady turbulent boundary layer. This quantity decreases monotonically with distance from the wall and is independent of the axial distance. As the vortex enters the domain of measurement (Figures. 3.14(b) and (c)) a region of increased turbulent kinetic energy appears which coincides approximately with the region of high vorticity (see Figure 3.7). By the time $T/\Delta T = 32$, the high intensity turbulence level has spread across the entire field. Even though the coherence of the vorticity is by now virtually eliminated, the turbulence kinetic energy remains elevated and the distribution almost uniform across the entire boundary layer.

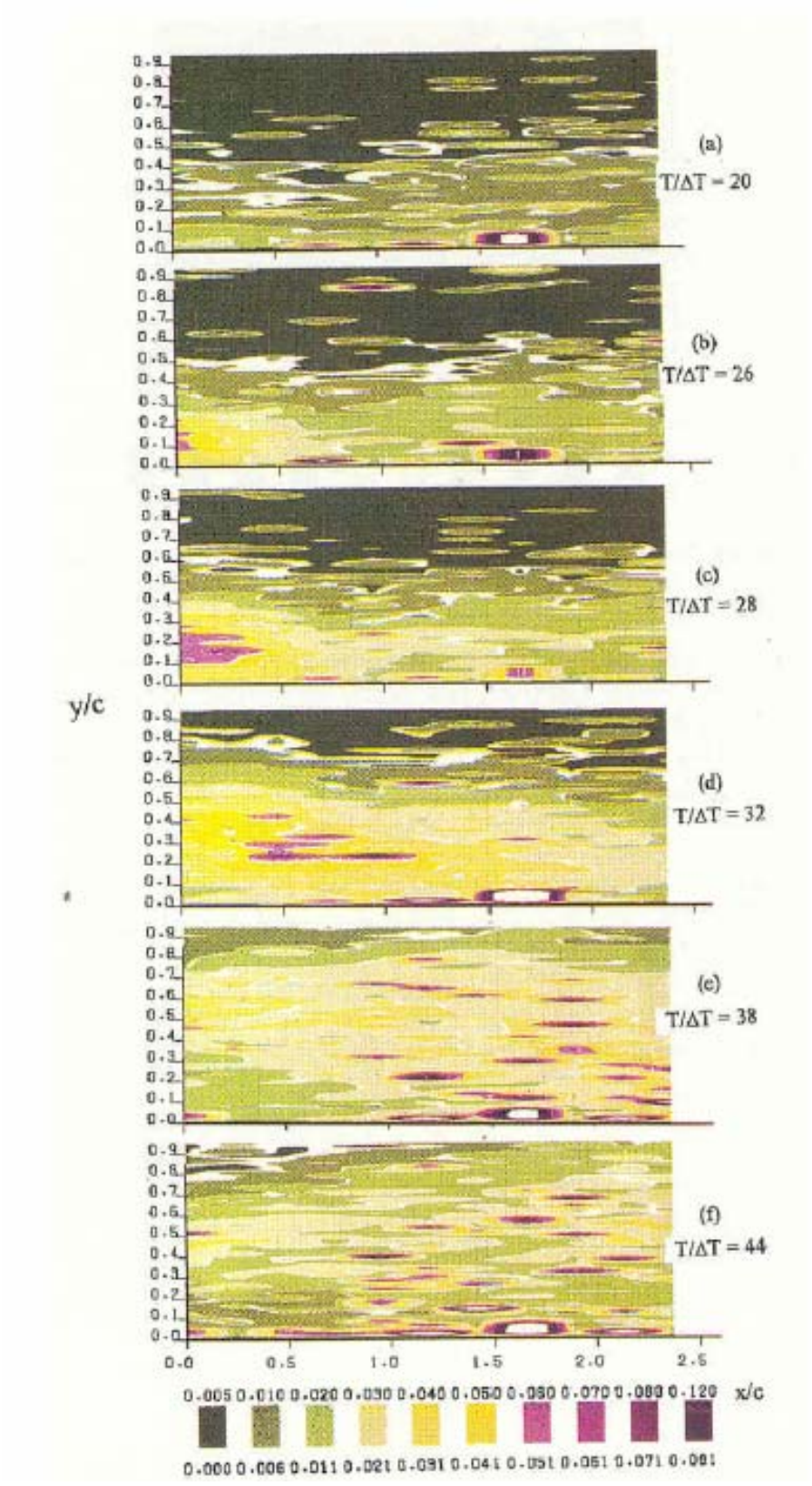

Figure 3.14. Turbulent kinetic energy contours for chordlength c=12.7 mm

Turbulent kinetic energy for the largest fence, c = 38.1 cm is displayed in Figure 3.15. The bulk of the turbulent energy which enters the domain and drifts downstream seems to be trailing the center of the disturbance. For example, at the time $T/\Delta T$ = 19 the center of the turbulent kinetic

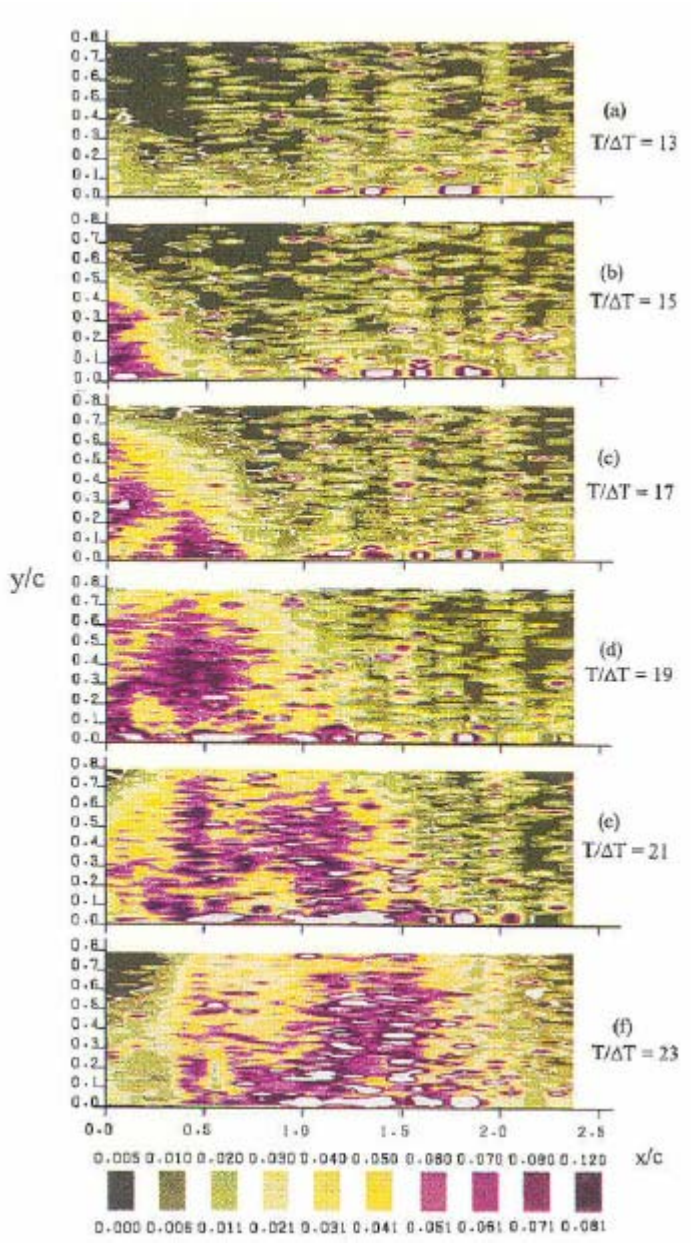

Figure 3.15. Turbulent kinetic energy contours for chordlength c=38.1 mm

energy appears to be a little upstream of $x/c = 0.5$ but in the corresponding frame of Figure 3.14, the center of the vortex is approximately at $x/c = 0.7$. It therefore appears that the vortex is lifting turbulence from the boundary layer. And yet, this mechanism could not account for the total amount of turbulence contained in the vortical structure. It therefore seems that vorticity in this vortical structure loses its organization and breaks down into turbulence. Eventually, the turbulent energy diffuses and passes out of the domain of measurement.

Conclusions

This experimental study indicates that a coherent spanwise vortex suddenly planted in the middle of a fully-developed turbulent boundary layer quickly loses its coherence if its size is comparable to the thickness of the boundary layer. At the beginning, up to two chordlengths downstream of its creation, it retains the character of a vortex with a viscous core. By the time the vortex drifts to three chordlengths downstream, its behavior is reminiscent of a wake behind a backward-facing step and by four to five chordlengths downstream, the effect of the disturbance has been practically eliminated.

For a disturbances about twice as large as the thickness of the boundary layer, the behavior is qualitatively similar. However, in this case, the identity of the vortex is preserved to a longer distance. The largest vortex tested, about three times the thickness of the boundary layer retains its character for the entire length of the measuring domain, but loses the coherence of its vorticity. On the other hand, the turbulence kinetic energy associated with the vortex experiences some diffusion, but its overall level appears to remain unaffected by the downstream drift. This indicates that vorticity in the vortex breaks down into turbulence which drifts downstream and leaves the domain of integration.

In all cases, the disturbing vortices appear to carry a higher level of turbulence than contained in the turbulent boundary layer. For the smaller vortex, turbulent kinetic energy quickly falls but in the case of the large vortex, the turbulence levels reach values as high as 25 percent. These high levels of turbulence are convected downstream with rather little diffusion and energize the mixing in the turbulent boundary layer for many chordlengths downstream.

Data Bank Contribution

The raw digital data obtained on this project are deposited to the JFE Data Bank. For the plates 12.7 mm and 26.5 mm, the data are presented for each integral value of $T/\Delta T$ in the range $0 < T/\Delta T < 40$ (see Figure 3.2). For each value of $T/\Delta T$, data are provided in columns corresponding to the four quantities x, y, u, and v. For the 38.1 mm plate, time records are provided for $20 < T/\Delta T < 40$. The files are organized in the same way. Enlarged and individual color figures are also deposited in the Data Bank.

Acknowledgments

The support of the Office of Naval Research under grant no. N00014-93-1-0264, Edwin Rood, monitor, is gratefully acknowledged.

References

Booth, E. R., Jr., and Yu, Y. C., 1986, ``Two-Dimensional Blade-Vortex Visualization Investigation,'' *AIAA Journal*, Vol. 24, pp. 1468-1473.

Booth, E. R., 1986, ``Surface Pressure Measurement During Low Speed Two-Dimensional Blade-Vortex Interaction,'' AIAA Paper No. 86-1856.

Consigny, H., Gravelle, A., and Molinaro, R., 1984, ``Aerodynamic Characteristics of a Two-Dimensional Moving Spoiler in Subsonic and Transonic Flow," *Journal of Aircraft*, Vol. 21, pp. 687-693.

Francis, M. S., Keesee, J. E., Lang, J. D., Sparks, G. W., and Sisson, G. E>, 1979, ``Aerodynamic Characteristics of an Unsteady Separated Flow,'' *AIAA Journal*, vol. 17, pp. 1332-1339.

Kida, S., Takaoka, M., and Hussain, F., 1991, ``Collision of Two Vortex Rings,'' *Journal of Fluid Mechanics*, Vol. 230, pp. 583-646.

Kothmann, B. C. and Pauley, W. P., 1992, ``Interaction of Unsteady Turbulent, Vortical Structures with a Turbulent Boundary Layer,'' AIAA Paper No. 92-0060.

Koromilas, C., and Telionis, D. P., 1980, ``Unsteady Laminar Separation – An Experimental Study,'' *Journal of Fluid Mechanics*, Vol. 97, pp. 347-384.

Littell, H. S., and J. K. Eaton, 1991, ``Unsteady Flowfield Behind a Vortex GeneratorRapidly Pitched to Angle of Attack,'' *AIAA Journal*, Vol. 29, pp. 577-584.

Macrorie, M., and Pauley, W. R., 1991, ``Experimental Developmeojnt of Spanwise Vortex Models with Streamwise Decay Due to Wall Interaction,'' AIAA Paper 91-2688.

Makita, H. K., Sassa, M., and Itabashi, A., 1989, ``Decay Processor of a Manipulated Large-Scale HorseshoeVortex in a Turbulent Boundary Layer,'' *AIAA Journal*, Vol. 27, pp. 155-160.

Mathioulakis, D. S. and Telionis, D. P., 1987, ``Velocity and Vorticity Distribution in Periodic Separating Flow,'' *Journal of Fluid Mechanics*, Vol. 184, pp. 303-333.

Morton, B. R., 1984, ``The Generation an Decay of Vorticity,'' *GeophysicoAstrophysics Fluid Dynamics*, Vol. 28, pp. 277-308.

Nagib, H. M., Reisenthel, P. H., and Koga, D. J., 1985, ``On the Dynamical Scaling of Forced Unsteady Flows,'' AIAA Paper No. 85-0553.

Nelson, C. F., Koga, D. J., and Eaton, J. K., 1990, ``Unsteady, Separated Flow Behind an Oscillating, Two-Dimensional Spoiler,'' *AIAA Journal*, Vol. 28, pp. 845-852.

Poling, D. R., Wilder, M. C. and Telionis, D. P., 1988, ``Two-Dimensional Interaction of Vortices with a Blade,'' AIAA Paper No. 88-0044.

Reisenthel, P. H., Nagib, H. M., and Koga, D. J., 1985, ``Control of Separated Flows Using Forced Unsteadiness,'' AIAA Paper No. 85-0556.

Shabaka, I. M. M. A., Mehta, R. D. and Bradshaw, P., 1985, ``Longitudinal Vortices Imbeddedin Turbulent Boundary Layers, Part 1, Single Vortex,'' *Journal of Fluid Mechanics*, Vol. 155, pp. 37-57.

Wilder, M. C., Pesce, M. M., Telionis, D. P., Poling, D. R., and Dadone, L., 1990, ``Blade-Vortex Interaction Experiments – Velocity and Vorticity Fields,'' AIAA Paper No. 90-0030.

White, F. M., 1974, *Viscous Fluid Flow*, McGraw-Hill, 2nd Edition, New York.

CHAPTER 4

The Three-Dimensional Character of the Interaction of Large Rollers with a Free Surface

Abstract

Trailing edge vortices are generated in a water tunnel by sharp hinged motions of a flap. These vortices are allowed to reconnect with the free surface and mix with a turbulent free shear layer. The flow is conditionally sampled via frame grabbing of free surface shadowgraphs. Laser-Doppler velocimetry is employed to map out the velocity fields at different elevations. It is found that the vortex core bends away from the plane of the shear layer. Moreover, contrary to earlier findings, organized velocity fluctuations decrease as the free surface is approached.

Introduction

The fluid mechanics of the interaction of vorticity and free surface is one of the few mechanics phenomena which remained unexplored until very recently. Ground was broken in this direction in the 1980's. Sarpkaya (1986) identified the basic elements of the free surface disturbances generated by stationary pairs of vortices parallel to the free stream. The first convincing demonstration that a vortex tube will disconnect in the vicinity of the surface and reconnect to the surface was provided by Bernal and Kwon (1989). The basic principles of vortex reconnection can be found in Kida and Takaoka (1994) and Hussain Melander (1993). A number of problems involving the interaction of discrete vortical structures with a free surface

have been investigated. Typical problems involve a pair or a single vortex with axis parallel to the free surface (Sarpkaya et al. 1988, Sarpkaya and Suthon 1990, 1991), a jet with its axis parallel to the free surface (Anthony and Willmarth 1992) or a pair of parallel linear vortices drifting towards to free surface (Marcus and Berger 1989, Willmarth et al. 1989, Willert and Gharib 1994). The most interesting feature of such flows, vortex reconnection with a free surface can be best demonstrated and studied by allowing vortex rings to approach a free surface along a path inclined with respect to the latter (Bernal and Kwon 1989, Gharib et al. 1992, Gharib 1994). Extensive numerical calculations of such problems have also been carried out as for example Ohring and Lugt (1989), Yu and Tryggvason (1990), Kommermuth Yue (1990), Swean et al. (1991). A crucial element in the peculiar physics of vorticity/free-surface interaction is that vorticity can actually escape from the free surface. Rood (1994a,b) indicates how the vorticity component parallel to the surface can be balanced with the surface particle acceleration and thus removed from the field. Gharib (1994) provides experimental evidence to this effect.

A variety of experimental methods have been employed but the reconnection problem has been explored only with flow visualization and particle image velocimety. In the present paper we study another vortex reconnection problem, namely the mechanics of a trailing-edge vortex drifting with its axis normal to the free surface. In this investigation we employ laser-Doppler velocimetry to map out the field at different elevations.

The interaction of turbulence, mostly in the form of turbulent boundary layers with a free surface has also been investigated (Komori et al. 1982, Lam and Banerjee 1988, Rashidi and Banerjee 1988, Swean et al. 1989, Longo et al. 1983, Stern et al. 1994). Here we consider the coherent vortex embedded in a fully-developed turbulent shear layer. In most earlier studies,

both analytical and numerical, assumptions or provisions are made respectively for the free surface disturbances to be small. This is not a limitation in this study. In fact, we aimed at studying the interaction of vortices with a free surface that can deform without limitations. The surface depression in the cases we studied is the order of magnitude of the diameter of the core of the vortex.

In the following sections we discuss briefly the facilities and the instrumentation employed. We then describe how the drifting of a vortex can be captured by triggering laser-Doppler measurements via a shadowgraph and a frame grabbing system. We reconstruct velocity fields and also present the temporal variation of ensemble-averaged velocity fluctuations.

Facilities and Instrumentation

Work was conducted in a free-surface water tunnel. This is a facility constructed by Engineering Laboratory Design, Inc., and installed in 1995 in the Engineering Mechanics Fluids Laboratory. The water tunnel operates in a closed loop, with up to 25,000 lbs of water. It is fabricated of a composite lamination of fiberglass-reinforced plastic and clear, acrylic Plexiglass. It is driven by a 4500 GPM, 20 HP axial flow pump. Its settling chamber is followed by a three-way convergence that leads into a 24" × 24" × 72" (61 cm × 61 cm × 183 cm) test section.

A TSI two-component laser-Doppler velocimetry (LDV) system was employed. Here LDV provides much greater frequency response than PIV (Particle-Image Velocimetry). The optical components of the system were arranged on an optical bench so that the beams can be directed into the test section via mirrors either from the bottom as shown in Figure 4.1, or from the side of the tunnel. The mirrors are mounted on traversing scales and their motion is

controlled by stepping motors. The laboratory computer controls the traversing of the measuring volume by pulses that are sent to the stepping motors.

Of the three beams one is shifted by 40 MHz, a second is shifted by 60 MHz and the third is unshifted. The Doppler signals are received by a single photomultiplier, separated by filters and processed by two TSI counters. The data acquisition process is fully automated. A measuring grid is defined by the user. The computer then directs the displacement of the measuring point along the nodes of the grid, receives the LDV data, performs some elementary operations like phase locking and ensemble averaging, and stores the data.

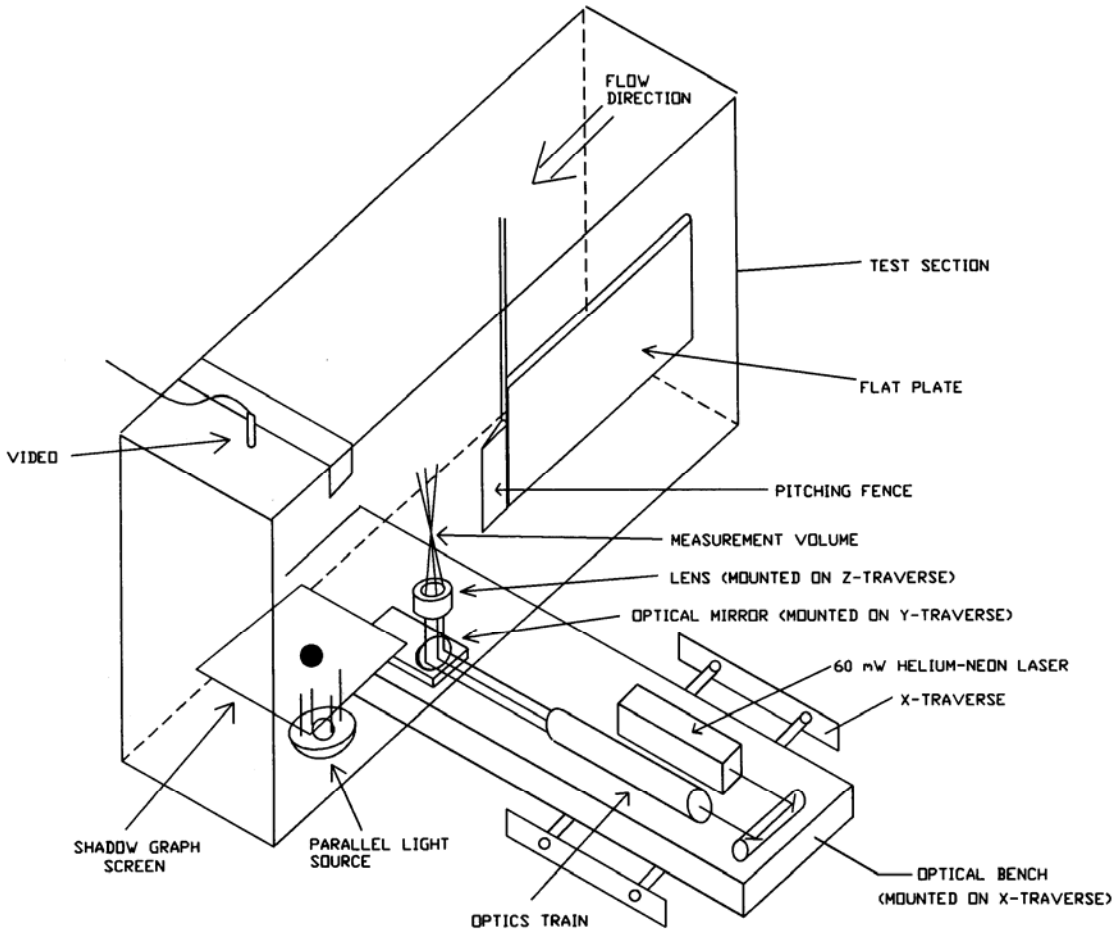

Figure 4.1. The test section – the model and the experimental rig.

To monitor the motion and insure repeatability, a frame grabber was also installed. A shadowgraph system was rigged, by directing parallel light from the bottom of the test section and normal to the free surface. Light passing through the free surface deformations was projected on a translucent screen which was positioned parallel to the free surface. A video camera was placed above the test section, aiming in a direction perpendicular to the screen as shown in Figure 4.1. Images were captured and digitized. This information was analyzed via image-processing software prepared for this purpose and the results were communicated with the data acquisition software. The procedure will be described in greater detail in the next section.

Experimental Procedure

A flat plate was positioned parallel to the stream and normal to the free surface as shown schematically in Figure 4.2. At the downstream edge of the plate, a flap with a chord of 38.1 mm was hinged which was controlled by a stepping motor. The span of the flap was 19 mm shorter than the depth of the water free surface. A flap reaching or penetrating the free surface would create surface waves which would interfere with the vortex surface signature. It was found that positioning the flat tip beneath the surface greatly reduced surface waves. On the other hand, the vortex generated by the motion of the flap quickly connected with the free surface.

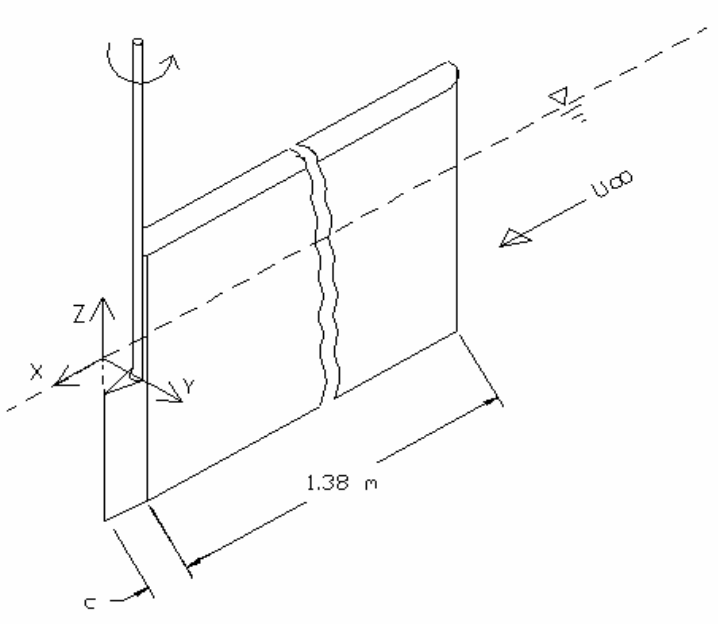

Figure 4.2. Schematic of flat plate and pitching fence.

Along cross-sectional planes parallel to the free surface, the flow field can be represented schematically as in Figure 4.3. The vortices thus generated were immersed in the fully developed turbulent shear layer of the flat plate. The temporal variation of the flap inclination contained a sharp increase to generate a strong vortex and a slower return to the initial position to avoid generating more disturbances. Just a few chordlengths downstream of the edge of the flap, a depression in the surface of the water appeared, which displaced downstream and survived for at least 10 flap chordlengths. This depression represents the reconnection of the vortex generated by the flap and was recorded on the shadowgraph screen. Typical instantaneous shadowgraphs capturing the passage of the vortex are shown in Figure 4.4

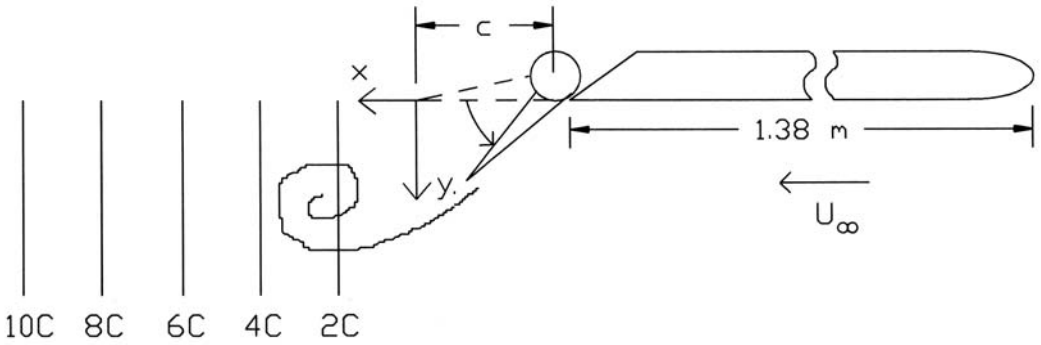

Figure 4.3. Top View of Fig 4. 2 with data acquisition locations indicated.

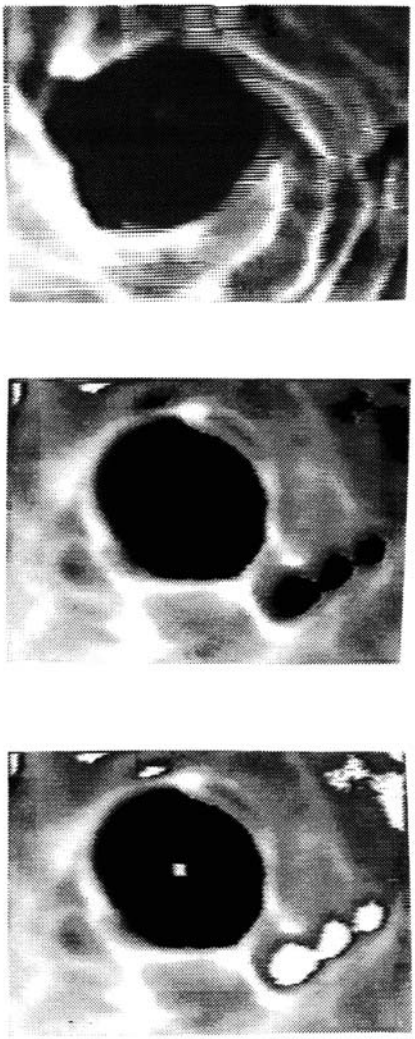

Figure 4.4. A sequence of instantaneous shadowgraph frames capturing the free-surface vortex depressions.

The experiments were controlled by two computers. The aim was to generate repeatable realizations of the motions, and then ensemble averages of the measured quantities. The automatic procedure was the following (see Figure 4.5). Computer PC1 sends a message to computer PC2 to initiate the motion. Computer PC2 in turn sends a pulse to the flap mechanism to generate a vortex. Computer PC1 grabs a frame at a specified time after the initiation of the motion. This is obtained by a shadowgraph via the video camera (Figure 4.1).

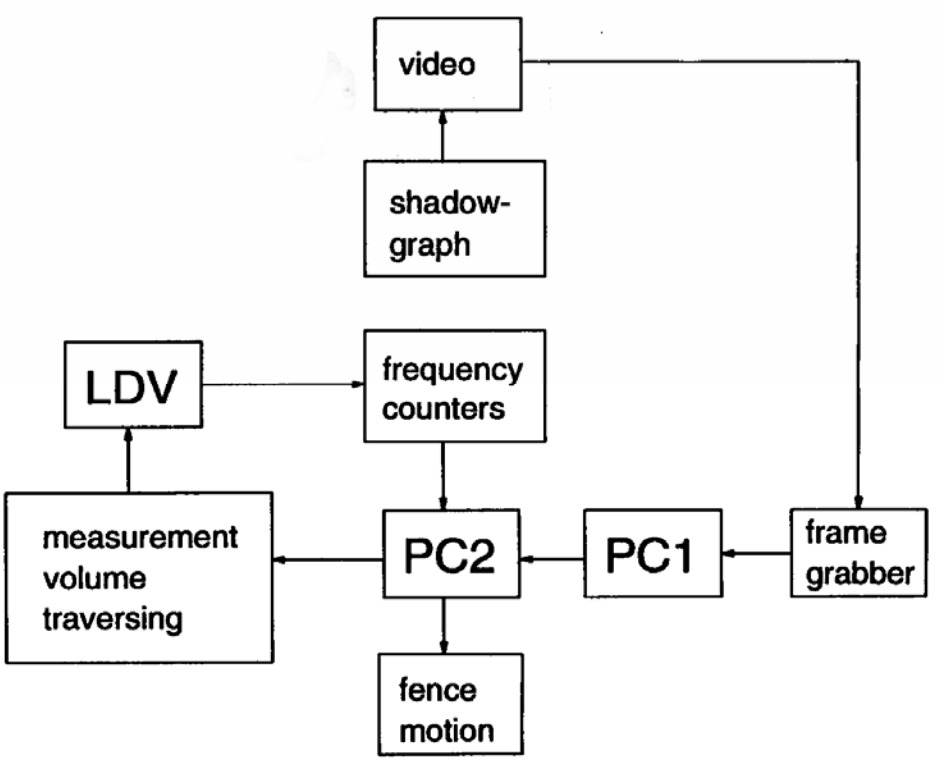

Figure 4.5. Data Acquisition/Peripheral communication diagram.

We wrote a program to process these optical data. PC1 then searches for dark areas, eliminates noise by virtue of logic built into the software, zeros in to the vortex image and calculates its centroid. The coordinates of the centroid are checked against earlier data and if found to be consistent, then PC1 sends an affirmative signal to PC2. The latter in the meantime has collected the temporal variations of two components of the velocity. If the coherence of the vortex is

weak, or if the coordinates of the centroid are not consistent with earlier data, the velocity values are discarded. In this way, twenty realizations are obtained at each point in space and ensemble averaged on line. Computer PC2 then orders a displacement of the measuring volume to another point in space and the process is repeated. In this way a three-dimensional grid is traced, and velocity component time series at each point are stored. Measurements were carried out with beams entering the test section from the bottom of the test section and later from the side, thus generating all three components of the velocity at each point.

Results and Discussion

Measurements were made along lines parallel to the y axis, namely in the direction normal to the plane of the plate, at five distinct elevations, namely z/c = -0.131, -0.262, -0.5, -1.67, -2.25, where c is the chordlength of the flap. Such measurements were obtained along five stations, at distances $x = 2c$, $4c$, $6c$, $8c$, and 10 c, as shown in Figure 4.3. Increments along the y direction were chosen to be Δy = 2 mm and data were obtained along 30 points in the y direction.

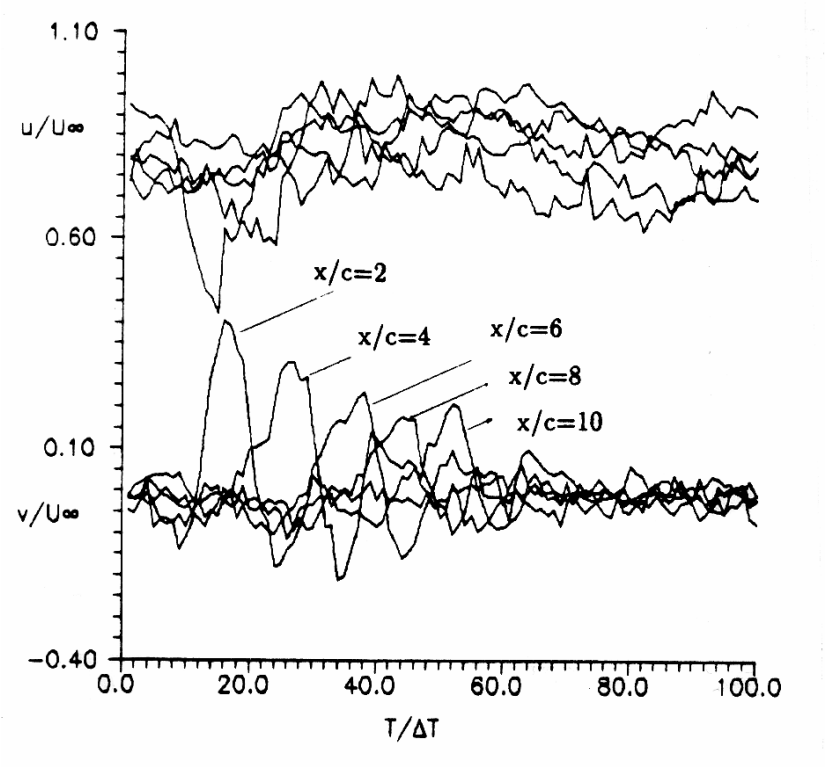

Figure 4.6. Temporal variations of the non-dimensional u and v components of velocity y/c = 0.052c, z/c = -5.01.

Typical results of time records are presented in Figures 4.6-4.8. In Figure 4.6 we display temporal records of the *u* and *v* components of the velocity at a distance of y=0.052 *c* from the plane *xz*. The familiar oscillation which indicates the passage of a vortex is apparent in the component parallel to the stream. The random character of the field at this location is also evident. This point is well within the turbulent free shear layer which is released from the trailing edge of the plate. In Figures 4.7 and 4.8 we display results obtained at y = 0.525 at distance z/c = -0.5 and -1.167 from the free surface,.

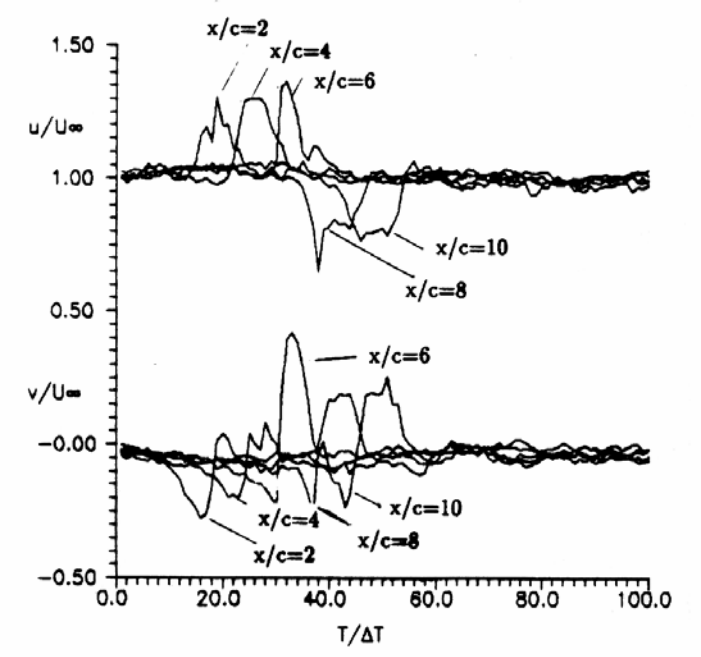

Figure 4.7. Temporal variations of the non-dimensional u and v components of velocity y/c = 0.525c, z/c = -0.5.

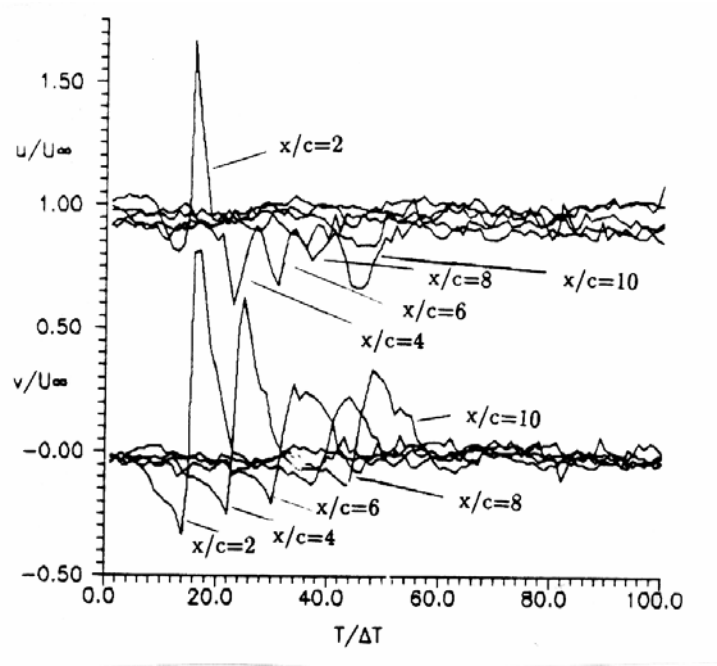

Figure 4.8. Temporal variations of the non-dimensional u and v components of velocity at y/c = 0.52, z/c = -1.167.

Now the background noise of the random fluctuations is considerably reduced. But surprisingly, the character of the vortex is distinct even if it is embedded in turbulence. Here another interesting phenomenon appears. In Figure 4.7 the signature of the vortex in the u component is reversed in the middle of the downstream distance. This implies that the vortex is crossing the y coordinate of 20 mm as it drifts in the downstream direction. In fact, inspecting the profiles of Figure 4.8, corresponding to point at a larger depth, we recognize that the change of the behavior and therefore the crossing of the core of the vortex occurs sooner, that is closer to the edge of the plate where vorticity is released. This implies that the axis of the vortex is not normal to the free surface, even though the generator edge is.

More descriptive of the vertical motion and more clearly indicating the position of the core are figures displaying quasi-two-dimensional velocity fields. The idea is the following. The free-stream velocity vector is first subtracted from all local velocity vectors. Velocity vectors in xy planes along a x = const line are then plotted next to each other for consecutive instants. This creates the impression of a two-dimensional vector field. This representation would be perfectly accurate if Taylor's hypothesis were valid. In the present case the figures that follow simply allow the reader to visualize the temporal variation of the velocity vectors. The horizontal axis is essentially time, increasing in the right-to-left direction.

In Figures 4.9 and 4.10 we display velocity vector fields for distances $x = 2c$ and $10c$ respectively. The z-component of the velocity is displayed in these figures in the form of color contours. The vertical motion of flow is now apparent. Moreover, it appears clearly that the vortex deviates in the spanwise direction as it drifts downstream. In fact, it appears as if its axis bends in a bow-like manner, displacing away from the x, z plane. This effect is more pronounced

away from the free surface. Very near the surface, no vortical motion is evident, because the velocity field is dominated by surface waves.

Quite interesting is also the fact that for small distances x, the center of the cross-section of the vortex is displaced in the axial direction as well. This represents a bending in a plane parallel to the x, z plane, which may be due to the reconnecting process because it is eliminated further downstream.

The vertical component of the velocity, i.e., the component normal to the oncoming stream indicates another unexpected pattern. Spanwise vortices like the vortices shed over cylindrical bodies placed normal to a stream sustain a considerable amount of axial motion in their core. But in the present case, the spanwise motion is outside the core. Moreover, the spanwise motion seems to be balanced, with positive z-component velocities ahead of the vortex and negative velocities behind it.

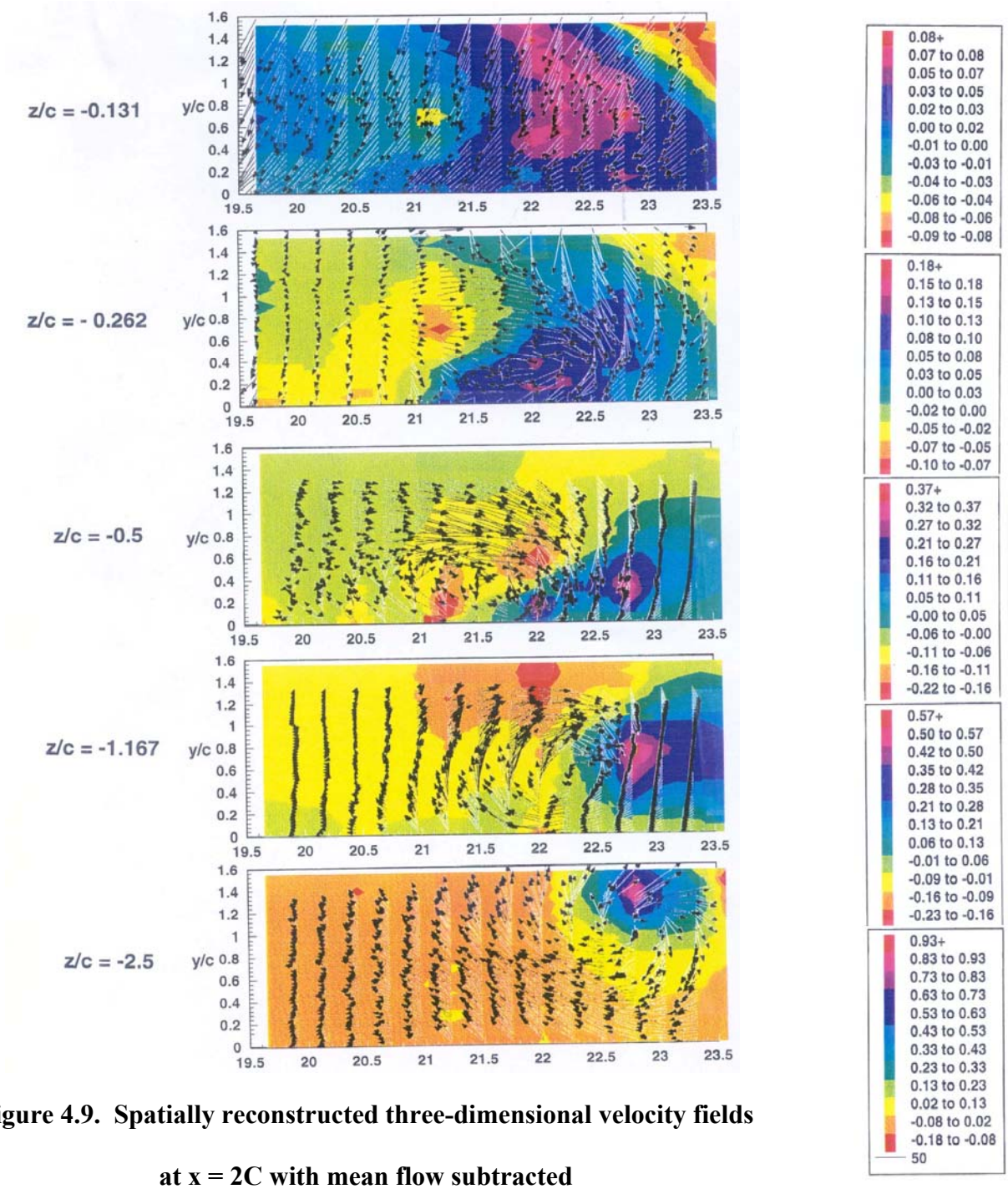

Figure 4.9. Spatially reconstructed three-dimensional velocity fields at x = 2C with mean flow subtracted

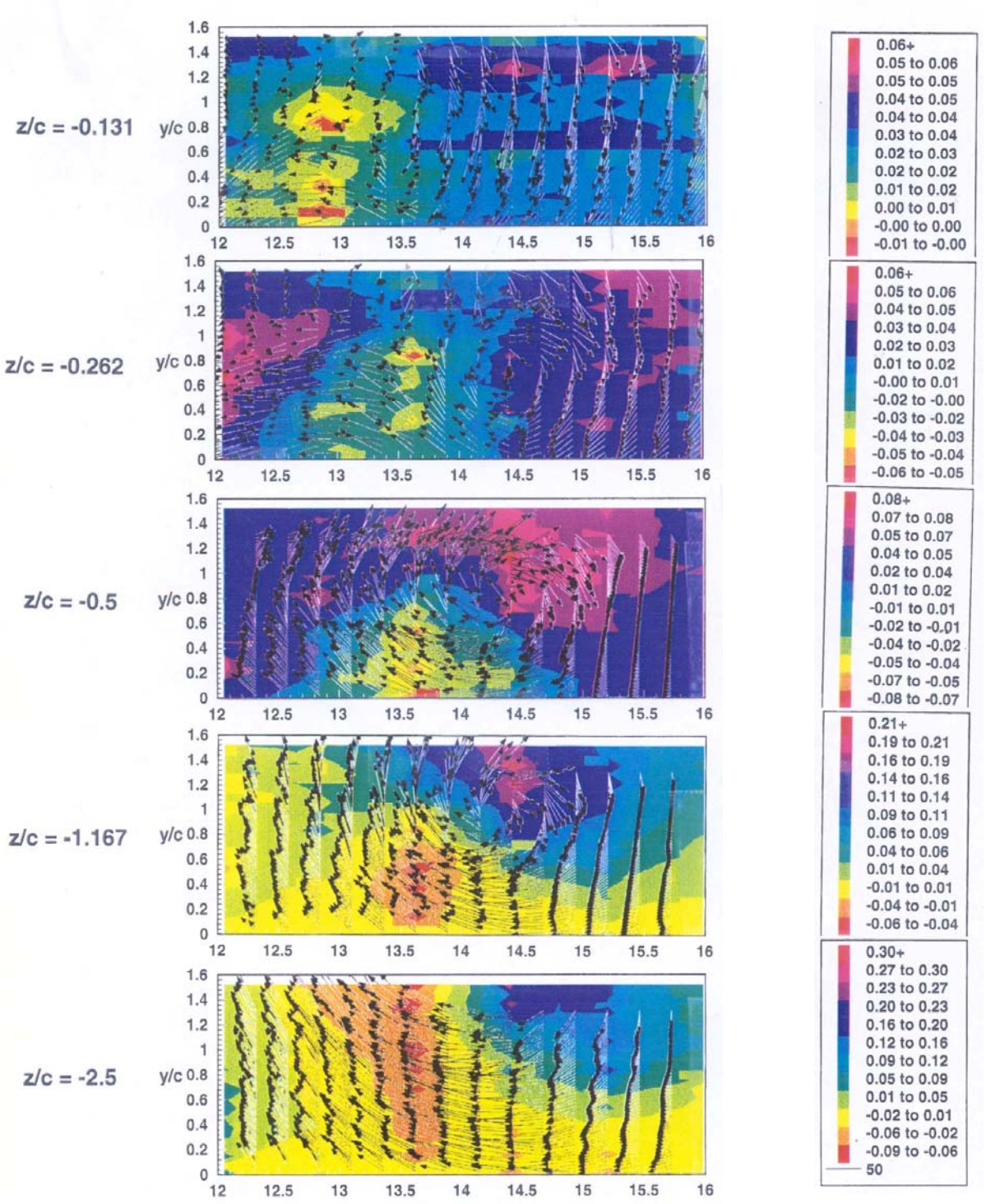

Figure 4.10. Spatially reconstructed three-dimensional velocity fields at x = 10C with mean flow subtracted.

In Figures 4.11 and 4.12 we display ensemble averaged RMS of the fluctuations in the *u*-component of velocity at different elevations. Here we observe that the fluctuation of the component parallel to the surface increases towards the surfaced and the normal component decreases in qualitative agreement with earlier measurements on turbulent fluctuations. However, the trend is reserved with increasing depth.

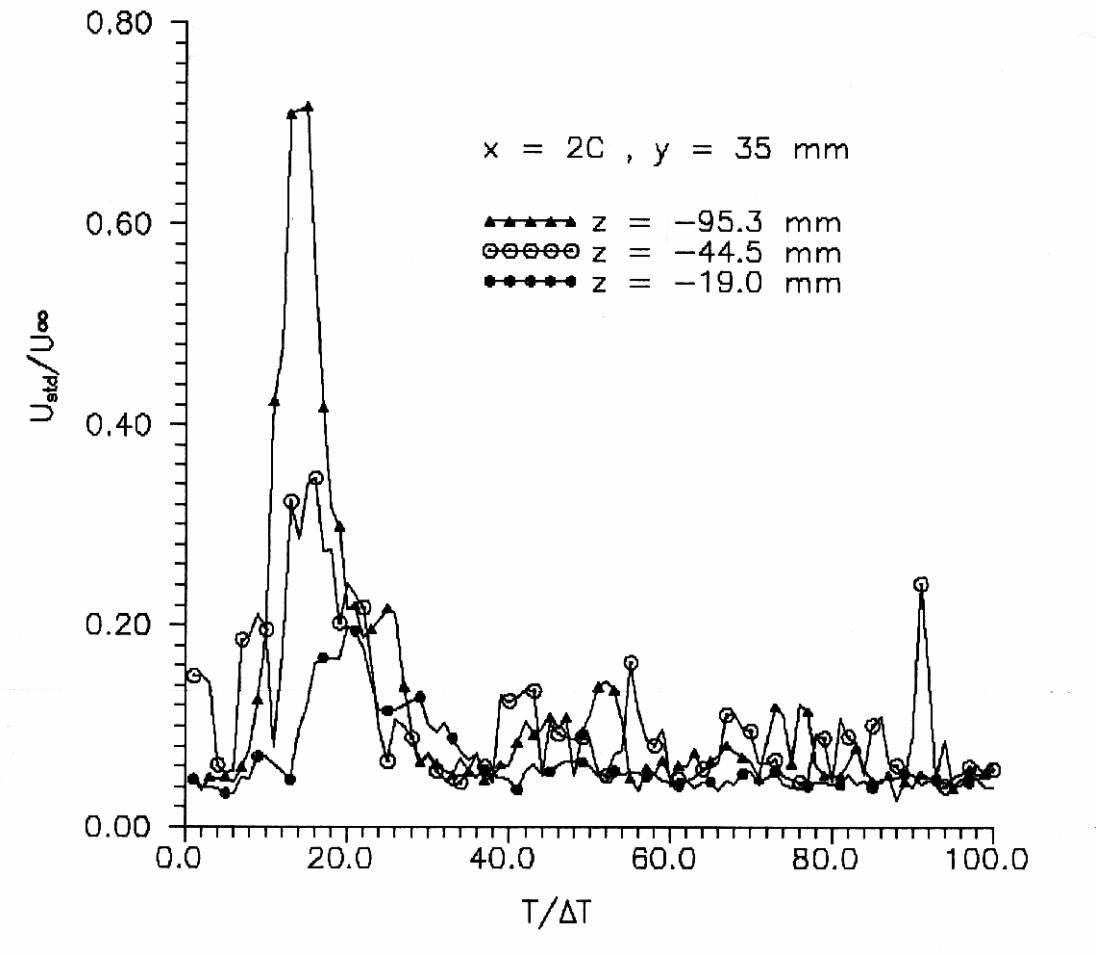

Figure 4.11. Ensemble-averaged RMS fluctuations of the u-component of velocity.

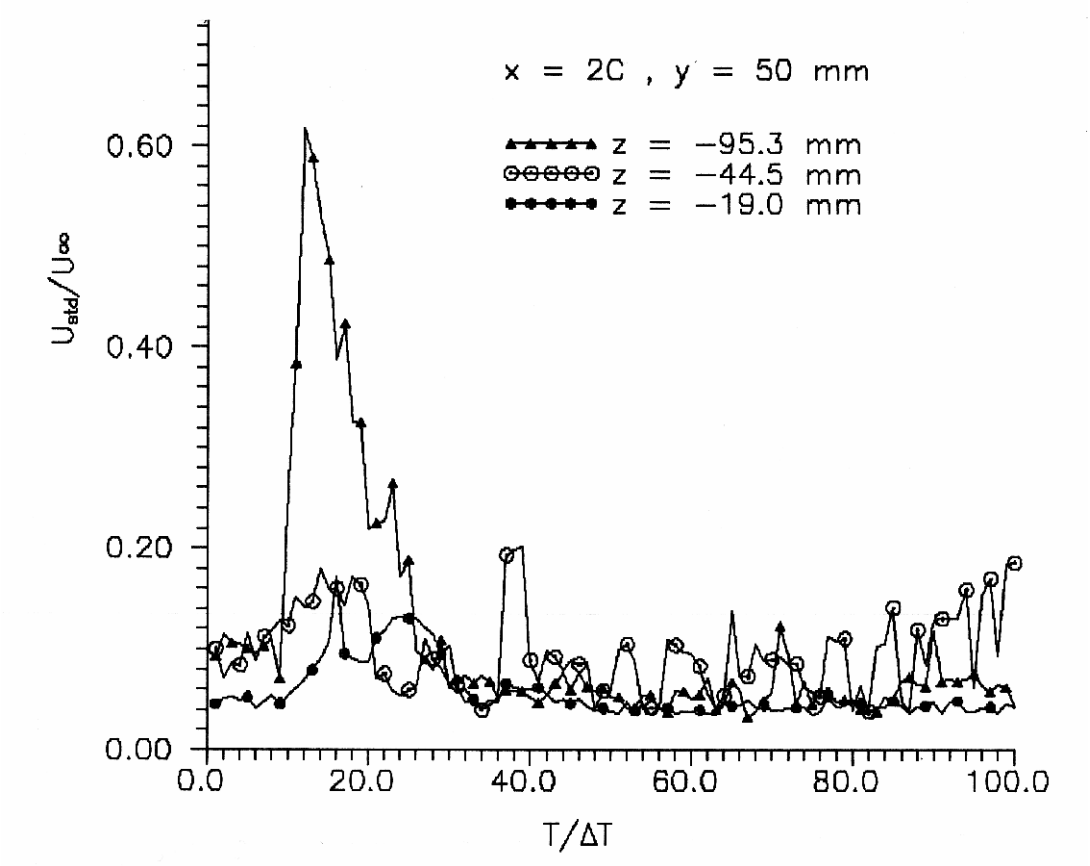

Figure 4.12. Ensemble-averaged RMS fluctuations of the v-component of velocity.

Conclusions

A classical trailing-edge vortex was generated by pitching a flap attached to a flat plate. Such vortices have been thus generated in closed wind tunnels and were found to drift with the stream preserving their straight core parallel to the generating trailing edge. In the present case, with the tip of the flap beneath the surface, a horse-shoe vortex is released which quickly disconnects opening up and reconnects to the free surface. Evidence to this effect was provided by LDV measurements indicating that the core of the vortex near the free surface is somewhat left behind sectional cores beneath the surface.

A little further downstream the core of the vortex straightens up, but starts bending in a plane normal to the plane of the flap. We can provide no physical explanation for this phenomenon. The turbulent fluctuations after the organized part of the vortex has been subtracted, indicate the familiar shift from the normal component to the surface which decreases to the component parallel to the surface.

Acknowledgement

The support of the Office of Naval Research under Grant No. N00014-93-1-264, Edwin Rood, monitor is gratefully acknowledged.

References

Anthony, D. G. and Willmarth, W. W., 1992, "Turbulence measurements in a round jet beneath a free surface," *J. of Fluid Mechanics*, Vol. 243, pp. 699-720.

Banerjee, S., 1994, "Upwelling, Downdrafts and Whirlpools: Dominant Structures in Free Surface Turbulence," *Appl. Mech. Rev.*, Vol. 47, paper S166.

Bernal, L. P., Hirsa, A., Kwon, J. T. and Willmarth, W. W., 1989 "On the interaction of vortex rings and pairs with a free surface for varying amounts of surface active agent." *Phys. Fluids A*, Vol. 1, pp. 2001-2004.

Bernal, L. P. and Kwon, J. T. 1989 "Vortex Ring Dynamics at a Fee Surface," *Phys. Fluids*, Vol. A1, pp. 449-451.

Dommermuth, D. S., and Yue, D. K. P., 1990, "A Numerical Study of Three-Dimensional Viscous Interactions of Vortices with a Free Surface," in *Proc. 18th Symp. on Naval Hydro*, Ann Arbor.

Gharib, M. 1994, "Some Aspects of Near-Surface Vortices," *Appl. Mech. Rev.*, Vol. 47, June 1994.

Gharib, M., Weigand, A., Willert, C. E., and Liepmann, D., 1992, "Experimental Studies of a Vortex Reconnection to a Free Surface: A Physical Flow Model," Proc. of the Nineteenth Symp. of Naval Hydrodynamics, Seoul, Korea.

Hussain, F. and Melander, M.V. 1993, "Model coherent structure dynamics: vortex reconnection, core dynamics and interaction with turbulence" Vol. 395, pp239

Kida, S. and Takaoka, M., 1994, "Vortex Reconnection" Annual Review of Fluid Mechanics, Vol. 26, pp169

Komori, S., Ueda, H., Ogino, F., and Mizushima, T., 1982, "Turbulence structure and transport mechanism at the free surface in an open channel flow," *International J. Heat and Mass Transfer*, Vol. 25, pp. 513-521.

Lam, K. and Banerjee, S., 1988, "Investigation of turbulent flow bounded by a wall and free surface," Proc. of the ASME Winter Annual Meeting, Chicago, Illinois.

Longo, J., Stern, F., and Toda, Y., 1993, "Mean flow measurements in the boundary layer and wake and wave field of a series 60 C_B = 0.6 ship model – part 2: scale effects on nearfield wave patterns and comparisons with inviscid theory," *J. of Ship Research*, Vol. 37, No. 1, pp. 16-24.

Marcus, D. L., and Berger, S. A., 1989, "The Interaction between a Counter-Rotating Vortex Pair in Vertical Ascent and a Free Surface," *Phy. of Fluids*, Vol. A1, pp. 1988-2000.

Ohring, S., and Lugt, H. J., 1989 "Two counter-rotating vortices approaching a free surface in a viscous fluid." *David Taylor Research Center Rep. DTRC-89/013.*

Rashidi, M. and Banerjee, S., 1988, "Turbulence structure in free-surface channel flows," *Physics of Fluids*, Vol. 31, pp. 2491-2503.

Rood, E. P., 1994, "Myths, Math and Physics of Free-Surface Vorticity," *Appl. Mech. Rev.*, Vol. 47, paper S-152.

Rood, E. P. 1994, "Interpreting Vortex Interaction with a Free Surface," *J. Fluids Engineering*, Vol. **????**

Sarpkaya, T. and Neubert, D., 1993, "Interaction of a streamwise vortex with a free surface," AIAA Paper 93-0556.

Sarpkaya, T., and Suthon, P. B. R., 1991, "Interaction of a Vortex Couple with a Free Surface," *Experiments in Fluids*, Vol. 11, pp. 205-217.

Sarpkaya, T., and Suthon, P. B., 1990 "Scarred and striated signature of a vortex pair on the free surface." *Proc. 19th Symp. on Naval Hydrodynamics*. National Academy Press (to appear).

Sarpkaya, T., Elnitsky, J., and Leeker, R. E. 1988 "Wake of a vortex pair on the free surface." In *Proc. 17th Symp. on Naval Hydrodynamics*, pp. 47-54. Washington: Naval Studies Board.

Sarpkaya, T., 1986 "Trailing vortex wakes on the free surface." *In Proc. 16th Symp. on Naval Hydrodynamics*, Berkeley, pp. 38-50.

Stern, F., Parthasarathy, R., Huang, H. P. and Longo, J., 1994, "Effects of Waves and Free Surface on Turbulence in the Boundary Layer of a Surface-Piercing Flat Plate," ASME Free-Surface Turbulence, FED-Vol. 181, pp. 37-51.

Swean, Jr., T. F., Leighton, R. I., Handler, R. A., and Swearingen, J. D., 1991, "Turbulence modeling near the free surface in an open channel flow," AIAA Paper 91-0613.

Tryggvason, G., 1988 "Deformation of a free surface as a result of vertical flows." *Phys. Fluids*, 31, 955-957.

Willmarth, W. W., Tryggvason, G., Hirsa, A. and Yu, D., 1989 "Vortex pair generation and interaction with a free surface." *Phys. Fluids A*, Vol. 1, pp.p 170-172.

Willert, C. E., and Gharib, M., 1994, "The Interaction of Modulated Vortex Pairs with Free Surfaces," Proc. of ASME Symposium of Free-Surface Turbulence," Lake Tahoe, CA.

Yu, D. and Tryggvason, G., 1990. "The Free Surface Signature of Unsteady, Two-Dimensional Vortex Flows," *J. Fluid Mech*, Vol. 218, pp. 547-553.

CHAPTER 5
Conclusions and Recommendations

The aim in this dissertation was to study the interaction of coherent vortices with attached or separated shear layers, and with flat solid walls. Coherent vortices are generated in nature and in engineering applications when flow is passing over a sharp edge at incidence. Such vortices are very nearly ideal, characterized by an irrotational velocity field and a small rotational core. These structures usually retain their coherence even if they encounter solid surfaces. Typical cases of interest to engineering are vortices shed by helicopter blades that impinge upon following blades. This is the typical "blade-vortex interaction" problem.

Of particular interest to this work and its sponsor is the free surface signature of a ship wake and its ability to retain its distinct character for a significant distance downstream of the ship. A ship wake is primarily comprised of the Kelvin wake, a turbulent momentum wake and large vortical structures. These large vortical structures could be the result of wave induced motion with the added complexity of breaking waves adding high concentrations of bubbles. The study of ship wakes are hindered by a combination of the complexity of the flow field and the limited experimental techniques available at the time. The approach taken here is to break the problem down into three simplified experimental setups intended to build knowledge about vortex interaction phenomena. This step-by-step approach has been adopted by most of the researchers working in this field in the hope that studies of simplified versions of wake flows will reveal insight not obvious when many different factors are acting together in the wake of

a ship. For completeness the results of each individual experiment are initially discussed below.

In this dissertation we examined two vortices that propel each other towards a flat plate. Their interaction with the flat plate gives rise to secondary vortices, a phenomenon that has been also observed when delta wing vortices interact with the suction side of a wing. Flow visualizations and subsequent plots of the primary vortex trajectories, for a variety of pitch rates reveal that the development of secondary vorticity is dependent on initial vortex strength. Weaker vortices follow trajectories consistent with an inviscid analysis. The trajectories of stronger vortices are characterized by meandering, which indicates the presence of secondary vorticity. Once the pair of vortices impinge on the wall they start moving apart from each other in directions parallel to the wall, until they reach nondimensional distances $x = 1$, with distances non-dimensionalized by the chordlength of the vortex generating flap. At this point velocity vectors, instantaneous streamlines, and vorticity surfaces and contours reveal an initial movement away from the wall followed by a return towards the wall. Once the data acquisition grid was moved far enough in the x-direction actual evidence of secondary vorticity could be observed. This smaller secondary vortex was seen to quickly roll up and move out of the field of measurement around the primary vortex.

Our main interest in this dissertation was to study the interaction of coherent vortices embedded in shear layers. We considered both wall shear layers, namely boundary layers and free shear layers. Our attention was focused on spanwise vortices, i.e. vortices with their axes normal to the stream. Such vortices could be generated by wall steps or protrusions. In practice, such vortices are generated within the boundary

layers over the hull of a ship in response to pressure gradients induced by free surface waves. Our results indicate that a coherent spanwise vortex suddenly planted in the middle of a fully-developed turbulent boundary layer quickly loses its coherence if its size is comparable to the thickness of the boundary layer. At the beginning, up to two chordlengths of the vortex generating flap downstream of its creation, the vortex retains its character with a viscous core. By the time the vortex drifts to three chordlengths downstream, its behavior is reminiscent of a wake behind a backward-facing step and by four to five chordlengths downstream, the effect of the disturbance is practically eliminated.

For disturbances about twice as large as the thickness of the boundary layer, the behavior is qualitatively similar. However, in this case, the identity of the vortex is preserved for a longer distance. The largest vortex tested, about three times the thickness of the boundary layer retains its character for the entire length of the measuring domain, but loses the coherence of its vorticity. On the other hand, the turbulence kinetic energy associated with the vortex experiences some diffusion, but its overall level appears to remain unaffected by the downstream drift. This indicates that vorticity in the vortex breaks down into turbulence which drifts downstream and leaves the domain of interrogation.

In our study of the interaction of a vortex with a free shear layer we found that such vortices drift with the stream preserving their straight core parallel to the generating trailing edge. With the tip of the generating flap beneath the surface, a wing tip vortex is released which quickly disconnects, opening up and reconnecting to the free surface. Evidence to this effect was provided by LDV measurements indicating that the

propagation of the vortex near the free surface is delayed when compared to sectional cores beneath the surface.

A little further downstream the core of the vortex straightens up, but starts bending in a plane normal to the plane of the flap. We can provide no physical explanation for this phenomenon. The turbulent fluctuations after the organized part of the vortex has been subtracted, indicate a shift from a component normal to the surface into the component parallel to the surface creating a nominally two-dimensional surface layer.

In all cases, the disturbing vortices appear to carry a higher level of turbulence than contained in the turbulent boundary layer. For the smaller vortex, turbulent kinetic energy quickly falls but in the case of the large vortex, the turbulence levels reach values as high as 25 percent. These high levels of turbulence are convected downstream with rather little diffusion and energize the mixing in the turbulent boundary layer for many chordlengths downstream.

With the overall goal of each experimental setup building on our previous knowledge the question remains is how these individual conclusions tie together. Much insight can be gained by comparing the present observations to the results of Luton (1996) whose Ph.D. dissertation was entitled “Numerical Simulations of Vortices Near Free and Solid Surfaces” and was completed prior to this experimental effort. The major difference in this work is the low Reynolds numbers of the flow fields investigated and hence the laminar boundary layers. In the computational investigation of a vortex approaching a solid boundary the secondary vortex generated at the wall spirals around the primary core even generating a tertiary vortex. It is assumed that the path of the

secondary vortex is similar in the experimental results even though only the initial generation and peeling off the wall were captured. In the case of a vortex superimposed on a boundary layer the computational results again show the secondary vortex generated at the wall. Due to the rotation of the vortex the secondary vortex is squeezed between the primary core and the wall before lifting off behind the primary vortex. The experimental results which have a turbulent boundary layer inflow also show the formation of a secondary vortex that is elongated as it is pushed between the plate and the primary vortex due to a flow reversal at the wall. The vortex however does not lift off the wall but remains attached and begins to propagate downstream. In the case of the primary vortex fully embedded in the boundary layer this movement downstream occurs after the breakdown of the primary vortex. For the cases with a larger fence, generating a vortex 3 times the thickness of the boundary layer this movement downstream occurs later, after the primary vortex has moved sufficiently downstream to allow the inflow boundary layer to reestablish downstream velocity. In neither case are the results of the computational studied repeated. But what significance does this have to the problem of a ship wake and hull generated vortices? From the results of these experiments it is seen that a fully embedded vortex is quickly destroyed, within 1-2 chord-lengths of the vortex generating flap. Secondary vorticity at the wall generated by an already dissipated vortex could act on another primary vortex pushing it away from the wall into the outer mean flow where it would feed into the wake structures. The experiment in which a vortex interacts with a shear layer and the free surface was not investigated computationally. Building on the vortex decay rates from the interactions with the turbulent boundary layer it was assumed that the interaction with the free-shear layer would also result in reduced

if not similar decay rates. In fact the vortex generated at the trailing edge of the plate propagates 10 chord-lengths downstream while the turbulent fluctuations of the shed boundary layer are concentrated within the vortex core.

The question remains as to how the individual insights gained here contribute to our overall understanding of ship wakes and the nature of a ship wake to retain its character for a significant distance behind the ship. As observed in the interactions of a spanwise vortex with a turbulent boundary layer, two-dimensional turbulence kinetic energy can be elevated to three times the normal levels due to the breakdown of the primary vortex. These elevated turbulence levels fed by the energy from the mean flow are pushed into the lower levels of the boundary layer by the still coherent vortex. Even after the primary vortex breaks down the elevated turbulence levels continue to propagate downstream. Repeated occurrences of this phenomenon would lead to elevated turbulence levels in the wake of the ship, which are then concentrated in the distinct Kelvin wake V observed by satellite imagery. Using a nominal hull size and ship speed it can be determined that Reynolds numbers above 10^8 are common in full scale wakes, while the experiments were conducted around 3×10^5 based on length of the inflow plate and test section velocity. Full-scale boundary layers using the Blasius formula would then be on the order of fifteen times the size of the model scale 99% boundary layer thickness. Using a nominal distance of ten chord-lengths for propagation of the vortex core observed in the vortex shear layer free surface interactions, would result in a distance of only 6 meters full scale. It is obvious then that a shed primary vortex could only contribute to elevated turbulence levels in the near wake of the ship, not the extended distances observed downstream. Due to the complexity of a ship wake it is not

known whether this problem will be fully understood or aspects of these interactions illuminated by anything less than full-scale experimentation.

APPENDIX A

SUPPLEMENTAL MATERIAL

Experimental Setup and Design

While this dissertation consists of a summary of published papers reflecting the authors work in the area of vortex interactions, it does not document the level of effort spent on experimental preparation. It is the author's opinion that this period of experimental design and setup is as significant a part of the learning experience as the documented results.

During the execution of this experimental investigation many different experimental methods were utilized and developed. Some of these methods were existing techniques, including laser Doppler velocimetry, and flow visualization, that were updated or modified to meet the experimental requirements. Other methods including high speed particle image velocimetry were state of the art and required a significant investment of time to develop into useable tools. This development of experimental techniques and instrumentation was a significant part of my overall education and is not reflected in this summation of published work.

In order to assess complex three-dimensional fluid mechanics problems it was essential to integrate the measurement technique with automated model motions. At the time this research was conducted, primarily 1995 through 1999, laboratory based computer automation was in its infancy. This along with limited budgets required the development of analog circuits to activate computer controlled stepping motors, count

encoder pulses to measure angular motion, and reverse the direction of motors. In this manner repeatable vortices were generated with the motion of sharp edged flat plates.

The motion of the flap would then trigger the collection of laser Doppler velocimetry, frequencies converted to analog voltages proportional to flow velocity, with a analog to digital converter. In addition to controlling the model motions and data collection, tunnel conditions would be continuously monitored. This included tunnel velocity through feedback from the tunnel impeller, and water level for free surface experiments through a level sensor. Measurements would be paused and the user notified if tunnel conditions were not within specified parameters. This level of automation was required in order to collect the large three dimensional data sets reported here that were acquired over a number of days and weeks.

One of the measurement techniques utilized in the collection of data was particle image velocimetry. Again during the period this research was conducted, many universities were implementing these systems but they were still not commercially available. The system developed in the fluid mechanics laboratory in the Engineering Science and Mechanics was unique in that it was one of the first attempts at high speed image collection, 1000 Hz, with a frequency controlled Copper vapor laser. These early attempts suffered from many problems primarily related to low energy density per laser pulse. This resulted in too few particles illuminated within the measurement region to compute correlations between image pairs and compute velocity vectors. The author along with other members of the team tried many different seeding particles, including standard silicon carbide used for laser Doppler velocimetry, silver coated spheres, and custom fluorescent particles developed by Johns Hopkins University, in an attempt to

solve this problem. These efforts met with limited success. Modifications to the laser were then investigated in order to increase the energy density per pulse, including realignment, recharging, replacement of oscillator, and frequency controller. Even with the laser operating at its peak efficiency insufficient particles were being illuminated. The final resolution of this issue was to pulse the laser multiple times during a single shutter opening on the high speed digital camera. The frequency of the laser could then be kept within its optimal range as a multiple of the image acquisition rate. With this issue resolved the issues of integration with computerized data acquisition, condition monitoring and model motion automation had to be addressed. While these efforts are summarized in a single paragraph this effort took approximately 2 years before the particle image velocimetry system was fully operational.

This level of experience with experimental automation, different measurement techniques, and how they can be applied to unique experimental objectives is a key part of any experimental effort at the graduate student level.

Research Carried out by the Author at VA Tech

This section includes paragraphs listed at the end of the introduction, but some of this material is repeated here for completeness. The present dissertation is based on three papers with the author of the dissertation as a first author. The topic of these papers is essentially the topic of the dissertation. Each is concerned with different aspects of the interaction of coherent vortices generated by moving sharp edges. In Chapter 2 we present the interaction of two such vortices that approach a solid surface in a direction

normal to it. They then turn and follow trajectories parallel to the wall. But in this case there is no mean flow, and therefore no significant boundary layer. In the following two chapters we examine the interaction of vortices with developed boundary layers, with thickness the order of magnitude of the diameter of the core of the vortex. In Chapter 3, we study the interaction of vortices with a wall boundary layer, and in Chapter 4, we present data for vortices that are released in the wake of a flat plate. This is essentially the interaction of a coherent vortex with a free shear layer. In the latter chapter we also examine the effects of a free surface.

During his years at VA Tech, the author of this dissertation has worked on many other projects. His collaboration with other members of the fluid mechanics laboratory has resulted in many other publications. He has thus co-authored another six papers. All ten of these papers are listed in the following section of this Appendix. All these papers have been presented at various conferences. Two have appeared in archival journals. Another two have been submitted for publication.

On one of the papers that are not included in the main body of the dissertation, the author was the first author. But the topic was not directly linked to the dissertation, and thus was omitted from the present document. In the other five papers, the present author has made contributions that are outlined in the following Appendices, but his name did not appear as a first author. Two of these papers with content closely linked to the topic of this dissertation are included in the Appendices.

Publications Generated by Author at VA Tech

1. Zeiger, M. D., Rediniotis, O. K., Donnelly, M. J., and Telionis, D. P., "The Temporal Evolution of the Flowfield Over a Pitching Tangent Ogive Cylinder," *AIAA Aerospace Sciences Meeting,* AIAA Paper No. 95-0441.

2. Donnelly, M.J., Rediniotis, O.K., Ragab, S.A., Telionis D.P., "The Interaction of Rolling Vortices with a Turbulent Boundary Layer," Journal of Fluids Engineering, Volume 117, Number 4, pp 564-570, December 1995.

3. Donnelly, M. J., Rediniotis, O. K., and Telionis, D. P., "The Three-Dimensional Character of the Interaction of Large Rollers with a Free Surface," *ASME Fluids Engineering Division*, FED-vol. 217, pp. 191-198, 1995.

4. Zeiger, M.D., Donnelly, M.J., and Telionis, D. P., "An Experimental Investigation of Pitch Axis Effects on Flow Over an Ogive Cylinder," *27th AIAA Fluid Dynamics Conference*, June 17-20, 1996, New Orleans, LA.

5. Donnelly, M. J., and Telionis, D. P., "On the Interaction of a Spanwise Vortex with a Boundary Layer Near a Free Surface," PACAM 97 (Panamerican Congress of Applied Mechanics), Jan. 1-3, 1997, by, also, *Applied Mechanics in the Americas*, M. Rysz, L. A. Godsy and L. E. Suarez, Eds. Vol. 5, pp. 9-62, 1997.

6. Donnelly, M J., Vlachos, P., and Telionis, D. P., "A Vortex Pair Impinging on a Solid Boundary," *AIAA Aerospace Sciences Meeting*, Reno, Nevada, AIAA Paper No. 98-0673.

7. Vlachos, P.P., M. J. Donnelly, D. P. Telionis, "On the Wake of a Circular Cylinder Piercing a Water Free Surface," ASME FED Summer Meeting No.98-5177.

8. Vlachos, P.P., M. J. Donnelly, T. Potter, D. P. Telionis and N. W. Schaeffler, "Post-Stall Control of Sharp-Edged Wings," *AIAA Aerospace Sciences Meeting,* Jan, 1999, AIAA Paper No. 99-0924.

9. Donnelly, M. J., P. P. Vlachos, and Telionis, D. P., "The Design and Testing of a Smart Balance System," *AIAA Aerospace Sciences Meeting,* AIAA Paper No. 99-3165.

10. Stamos, D. G., M. J. Donnelly and Telionis, D. P., "Interaction of Free Surface Waves with a Submerged Rigid Hemisphere," *ASME Fluids Engineering Division Summer Conference*, Paper No. FEDSM99-7093.

APPENDIX B

Interaction of Free Surface Waves with a Submerged Rigid Hemi-Cylinder

The following paper was presented at the 1999 ASME Fluids Engineering Summer Conference. This paper is reproduced here with the permission of the first author Dr. Dimitri G.Stamos.

FEDSM99-7093

Interaction of Free Surface Waves with a Submerged Rigid Hemi-Cylinder

D. G. Stamos, M. J. Donnelly and D. P. Telionis
Department of Engineering Science and Mechanics
Virginia Tech, Blacksburg VA 24061-0219 USA
E-mail: dstamos@vt.edu

ABSTRACT

Laboratory experiments have been conducted to investigate flow separation effects induced by free-surface water waves travelling over a submerged, semi-circular, rigid obstacle. Fluid velocities were obtained for a range of wave conditions. The wave transmission process is modified significantly from the interaction of the obstacle with the wave field. The reflection process is not affected. The presence of the obstacle may induce vortex breakdown which in turn introduces vorticity in the flow. The most important consequence of vorticity production is energy dissipation at the expense of the transmitted waves. The results indicate that the flow does not separate over the body.

INTRODUCTION

Submerged breakwaters are often used for shoreline or harbor protection. The purpose of these structures is mainly to attenuate the wave height and control erosion effects. The problem of propagation of water waves over an obstacle has been studied experimentally and theoretically. Previous studies have been basically concerned with determining the reflection and transmission characteristics of surface waves travelling over an obstacle with a specific geometry.

Grue (1992), Driscoll et al. (1993), and Ohyama and Nadaoka (1993) have modeled the nonlinear interaction of water waves with a submerged rectangular obstacle using potential theory. A comparison of results from theory and experiment indicates that inviscid theory cannot accurately reproduce the experimental observations at the lee of the obstacle. The discrepancies between theory and experiment are due to flow separation and energy dissipation, which cannot be modeled by potential theory. Beji and Battjes (1993) have conducted similar study with trapezoidal object. There are several researchers, who have investigated vortex shedding from submerged objects in waves. Knott and Mackley (1980) studied formation and growth of vortices near plates and surface-piercing tubes using flow visualization, and estimated the energy losses due to eddy motions from measurements of water surface elevations. Stiassnie et al. (1984) studied energy losses due to vortex shedding from the lower edge of a surface-piercing plate. They estimated the energy of the shed vortices, and related that energy to the loss of energy in the surface wave train. These studies have provided important insights into the dynamics of vortex shedding. Francis et. al. (1994) conducted laboratory experiments to investigate flow separation over a submerged rectangular obstacle. From these

measurements, the kinematics and dynamics of eddy motions were studied. The strengths of eddy motions were calculated from the velocity fields, and the energy bound up in the eddies, obtained from integration of kinetic energy, is compared to the energy losses in the surface wave train. The measured velocities were compared to the theoretical predictions of a linear inviscid model. It was found that the formation and growth of separation region respond directly to the wave transformation above the submerged obstacle, leading to a variety of different eddy geometries. Fluid velocities were measured using a two-component laser-Doppler anemometer.

The purpose of this paper is to investigate the flow over a submerged semi-circular obstacle. This interaction may induce vortex breakdown and flow separation over the obstacle. Both processes are highly interactive where the eddy motions, induced by gravity waves, modify the flow around the obstacle, which in turn, affect the surface waves. The large rates of shear associated with the individual vortices can cause energy dissipation. Thus a major effect of vorticity generation is to decrease the amplitudes of the transmitted waves and to change their shapes. Thus the reflection and transmission processes can no longer be predicted by potential inviscid theory. In this study, fluid velocities in the near field of a submerged semi-circular obstacle in waves are measured using particle image velocimetry (PIV). Water surface elevations in front of the submerged object are measured using water level transducers. From these measurements the formation and growth of the separation region are studied.

EXPERIMENTAL SETUP

The experiments were conducted in the Engineering Mechanics wave tank of Virginia Tech. The tank is 25 m long, 2 m wide, and 1.5 m deep with glasswalls to provide optical access at the middle. A piston provides wave generation. The wavemaker accepts an input voltage from a function generator. It is capable of producing regular surface waves with frequencies ranging from 0.6 Hz to 1.4 Hz. The tank is equipped also with a permeable wave-absorbing beach downstream in order to reduce end reflections.

The model is 178-cm long with 30.5-cm diameter. It is constructed of a semi-circular PVC tube mounted on an aluminum plate. Four stainless steel pad eyes were placed at each corner and used to anchor the structure to the bottom of the tank, Figure 1. Thus the model did not float or move when subjected to wave action.

Water surface elevation was measured using a water level transducer, mounted on an instrument carriage, 3-m in front of the model. Wave measurements were conducted to determine the variations of the wave amplitudes in front of the submerged obstacle. A sampling rate of 0.1 s was used. The amplitudes and the corresponding frequencies of fundamental waves are determined from the measured water surface elevations using a fast Fourier transform method.

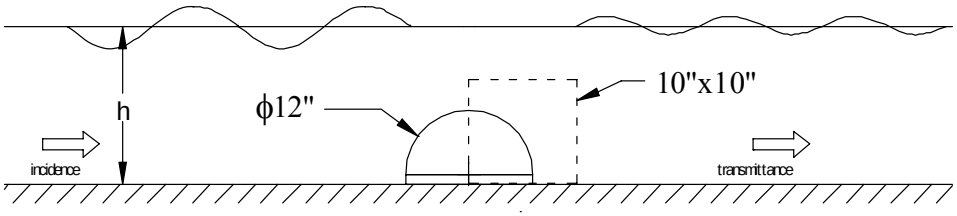

Figure 1: Experimental set up.

Velocity measurements were obtained using particle image velocimetry (PIV). The PIV technique relies on the images of double-or multiply-exposed seed particles within a thin sheet of light in the flow. In this experiment a copper vapor 45-Watt pulsing laser delivering approximately 5 mJ/pulse at its optimum operation provides the light source. The appropriate number of optical components were mounted on the carriage of the wave tank to deliver the laser beam into the flow, Figure 2. The resultant laser sheet was parallel to the propagating waves and was adjusted to cover the flow field, placed on the half-backward circumference of the obstacle, Figure 3. The viewing area of interest was approximately 10x10 in, shown by a dashed frame in Figure 1. The temporal evolution of the flow and the formation and growth of vortical structures were visualized from the reflection of the light on the surface of the suspended and floating particles. PLIOLITE VT particles were used to follow and capture the paths of flow particles. They are vinyl toluene/butadiene copolymers constructed by Good-Year. Their mean diameter was about 400 μm.

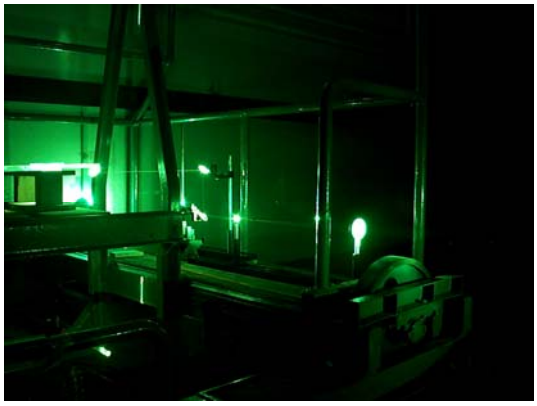

Figure 2: The optical components mounted on the carriage of the wave tank.

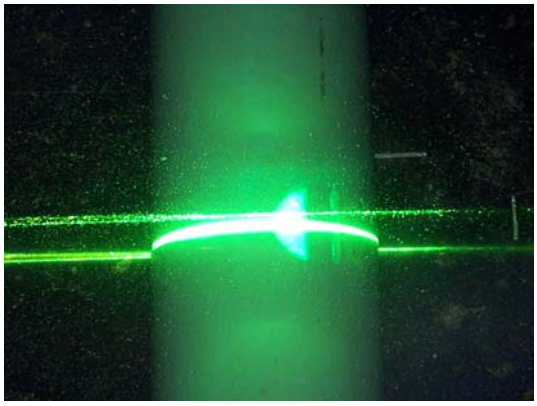

Figure 3: The laser sheet parallel to the propagating waves.

For two different water depths, 22.5-cm and 25-cm and several wave conditions, flow images were acquired with a high speed CCD camera able to take 1000 images/sec with a resolution 256x256 pixels. The camera was synchronized with the laser in order to capture 87 pulses/frame and was interfaced with a Pentium 200-based PC to store the images. The digitally recorded images were analyzed computationally using VISIFLOW software, developed by AEA.

Results and Discussion

Figure 4-a shows a time record of water elevation at $x = 3m$ upstream of the model. The corresponding frequency domain spectrum is presented in Figure 4-b. The water depth is 22.5 cm. Figures 5-a and 5-b also show time record elevations and frequency domain spectra, respectively for another wave condition. The water depth is 25-cm. The results show a strong frequency component in all records at the generated wave frequency.

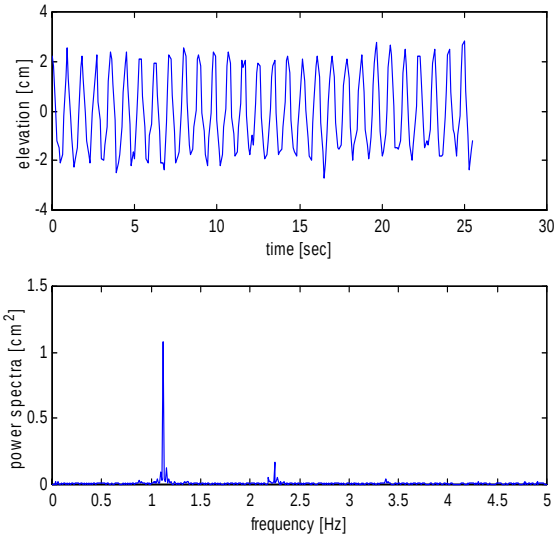

Figure 4.

4-a: Time record elevation for water depth $h = 22.5cm$ and wave frequency $f = 1.2Hz$.

4-b: Wave spectra of the record.

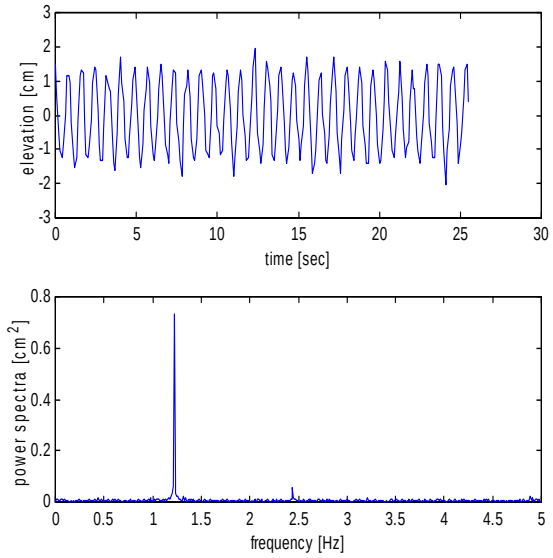

Figure 5.

5-a: Time record elevation for water depth $h = 25cm$ and wave frequency $f = 1.3Hz$.

5-b: Wave spectra of the record.

Figure 6 shows some frames captured by the CCD camera. The free surface can be easily detected. The water depth is 22.5-cm and the fundamental wave frequency is 1.2-Hz. We acquire 150 such frames with sampling frequency 70-Hz. The vectors shown in this figure have lengths and directions indicating the magnitudes and directions of the velocity above and behind the structure.

For the conditions of Figure 6 we combine in Figure 7 flow visualization frames with the results of particle-image velocimetry. The instantaneous velocity field is shown for half period of the generated wave. The free surface can thus be readily identified above the vector field created by the PIV software.

The case depicted in Figures 6 and 7 is a typical case which involves vortex breakdown. The steepening of the wave front is apparent in the flow visualizations. In Figure 6 we observe that the seeding particles recede from the breaking wave. As a result it will not be able to detect the flow motion in this region. Seeding is a difficult process here because there is no continuos motion of the fluid. In regions of poor seeding, the software creates vectors which are in gross error of the velocity. Such regions can be observed on Figure 7. Pockets of recirculating flow can be detected in the neighborhood of the breaking wave but the flow over the obstacle appears to be free of separation.

In Figure 8 we present results of particle-image velocimetry for the case where the water depth is 25-cm and the fundamental wave frequency is 1.3-Hz. The instantaneous velocity field is shown for half period of the generated wave. The front of a wave takes the form of converging streamlines in the form of a fountain. Its interference with an object protruding from the flat bottom of the tank leads to a point of stagnation, which propagates in the direction of the wave motion. As expected the velocity magnitudes decrease with depth. The direction of the flow locally and the decreasing velocity magnitudes are apparently compatible with the geometry of the hemi-cylinder. This explains the fact that no separation is observed over the obstacle. Such a shape would therefore be inappropriate for a breakwater. A rectangular object would be much more appropriate as indicated by Francis et al. (1994) who have observed extensive separation regions over the corners of their body.

Summary and Conclusions

In the present study we demonstrated how flow visualization could be combined with particle -image velocimetry to provide the instantaneous shape of free surface waves and the instantaneous velocity fields. The method was employed to study the interaction of propagating free surface waves with a semi- cylinder mounted on the flat bottom of a channel. In all cases tested it was found the flow over the submerged body is free of separation. However, when the obstacle induces breaking of the wave, vorticity is generated which is leads to energy dissipation and therefore attenuation of the transmitted wave.

References

Beji, S. and Battjes, J.A., 1993. Experimental investigation of wave propagation over a bar. *Coastal Engineering* 19, pp. 151-162.

Driscoll, A.M., Dalrymble, R.A. and Grilli, S.T., 1993. Harmonic generation and transmission past a submerged rectangular obstacle, *In Proc. 23rd Int. Coastal Engineering* Conf., Venice, 1992. ASCE, pp. 1142-1152.

Francis C.K. Ting, Young-Ki Kim, 1993. Vortex generation in water waves propagating over a submerged obstacle. *Coastal Engineering*, 24, pp. 23-49.

Grue, J., 1992. Nonlinear water waves at a submerged obstacle or bottom topography. *J. Fluid Mech.*, 244, pp. 455-476.

Knott, G.F. and Mackley, M.R., 1980. On eddy motions near plates and ducts induced by water waves and periodic flows. Philos. Trans. R.Soc. Lond., A294, pp. 559-623.

Ohyama, T. and Nadaoka, K., 1993. Modeling the transformation of nonlinear waves passing over a submerged dike. *In Proc. 23rd Int. Coastal Engineering* Conf., Venice, 1992. ASCE, pp. 526-539.

Stiassnie, M., Naheer, E. and Boguslavsky, I., 1984. Energy losses due to vortex shedding from the lower edge of a vertical plate attacked by surface waves. Proc. R. Soc. Lond., A396 pp. 131-142.

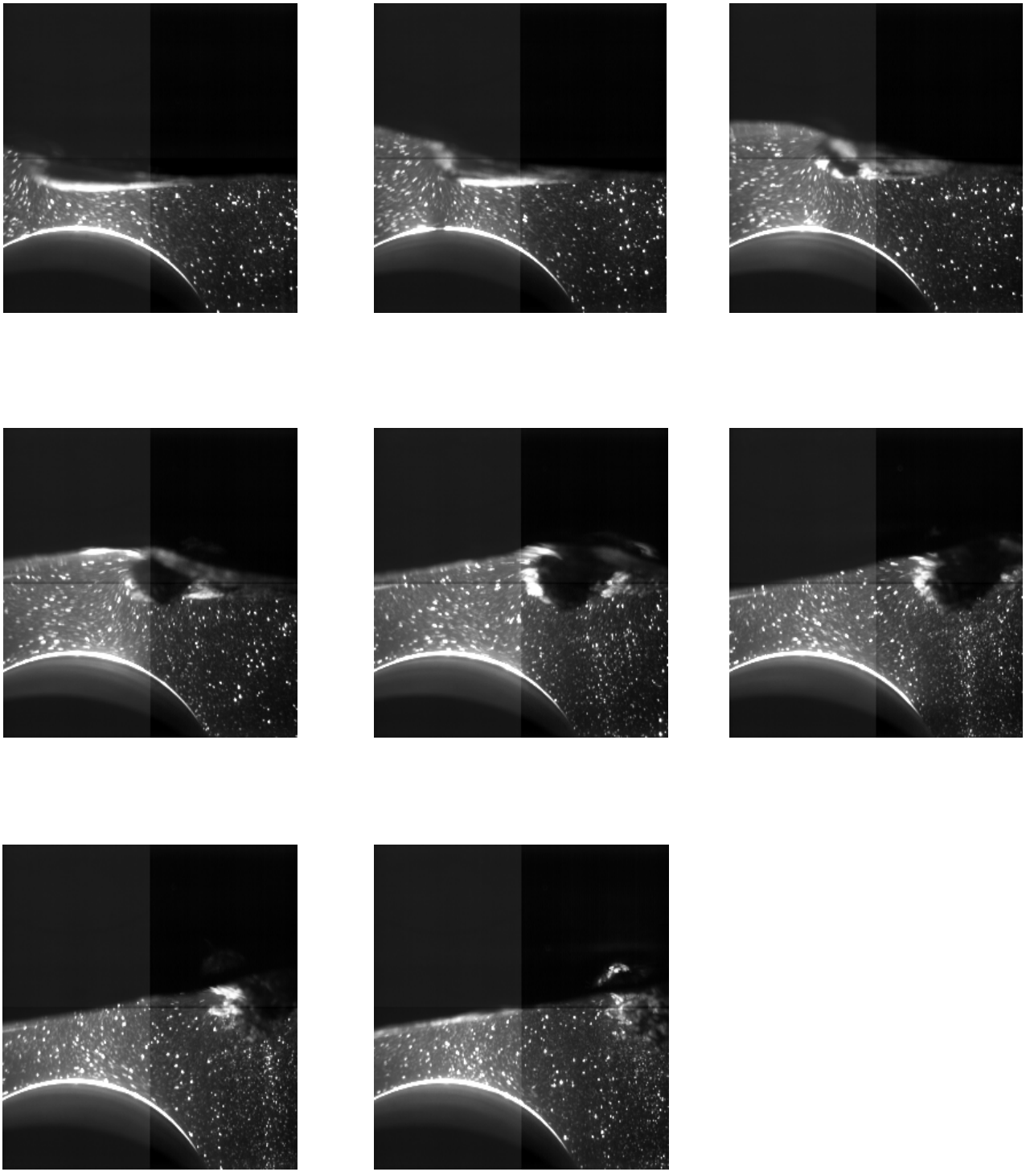

Figure 6: Frames captured by the CCD camera. The water depth is 22.5-cm and the fundamental wave frequency is 1.2-Hz.

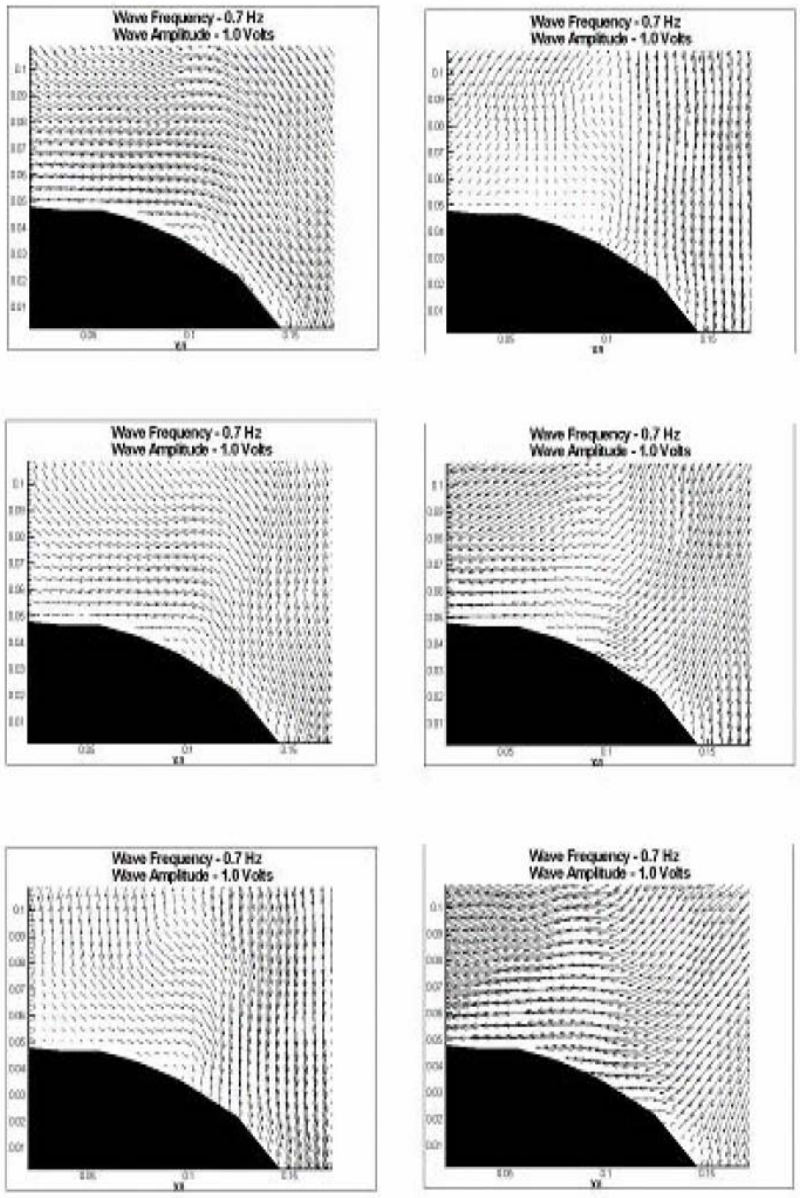

Figure 7: Results of particle-image velocimetry for the case where the water depth is 25-cm and the fundamental wave frequency is 0.7 Hz.

APPENDIX C

Post-Stall Flow Control of Sharp Edged-Wings

The following paper was presented at the 1999 AIAA Winter Annual Meeting, Reno, Nevada. This paper is reproduced here with the permission of the first author Dr. Pavlos P. Vlachos.

Post-Stall Flow Control of Sharp Edged-Wings

Pavlos P. Vlachos*, Martin J. Donnelly*, Tavis L. Potter*, Demetri P. Telionis℘

Department of Engineering Science and Mechanics
Virginia Tech
Blacksburg, VA 24061-0219

and

Norman W. Schaeffler ζ
Aeroprobe Corporation

Blacksburg, VA 24060

Abstract:

In this experimental study we investigate the flow over a sharp-edge airfoil and methods to effectively control it. Digital Particle Image Velocimetry (DPIV) is implemented to investigate the physics related to the flow. Results for a range of angles of attack over a reference airfoil are compared to a flow control model. State of the art piezoelectric actuators are used to introduce a disturbance in the flow via a leading edge flap. For post-stall conditions examined the alternate vortex shedding is unavoidable. Flow control at the appropriate frequency can increase the vorticity content of the stall vortices and induce its motion close to the airfoil surface.

Nomenclature:

C = airfoil chord length
x* = dimensional length (downstream)
y* = dimensional length (normal to airfoil)
x = non-dimensional length (x*/c)
y = non-dimensional length (y*/c)
Re_c = Reynolds number based on chord length

* Graduate Research Assistant, Student Member AIAA

ζSenior Scientist, Aeroprobe Corp., Blacksburg, VA

℘Professor, Associate Fellow AIAA

Introduction:

The physical mechanisms responsible for separated and post stall flow over airfoils have been studied extensively in the past because of their importance to applications. Both numerical and experimental studies have been conducted to provide a better understanding of the physics and to indicate the most effective means of control. Most of these investigations deal with airfoils with rounded edges at small angles of attack (AOA < 15° to 16°). Airfoils with sharp leading and trailing edges and for angles of attack over the stall limit have not received much attention. In the case of the sharp-edge airfoil the flow will separate at very small angles and as we further increase the angle of attack, a fully separated flow develops and the wing behaves as a bluff body. The need of performance enhancement mechanisms becomes evident.

The control of flow separation has been discussed extensively in recent review articles (Gad-el-Hak, 1990, Gad-el-Hak and Bushnell 1991). A variety of methods have been employed with considerable success for flows about airfoils with rounded leading edges. Most recently, Seifert and Pack (1998) demonstrated that unsteady blowing (Seifert, et al. 1996) can be effective in controlling boundary layer separation over a wide range of chord Reynolds numbers. However, all this work is limited to angles of attack only a few degrees beyond stall, i.e., 15° to 16°. For the case of deep stall, separation is unavoidable and the wakes of all

wings are dominated by alternately shed vortices. The challenging task is now to control and manage this naturally unsteady phenomenon. A few recent experimental and numerical studies proved that this is indeed possible. These studies have indicated that, for a wide range of post-stall angles of attack of a two-dimensional airfoil or a wing with large aspect ratio and small sweep angle, the lift can be greatly enhanced by unsteady flow control (Zhou et al. 1993; Hsiao et al. 1990, 1993, 1994; Chang et al. 1992; McManus and Magill 1996; Wu et al 1997a,b).

Employing acoustic disturbance, or oscillating flap excitation, Hsiao and his associates were able to increase the lift of a NACA 63-018 airfoil by 60%. The numerical investigation of Wu et al. (1997a,b) provided further evidence on the effectiveness of this unsteady control technique. They computed lift increases for a NACA-0012 airfoil with the Reynolds number based on chord length $Re_c = 5x10^5$ at a wide range of post-stall angles of attack. They indicated that the "lift valley" beyond the stall angle of attack is almost filled up, except for a narrow region very close to stall and that the effective control range may extend to about $\alpha = 35°$ for this airfoil. They also pointed out that in a wide range of post-stall angles of attack, a disturbance near the leading edge of an airfoil may lead to lift enhancement, drag reduction and buffet suppression.

The significant finding of Zhou and his associates (Zhou et al. 1993) is that a control mechanism is equally effective with sharp leading edges. They mounted a small oscillating flap on the sharp leading edge of an airfoil and showed that if the flap is oscillated in pitch with a 5° amplitude, at the frequency of vortex shedding, the lift could be increased by over 50%.

There is also evidence that vortex shedding over highly swept wings at high angles of attack. Members of this group (Rediniotis, et al. 1993) demonstrated this with a 70°-sweep delta wing. Application of an oscillating leading edge flap in this case may also lead to increased lift.

In this paper we will discuss our efforts to extend the concept of flow control to sharp-edge airfoils at high angles of attack. The success of this idea hinges on the better understanding of periodic vortex shedding over such airfoils and apparently this aspect of the problem has not yet been investigated.

Facilities and Instrumentation:

The experimental study was conducted in the Engineering Science and Mechanics Water Tunnel facility at Virginia Tech, using digital particle image velocimetry (DPIV). The advantages of DPIV method have been discussed extensively by many authors (R. J. Adrian, 1991, Willert and Charib, 1991, R. J. Adrian, 1996).

The ESM water tunnel can be run both as a closed and as a free-surface facility. The tunnel operates in a closed loop with up to 2,500 gallons of water. After the settling chamber, a three-way convergence leads to the 24″ x 24″ x 72″ test section made of a clear, acrylic Plexiglas. A 4500 GPM axial flow pump drives the flow at speeds up to 1 m/s, with free stream turbulence levels less than 2%.

Two-dimensional velocity plane measurements were acquired providing qualitative and quantitative information for the flow. For the PIV laser sheet, the light source was a copper vapor 45 Watt pulsed laser, delivering approximately 15 mJ/pulse at its optimum operation. Using a set of sheet forming optics, a laser sheet was delivered in the test section, shown schematically in Figure 1. The laser was synchronized with a high speed CCD camera able to take 1000 images/sec with a resolution of 256x256 pixels. Hollow glass spheres of 10 microns mean diameter were used as flow tracers.

Two models were constructed for this investigation, a reference model and a flow control model. Both models were constructed with sharp leading and trailing edges. The upper and lower surfaces are circular arcs and the airfoil has a thickness to chord length ratio of 0.15. The flow control model has a leading edge flap actuated by piezoelectric actuators, see Figure 2. The leading edge flap is 6.25% of the airfoil chord length.

Thunder piezoelectric actuators were employed for this study. Based on patented technology licensed from NASA, these devices are durable, solid-state construction and can provide significant mechanical output under load. At excitation frequencies of 2,4,and 8 Hz they oscillate the leading edge flap through an angle of 3.3°, 2.68°, and 2.1° respectively.

DPIV measurements were taken over both airfoil configurations for 10, 20 and 30-degree angles of attack. These angles of attack correspond to approximate vortex-shedding frequencies of 3, 2, and 1 Hz respectively,

determined from flow visualizations. All measurements were taken at a flow speed of 1.5 ft/s, which corresponds to a Re_c of 22114.

Results and Discussion:

The flow over any sharp leading edge separates at the edge. No flow control mechanism could avoid separation. But there is a possibility to manage the separated region in order to reduce the suction side pressure and therefore increase the lift. This can be achieved in two ways. The first is to force the free shear layer closer to the wing. This is equivalent to pushing separation downstream over an airfoil with a rounded leading edge. The second mechanism is to energize the wake by adding vorticity to it. This is equivalent to the Weiss Fogh mechanism whereby a vortex is trapped on the suction side of the airfoil. In the present case this is not possible because the flow is going through a dynamic process of vortex shedding. But it is possible in an average sense, as Wu et al have pointed out.

There is a natural vortex shedding activity over the airfoil, which is characterized by a distinct shedding frequency. In each case we captured two thousand instantaneous frames, at a rate of 500 Hz, covering several periods. We then averaged these data to generate averaged velocity, streamlines and vorticity fields. In all of the plots shown the flow is from left to right and the leading edge of the airfoil is at x=1.0 and the trailing edge is at x=0.0. In Figure 3 we present two average vector fields at 20° AOA from which we calculate vorticity, stream function, and streamlines. In Fig. 4, we present the vorticity field over the airfoil placed at an angle of attack of 10. Rather little influence of the placement of a fixed flap or an oscillating flap is observed. Apparently the vortex shedding activity is developing downstream of the airfoil and it is not easy to influence it by introducing disturbances in the free shear layer.

For the case of an airfoil at an angle of attack of 20 the results are presented in Fig. 5. Here we observe a very interesting phenomenon. The placement of a fixed flap as shown in Fig. 2 is enough to create a disturbance in the free shear layer which forces it to incline closer to the surface of the airfoil. The greatest influence on the free-shear layer inclination we obtained by disturbing the free-shear layer at a frequency of 2Hz. The frequency of the leading edge actuation which most clearly matches the natural shedding frequency of the airfoil at this angle of attack. Moreover, the actuated cases indicated the transfer of some vorticity in the wake to a region closer to the airfoil. This is reminiscent of a trapped vortex for this time-averaged data.

The case of 30 degrees shown in Fig. 6 shows a somewhat different influence of the leading edge flap actuation. Again the contours of vorticity show a transfer of vorticity into the wake of the airfoil. This vorticity, although lower in magnitude of the 20° case, is closer to the leading edge of the airfoil. The difference between these two cases could be due to the need for larger amplitude disturbances at higher angles of attack. These results or the lack of significant influence is in disagreement with the results of Zhou et al. The discrepancy between these two cases could be due to the fact that the amplitude of flap oscillation is lower for the 30°case than the amplitudes employed by Zhou et al. Moreover, it is known. that the flow control mechanism is most effective if the disturbance is introduced at the shedding frequency, which for the 30° case is lower than initial disturbance frequency of 2 Hz used in this study.

Figures 7 and 8 show streamlines plotted from a calculation of the stream function. Again these plots are time averaged over several periods of vortex shedding. Figure 7 shows the 20°angle of attack case for the reference airfoil and all frequencies of actuation. The conclusions from the streamlines coincide with those from the vorticity plots. Both a reduction in the shear layer angle, pushing it closer to the wing, and a time averaged vortex structure closer to the wing can be seen for all cases. Again the most effective actuation frequency is 2 Hz which is the closest frequency to the natural vortex shedding frequency. However, this time-averaged vortical structure is off the trailing edge of the airfoil, thereby reducing its contribution to the lift of the airfoil. Figure 8 again shows the reference airfoil and all frequencies of actuation at 30° angle of attack. In this case both for the reference airfoil and 0 Hz actuation control model multiple time-averaged vortical structures can be observed. Actuation of the leading edge flap at any of the frequencies tested shows the creation of a single time-averaged vortical structure off the leading edge. It is proposed that the fixing of the shedding process into a single structure could increase lift.

Conclusions:

The present investigation indicated that for the three angles of attack tested the most effective flow control results were obtained for the 20° angle of attack case and excitation at the natural frequency. The disturbance forces the free shear layer to lean closer to the airfoil surface, thus bringing it closer to attached flow. Moreover in all cases, we observed some increase in the vorticity level within the wake, which implies a more energized vortex. However, the results do not represent significant departures from the reference case. A more careful detection of the natural shedding frequency will be required. Moreover, it is proposed to increase the amplitude of the flap oscillation.

Acknowledgements:

We appreciate the support of Face International who provided the Thunder piezoelectric actuators and the necessary controller.

References:

Adrian R. J., 1991,"Particle Imaging Techniquesfor Experimental Fluid Mechanics" *ARFM, 1991, 23:261-304.*

Adrian R. J, 1996, "Strategies for Imaging FlowFields with PIV" *AIAA 96-1988*

.Chang, R C., Hsaio, F.-B., and Shyu, R.-N., 1992. Forcing Level Effects of Internal AcousticExcitation on Improvement of Airfoil Performance. *J. Aircraft* **29**, 823-829.

Willert C.E. and Charib M. "Digital Particle Image Velocimetry", 1991, Experiments inFluids 10, 181-193. Gad-el-Hak, M., 1990, "Control of Low-Speed Airfoil Aerodynamics," *AIAA Journal*, Vol. 28, pp. 1537-1552.

Gad-el-Hak, M., and Bushnell, D. M., 1991, "Separation Control: Review," *Journal of FluidsEngineering*, Vol. 113, pp. 5-29.
Hsiao, F. B., Liu, C.-F., and Shyu, J.-Y., 1990. "Control of Wall-Separated Flow by InternalAcoustic Excitation." *AIAA J*, **28**, 1440-1446.

Hsiao, F.-B., Wang, T.-Z., and Zohar, Y. 1993. "Flow Separation Control of a 2-D Airfoil by a Leading-Edged Oscillating Flap." Intern. Conf. Aerospace Sci. Tech., Tainan, Taiwan, Dec. 6-9, 1993.

Hsiao, F.-B., Shyu, R.-N., and Chang, R. C., 1994. "High-Angle-of-Attack Airfoil Performance Improvement by Internal Acoustic Excitation." *AIAA J*, **32** j655-657.

McManus, K., and Magill, J., 1996, "Separation Control in Incompressible and Compressible Flows Using Pulsed Jets," AIAA Paper 96-194

Rediniotis, O. K., Stapountzis, H., and D. P. Telionis, 1993, "Periodic Vortex Shedding over Delta Wings," *AIAA Journal* Vol. 31, pp. 1555-1562.

Seifert, A., and Pack, L. G., 1998, "Oscillatory Control of Separation at High Reynolds Numbers," AIAA 98-0214.

Seifert, A., Dorabi, A. and Wygnanski, I., 1996, "On the Delay of Airfoil Stall by Periodic Excitation," *AIAA J. of Aircraft*, Vol. 33, pp. 691-699.

Wu, J.M., Lu, X.Y., Denny, A.G., Fan, M., and Wu, J.Z. 1997. Post-stall lift enhancement on an airfoil by local unsteady control. Part I. Lift, drag, and pressure characteristics. AIAA paper 97-2063.

Wu, J.Z., Lu, X.-Y., and Wu, J.M. 1997. Post-stall lift enhancement on an airfoil by local unsteady control. Part II. Mode competition and vortex dynamics. AIAA Paper 97-2064.

Zhou, M. D., Fernholz, H. H., Ma, H. Y., Wu, J. Z., and Wu, J. M., 1993. "Vortex capture by a two-dimensional airfoil with a small oscillating leading edge flap." AIAA Paper 93-3266.

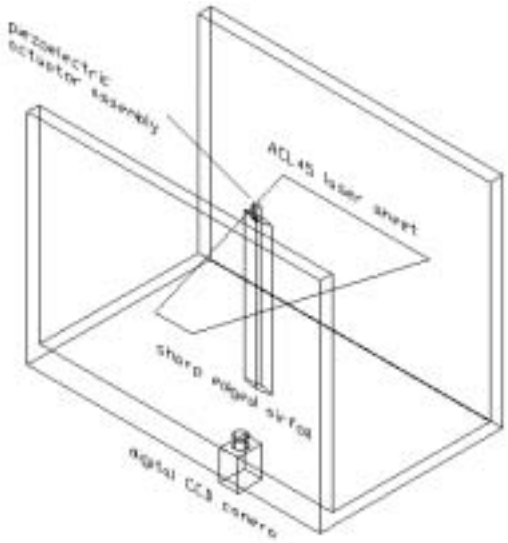

Fig. 1 Schematic of experimental setup

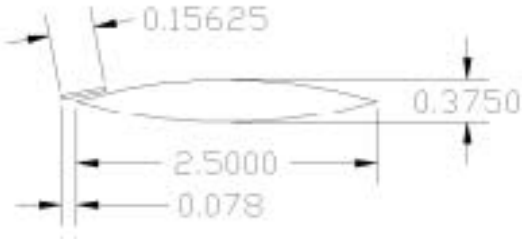

Fig. 2 Sharp edged airfoil dimensions(all dimensions in inches)

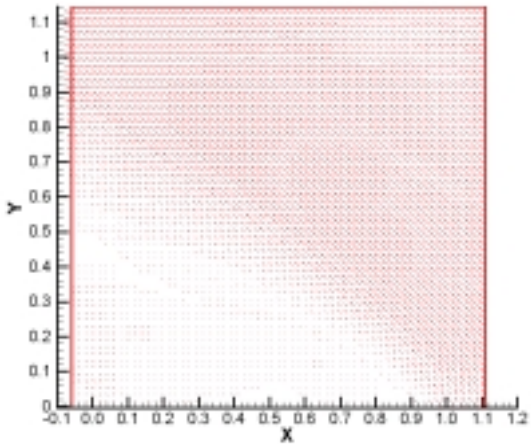

Fig. 3a Average Vector Field, 20° AOA, Reference Airfoil

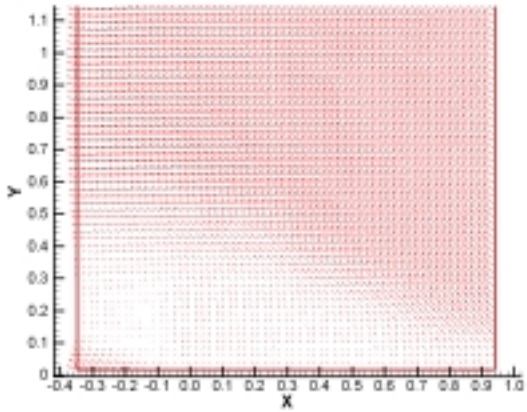

Fig. 3b Average Vector Field, 20° AOA, 2 Hz Actuation

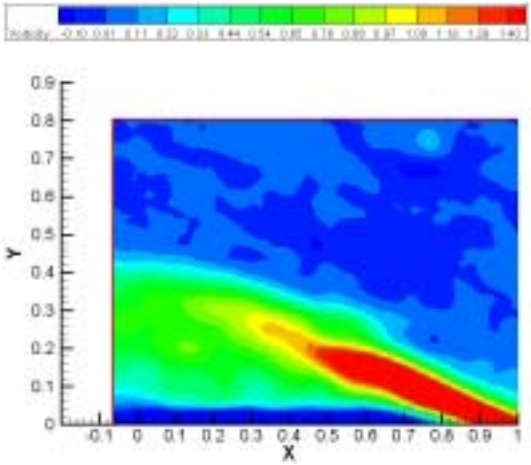

Fig. 4a Vorticity 10° AOA, Reference Airfoil

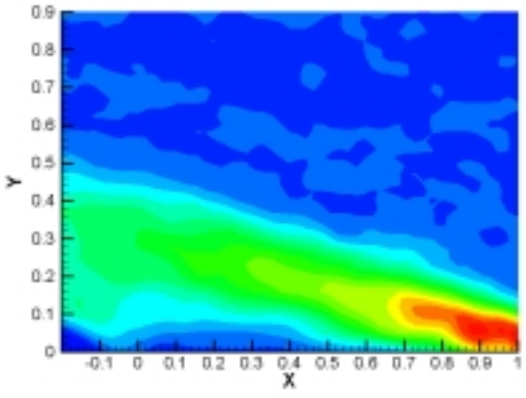

Fig. 4b Vorticity 10° AOA, 0 Hz Actuation

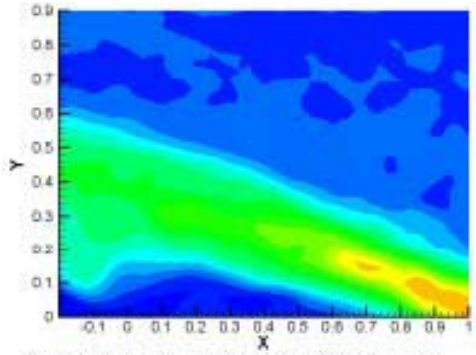

Fig. 4c Vorticity 10° AOA, 2 Hz Actuation

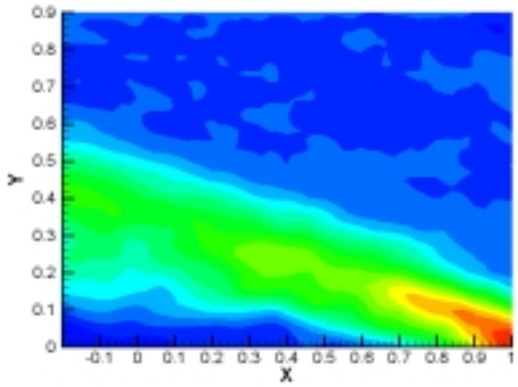

Fig. 4d Vorticity 10° AOA, 4 Hz Actuation

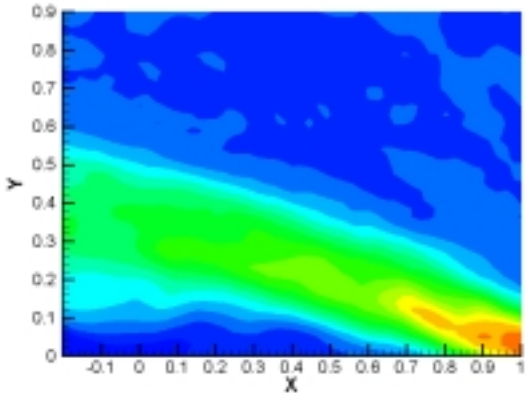

Fig. 4e Vorticity 10° AOA, 8 Hz Actuation

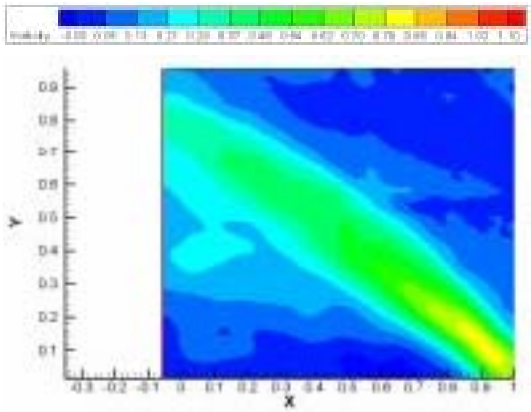

Fig. 5a Vorticity 20° AOA, Reference Airfoil

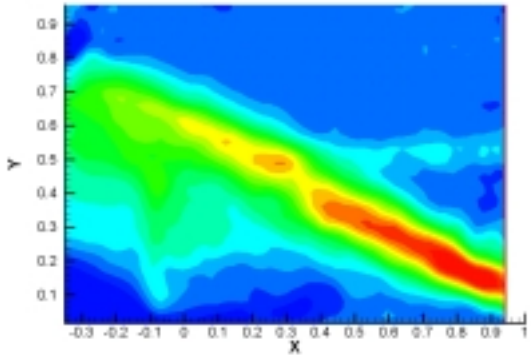

Fig. 5b Vorticity 20° AOA, 0 Hz Actuation

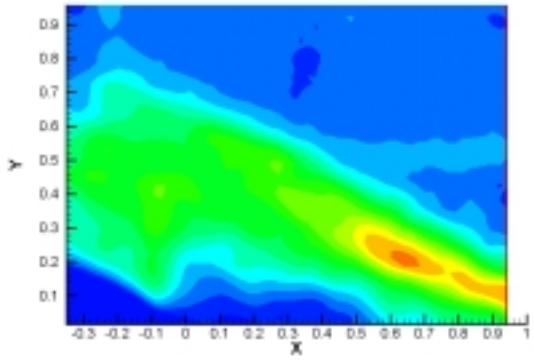

Fig. 5c Vorticity 20° AOA, 2 Hz Actuation

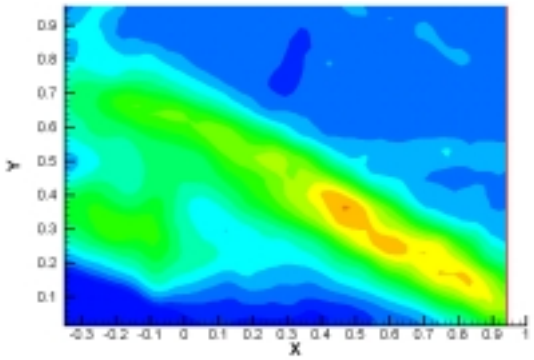

Fig. 5d Vorticity 20° AOA, 4 Hz Actuation

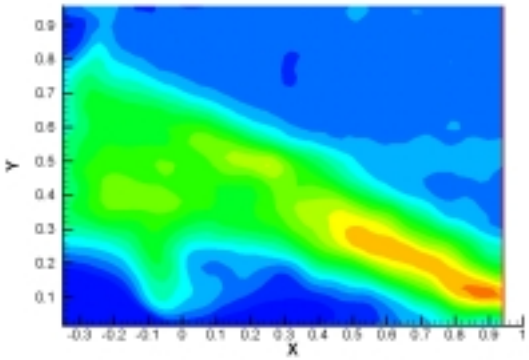

Fig. 5e Vorticity 20° AOA, 8 Hz Actuation

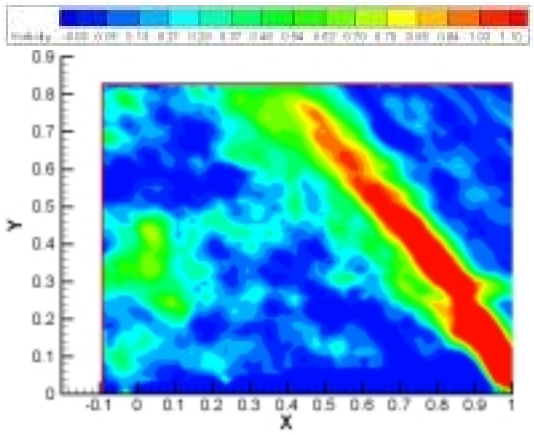

Fig. 6a Vorticity 30° AOA, Reference Airfoil

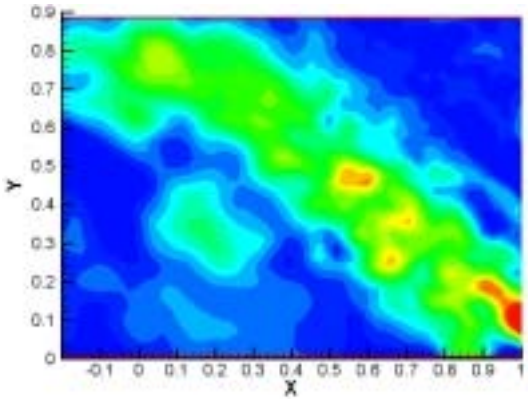

Fig. 6b Vorticity 30° AOA, 0 Hz Actuation

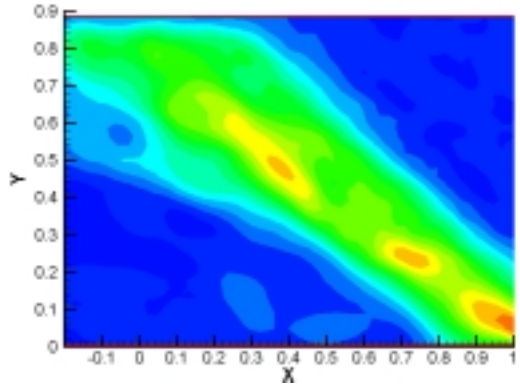

Fig. 6c Vorticity 30° AOA, 2 Hz

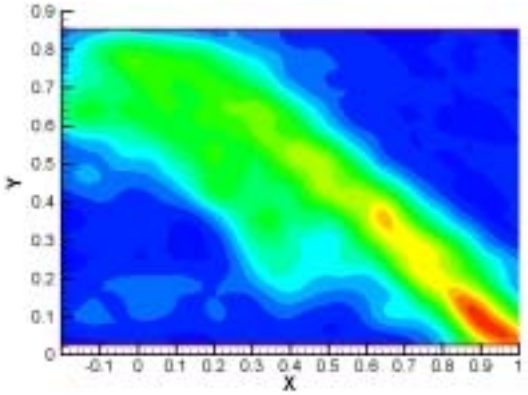

Fig. 6d Vorticity 30° AOA, 4 Hz Actuation

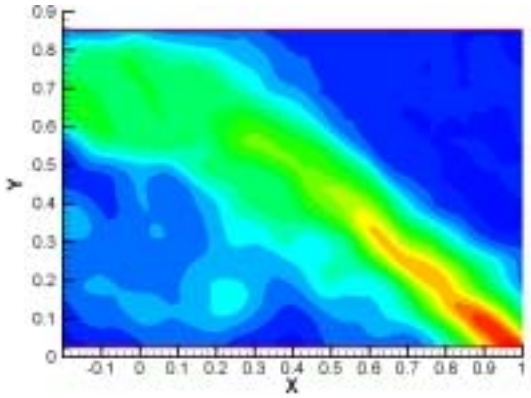

Fig. 6e Vorticity 30° AOA, 8 Hz Actuation

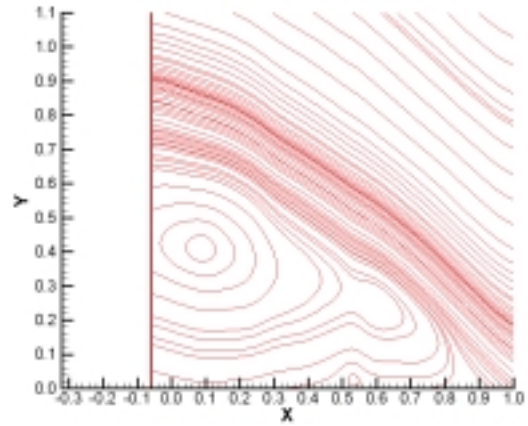

Fig. 7a Streamlines, Time Averaged Flowfield
20° AOA, Reference Airfoil

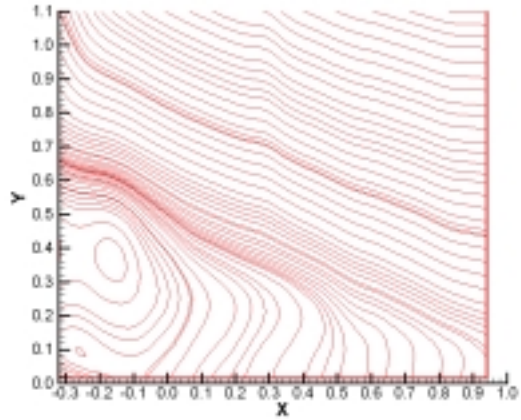

Fig. 7b Streamlines, Time Averaged Flowfield
20° AOA, 0 Hz Actuation

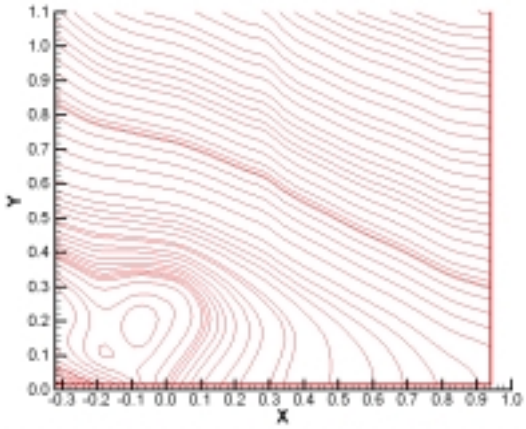

Fig. 7c Streamlines, Time Averaged Flowfield
20° AOA, 2 Hz Actuation

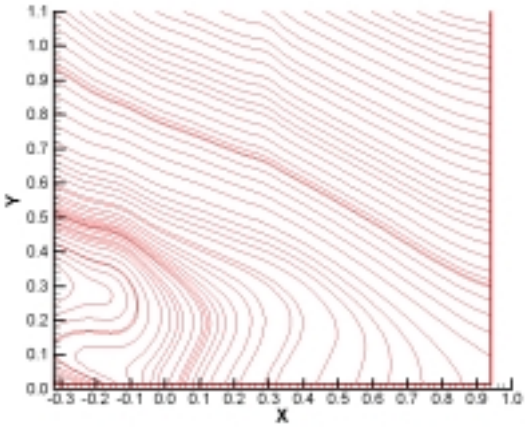

Fig. 7d Streamlines, Time Averaged Flowfield
20° AOA, 4 Hz Actuation

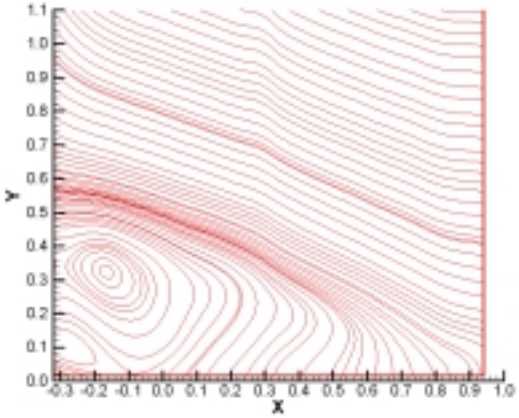

Fig. 7e Streamlines, Time Averaged Flowfield
20° AOA, 8 Hz Actuation

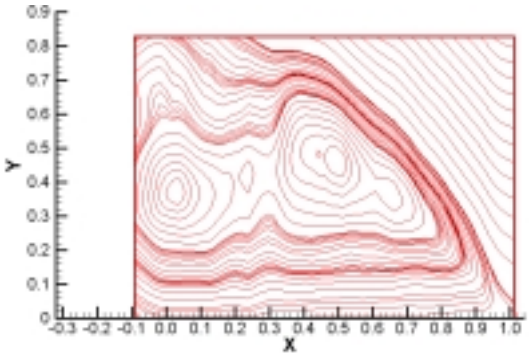

Fig. 8a Streamlines, Time Averaged Flowfield 30° AOA, Reference

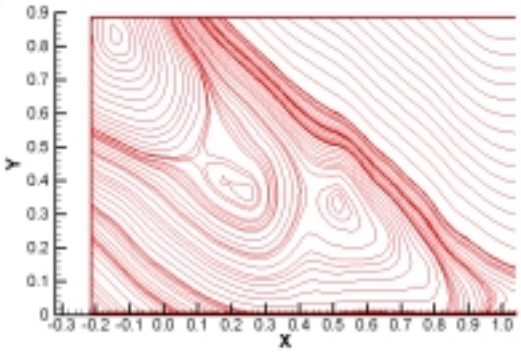

Airfoil Fig. 8b Streamlines, Time Averaged Flowfield 30° AOA, 0 Hz Actuation

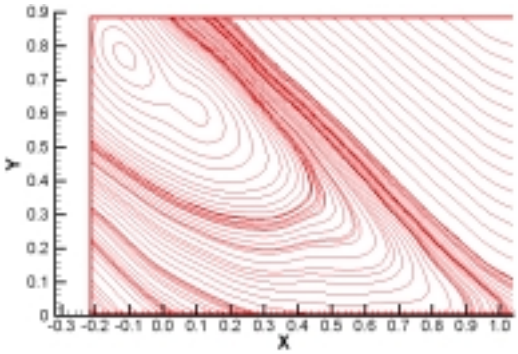

Fig. 8c Streamlines, Time Averaged Flowfield 30° AOA, 2 Hz Actuation

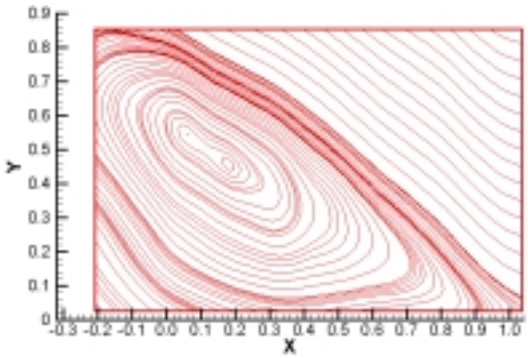

Fig. 8d Streamlines, Time Averaged Flowfield 30° AOA, 4 Hz Actuation

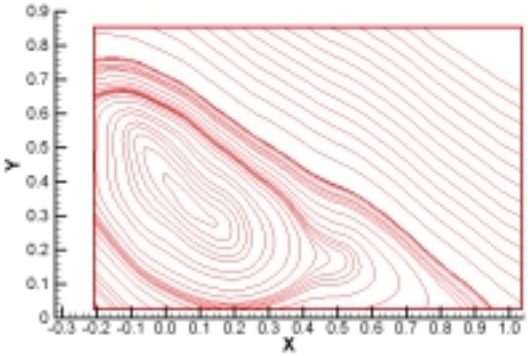

Fig. 8e Streamlines, Time Averaged Flowfield 30° AOA, 8 Hz Actuation